Numerical Methods in Lubrication Modelling

by

Elyas Gulam Nurgat

Submitted in accordance with the requirements
for the degree of Doctor of Philosophy

The University of Leeds
School of Computer Studies
September 1997

The candidate confirms that the work submitted is his own and that appropriate credit has been given where reference has been made to the work of others.

Abstract

Over the past two decades, many numerical schemes have been developed to solve elasto-hydrodynamic lubrication problems. New schemes are continuously being sought with the aim of improving efficiency and robustness. The two main issues of concern when solving these problems are large computational costs and numerical instabilities. The multigrid method, first used by Lubrecht et al. [68] when solving these problems, has proved to be very successful in dealing with the issue of computational costs. Venner [97] took this work further and developed a relaxation scheme which dealt with the issue of instability. However, Venner's scheme is not only difficult to understand because it is not presented in its entirety but also difficult to implement due its complexity. Hence, a new easy to understand and simple relaxation scheme will be developed and employed in this work, [74], to solve elasto-hydrodynamic lubrication problems.

The aim of this work is to present an efficient, robust and general purpose numerical solver for isothermal (Newtonian) elasto-hydrodynamic lubrication circular contact problems. The solver will be based on the FDMG Multigrid Software [92] and the new relaxation scheme. Elasto-hydrodynamic lubrication problems are very important in engineering applications and there is a need for general purpose solvers for industrial applications.

The multigrid solver will be used to solve both steady-state and time-dependent (transient) problems. A wide range of steady-state problems will be solved and the obtained solutions will be compared with those obtained using other numerical methods, [75]. Up to this date, transient problems are constantly being solved using fixed time step methods where the step sizes are chosen arbitrarily. We will present solutions to both fixed and variable time step methods. The governing equations of transient problems will be written as a system of differential algebraic equations and methods from this area will be employed in variable-step time integration and convergence testing, [90].

Acknowledgements

I would like to thank Dr Martin Berzins for his invaluable guidance, encouragement and advice throughout the course of this work. I would also like to thank Dr Laurence Scales (Shell Research and Technology Centre at Thornton) not only for providing much constructive advice and support but also for providing me with a very interesting and challenging problem.

Thanks are also due to Professor Duncan Dowson, Professor Chris Taylor, Dr Ducai Wang and especially Dr Pascal Ehret (Mechanical Engineering Department, Leeds Institute of Tribology) for their advice and support and Dr Gareth Shaw of NAG Ltd for supplying the FDMG Multigrid Software.

I am grateful to both EPSRC and Shell Research and Technology Centre at Thornton for funding this work.

Finally, I thank the Almighty for guiding me through both in good and bad times.

Contents

1 INTRODUCTION **1**

1.1 Hydrodynamic Lubrication 1

1.2 Elasto-Hydrodynamic Lubrication 2

1.3 EHL Review 3

1.4 Overview of Contents 7

2 GOVERNING EQUATIONS AND DISCRETISATION **10**

2.1 The Reynolds Equation 11

2.1.1 Viscosity 12

2.1.2 Density 13

2.1.3 Cavitation condition 14

2.1.3.1 Penalty method 14

2.2 The Film Thickness Equation 15

2.3 The Force Balance Equation 17

2.4 Non-Dimensionalisation 17

2.4.1 Moes and Hertzian dimensionless parameters 19

2.4.2 Hamrock-Dowson's dimensionless parameters 20

2.4.3 Relationship between Moes and Hamrock-Dowson's parameters 20

2.5 Discretisation 21

2.6 Finite Difference Discretisation of Governing Equations 22

2.6.1 Elastic deformation 25

2.7 Conclusion 27

3 SINGLE GRID ITERATIVE METHODS **30**

3.1 Iterative Methods 31

3.1.1 Inverse method 32
3.1.2 Gauss-Seidel method 33
3.1.3 Newton-Raphson method 34
3.1.3.1 Effective influence Newton method 35
3.1.4 Homotopy method 37
3.2 Single Grid Relaxation Schemes 40
3.2.1 Relaxation schemes of Venner and Ehret 44
3.2.1.1 Point Gauss-Seidel relaxation scheme 45
3.2.1.2 Gauss-Seidel line relaxation scheme 46
3.2.1.3 Jacobi distributive line relaxation scheme 48
3.2.2 A new relaxation scheme 50
3.2.3 Differences between Venner's relaxation scheme and the new relaxation scheme 53
3.3 Test Problem 55
3.3.1 Discussion 55
3.4 Smoothing Analysis 58
3.4.1 Fourier analysis of the Poiseuille terms 59
3.5 Conclusion 61

4 DEVELOPING AN EHL SOLVER USING MULTIGRID 64

4.1 Multigrid Method 65
4.1.1 Restriction operator 68
4.1.2 Prolongation operator 70
4.1.3 Coarse grid correction cycle 71
4.1.4 Full-multigrid 73
4.2 Overview of the Multigrid Method for Solving EHL Problems . . . 73
4.3 FDMG Multigrid Software 75
4.4 Multigrid Solver for EHL Problems 78
4.4.1 Driver Program 79
4.4.2 Modified FDMG 79
4.4.3 EHL Routines 80
4.5 Modifications Made to the Original FDMG Multigrid Software . . . 84

4.5.1 Modifications made due to the new relaxation scheme 84
4.5.2 Modifications made due to cavitation condition 84
4.6 Example Showing the Effectiveness of the Full-Multigrid Scheme . . 86
4.7 Conclusion 88

5 NUMERICAL EXPERIMENTS USING A MULTIGRID SOLVER BASED ON FDMG **90**

5.1 Case One 90
5.1.1 Results and discussion 91
5.1.2 Remarks 96
5.2 CPU Times 96
5.3 Case Two 97
5.3.1 Results 98
5.3.2 Discussion 102
5.4 Case Three 105
5.4.1 Results 106
5.4.2 Discussion 111
5.5 Case Four 116
5.5.1 Results and Discussion 117
5.6 Conclusion 123

6 TRANSIENT PROBLEMS **124**

6.1 Governing Equations 125
6.2 Differential Algebraic Equations and the Backward Euler Method . 128
6.2.1 Backward Euler method 129
6.3 Local Error Estimates, Convergence Test and Time Stepping 130
6.3.1 Local error estimates 130
6.3.2 Convergence test 134
6.3.3 Time stepping 135
6.4 Testing Convergence Criterion using a Fixed Time Step Method . . 137
6.4.1 Results and discussion 138
6.5 Comparison of Fixed and Variable Time Step Methods 147

6.5.1 Case one 147
6.5.1.1 Results 147
6.5.2 Case two 151
6.5.2.1 Results 151
6.5.3 Discussion 157
6.6 Conclusion 158

7 CONCLUSION **159**

List of Figures

1.1 Features of pressure and film thickness. 5

2.1 Fluid flow between two moving surfaces. 12
2.2 The representation of the lubricant film geometry. 15
2.3 Contact geometry of two surfaces and their reduced geometries. . . 16
2.4 Elastic deformation at a point (X, Y) due to pressure at (X_1, Y_1). . 26

3.1 Profile of the coefficient ϵ along the X axis. 41
3.2 Profile of viscosity $\overline{\eta}$ along the X axis. 42
3.3 Representation of domain for I-line relaxation. 44
3.4 Contact and non-contact regions of the computational domain. . . . 53
3.5 Amplification factor $\mu(\theta_1, \theta_2)$ for Gauss-Seidel line relaxation. 61

4.1 Restriction operator - Injection: $C_i = F_i$, $i = 1, \ldots, 4$. 69
4.2 Weighted restriction operator. 69
4.3 Prolongation operator - Linear Interpolation. 70
4.4 Structure of multigrid cycles. 72
4.5 Full-multigrid with one V cycle. 73
4.6 Structure of *Multigrid Driver* of the original FDMG multigrid software. 77
4.7 Structure of *Multigrid Driver* of the *Modified FDMG*. 81

5.1 Minimum and central film thicknesses for $L = 10$. 100
5.2 Minimum and central film thicknesses for $L = 14$. 101
5.3 Minimum and central film thicknesses for $L = 28$. 102
5.4 Pressure and film profiles for $L = 10$ along the X axis. 104
5.5 Pressure and film profiles for $L = 14$ along the X axis. 104

5.6 Pressure and film profiles for $L = 28$ along the X axis. 105
5.7 Minimum and central film thicknesses for $p_h = 0.72GPa$. 108
5.8 Minimum and central film thicknesses for $p_h = 1.05GPa$. 109
5.9 Minimum and central film thicknesses for $p_h = 1.21GPa$. 110
5.10 Pressure and film profiles for $p_h = 0.72\,GPa$ along the X axis. . . . 111
5.11 Pressure and film profiles for $p_h = 1.05\,GPa$ along the X axis. . . . 112
5.12 Pressure and film profiles for $p_h = 1.21\,GPa$ along the X axis. . . . 112
5.13 Film thickness contour: $p_h = 1.05\,GPa$ and $U = 0.468 \times 10^{-10}$. . . . 113
5.14 Pressure contour: $p_h = 1.05\,GPa$ and $U = 0.468 \times 10^{-10}$. 114
5.15 Pressure surface plot: $p_h = 1.05\,GPa$ and $U = 0.468 \times 10^{-10}$. 114
5.16 Film thickness contour: $p_h = 1.05\,GPa$ and $U = 1.87 \times 10^{-10}$. . . . 115
5.17 Pressure contour: $p_h = 1.05\,GPa$ and $U = 1.87 \times 10^{-10}$. 115
5.18 Pressure surface plot: $p_h = 1.05\,GPa$ and $U = 1.87 \times 10^{-10}$. 116
5.19 Minimum and central film thicknesses for $p_h = 0.72GPa$. 119
5.20 Minimum and central film thicknesses for $p_h = 1.23GPa$. 120
5.21 Minimum and central film thicknesses for $p_h = 1.95GPa$. 121
5.22 Pressure and film profiles for $p_h = 0.72GPa$ along the X axis. . . . 121
5.23 Pressure and film profiles for $p_h = 1.23GPa$ along the X axis. . . . 122
5.24 Pressure and film profiles for $p_h = 1.95GPa$ along the X axis. . . . 122

6.1 Pressure profiles along the X-axis (ConvergenceTest). 140
6.2 Pressure profiles along the X-axis (No ConvergenceTest). 140
6.3 Film thickness profiles along the X-axis (ConvergenceTest). 141
6.4 Film thickness profiles along the X-axis (No ConvergenceTest). . . 141
6.5 Pressure contour at time $t = 0$. 142
6.6 Pressure surface plot at time $t = 0$. 143
6.7 Pressure contour at time $t = 1.5$. 143
6.8 Pressure surface plot at time $t = 1.5$. 144
6.9 Pressure contour at time $t = 3.0$. 144
6.10 Pressure surface plot at time $t = 3.0$. 145
6.11 Film thickness contour at time $t = 0$. 145
6.12 Film thickness contour at time $t = 1.5$. 146

6.13 Film thickness contour at time $t = 3.0$. 146
6.14 Pressure profiles along the X-axis (65by65:Fixed TimeStep). 149
6.15 Pressure profiles along the X-axis (65by65:Variable TimeStep). . . . 149
6.16 Film thickness profiles along the X-axis (65by65:Fixed TimeStep). . 150
6.17 Film thickness profiles along the X-axis (65by65:Variable TimeStep). 150
6.18 Pressure profiles along the X-axis (129by129). 154
6.19 Film thickness profiles along the X-axis (129by129). 156
6.20 Graphical representation of fixed and variable step sizes. 157

List of Tables

3.1 Results obtained using the effective influence Newton method. . . . 56

3.2 Results obtained using the new relaxation scheme. 56

3.3 Results obtained using the Homotopy method. 57

3.4 Results obtained using the relaxation scheme of Ehret. 57

5.1 Input parameters for the problem in Case One. 91

5.2 NRS-S-Grid for M=20 & L=10. 93

5.3 NRS-M-Grid for M=20 & L=10. 94

5.4 H-S-Grid for M=20 & L=10. 94

5.5 Summary of Hcent and Hmin for M=20 & L=10. 95

5.6 Summary of Hcent and Hmin for M=20 & L=10 on different domains. 95

5.7 Input parameters for the problems in Case Two. 97

5.8 Summary of notation used in the Tables and Figures to follow. . . . 99

5.9 Minimum film thicknesses for $L = 10$, $U = 0.089 \times 10^{-10}$ and $G = 4869$. 99

5.10 Central film thicknesses for $L = 10$, $U = 0.089 \times 10^{-10}$ and $G = 4869$. 99

5.11 Minimum film thicknesses for $L = 14$, $U = 0.343 \times 10^{-10}$ and $G = 4869$. 100

5.12 Central film thicknesses for $L = 14$, $U = 0.343 \times 10^{-10}$ and $G = 4869$. 100

5.13 Minimum film thicknesses for $L = 28$, $U = 5.707 \times 10^{-10}$ and $G = 4869$. 101

5.14 Central film thicknesses for $L = 28$, $U = 5.707 \times 10^{-10}$ and $G = 4869$. 101

5.15 Input parameters for the problems in Case Three. 106

5.16 Summary of notation used in the Tables and Figures to follow. . . . 107

5.17 Minimum film thicknesses for $W = 0.7381 \times 10^{-6}$ and $p_h = 0.72GPa$. 107

5.18 Central film thicknesses for $W = 0.7381 \times 10^{-6}$ and $p_h = 0.72GPa$. 107

5.19 Minimum film thicknesses for $W = 2.273 \times 10^{-6}$ and $p_h = 1.05GPa$. 108

5.20 Central film thicknesses for $W = 2.273 \times 10^{-6}$ and $p_h = 1.05GPa$. . 109

5.21 Minimum film thicknesses for $W = 3.415 \times 10^{-6}$ and $p_h = 1.21GPa$. 110
5.22 Central film thicknesses for $W = 3.415 \times 10^{-6}$ and $p_h = 1.21GPa$. . 110
5.23 Input parameters for the problems in Case Four. 117
5.24 Summary of notation used in the Tables and Figures to follow. . . . 118
5.25 Minimum film thicknesses for $W = 0.664 \times 10^{-6}$ and $p_h = 0.72GPa$. 118
5.26 Central film thicknesses for $W = 0.664 \times 10^{-6}$ and $p_h = 0.72GPa$. . 118
5.27 Minimum film thicknesses for $W = 3.311 \times 10^{-6}$ and $p_h = 1.23GPa$. 119
5.28 Central film thicknesses for $W = 3.311 \times 10^{-6}$ and $p_h = 1.23GPa$. . 119
5.29 Minimum film thicknesses for $W = 13.22 \times 10^{-6}$ and $p_h = 1.95GPa$. 120
5.30 Central film thicknesses for $W = 13.22 \times 10^{-6}$ and $p_h = 1.95GPa$. . 120

6.1 Input parameters 137
6.2 Dimensionless parameters 138
6.3 Central and minimum film thicknesses (ConvergenceTest). 139
6.4 Central and minimum film thicknesses (No ConvergenceTest). . . . 139
6.5 Central and minimum film thicknesses (65by65:Fixed TimeStep). . 148
6.6 Central and minimum film thicknesses (65by65:Variable TimeStep). 148
6.7 Central and minimum film thicknesses (129by129:Fixed TimeStep). 151
6.8 Central and minimum film thicknesses (129by129:Variable TimeStep). 152

Chapter 1

INTRODUCTION

In 1966 [76] the word *tribology* was introduced and defined as the science and technology of interacting surfaces in relative motion and of the particles related thereto. This can be interprated as the lubrication, friction and wear of moving or stationary objects. A lubricant [30, 40, 43] is any substance that is used to reduce friction and wear of machine components. Besides this, it also provides smooth running and long life for the machine components. If a thin but continuous fluid film exists between machine components to prevent them from coming into contact then this is called *fluid film lubrication.* The applied load is carried by the pressure generated within the lubricant and the frictional characteristics arise purely from the shearing of the viscous lubricant. The two forms of lubrication regimes which fall into this category are *hydrodynamic* and *elasto-hydrodynamic* lubrication.

1.1 Hydrodynamic Lubrication

Hydrodynamic lubrication occurs when the lubricant film is sufficiently thick to prevent the opposing solids from coming into contact. Hence, wear will be nearly absent and the coefficient of friction will be small. Hydrodynamic lubrication is normally associated with conformal contacts. This is where there is a high degree

of geometrical conformity between the objects in contact. The behaviour of the contact is governed by the physical properties of the lubricant and the applied load. The applied load is carried by the pressure generated within the lubricant. This can be either due to the motion of the surfaces (squeeze film or sliding bearings) or externally motivated (externally pressurised bearing). The shearing of the viscous lubricant is responsible for the resistance to motion of the contacts. In hydrodynamic lubrication, the film thickness is normally greater than $1 \times 10^{-6}\, m$ and the magnitude of pressure developed is usually less than $5\, MPa$ which is not large enough to affect the geometry of the surfaces. Hence, the surfaces are rigid.

1.2 Elasto-Hydrodynamic Lubrication

Elasto-Hydrodynamic Lubrication (EHL) is a form of hydrodynamic lubrication where the elastic deformation of the contacts is no longer negligible and the pressure-viscosity effects are equally important. The magnitude of the generated pressure is typically between 0.5 and $4\, GPa$ and the minimum film thickness may be less than $0.1 \times 10^{-6}\, m$. Due to the high pressure, the lubricant exhibits piezoviscous properties. It is well known that for most lubricants [41], the viscosity increases rapidly with increasing pressure. Furthermore, the application of high contact loads can lead to substantial local deformation of the contacts, an effect which may drastically change the geometry of the lubricating film. Since the shape of the lubricant film in turn determines the pressure distribution, it is apparent that a solution to elasto-hydrodynamic lubrication problem must simultaneously satisfy the governing elastic and lubrication equations.

Elasto-hydrodynamic lubrication is normally associated with non-conformal contacts. This is where the surface contacts do not geometrically conform well to each other. Such contacts touch nominally along a line (line contact) or at a point (point contact). When studying elasto-hydrodynamic contacts, it is not necessary to consider the often rather complex geometry of the contacting elements. Since the film thickness and the contact width are generally small compared to the local radii of curvature of the running surfaces, the geometry of the surfaces in the contact

area can be accurately approximated locally by paraboloids. In general, two types of problems are distinguished, the one dimensional line contact problem and the more challenging two dimensional point contact problem considered here.

In a line contact problem, the contacting elements are assumed to be infinitely long in one of the principal directions. In an unloaded dry contact situation, the surfaces touch along a straight line whereas in a loaded situation, a strip-shaped contact is formed.

In a point contact problem, the contact width is very small in relation to the radii of curvature of the contacts. Thus, the contact width can be approximated by two parabolically shaped surfaces. This approximation allows a further simplification of the contact geometry into a reduced form which is between a single parabola with reduced radii of curvature and a flat surface. In an unloaded dry contact situation, that is in the absence of a lubricant, both surfaces nominally touch at a point whereas when a load is applied, the shape of the contact region depends on the ratio of the reduced radii of curvature in the X and Y directions. In general, the contact region is an ellipse and thus is called an elliptic contact. A special case of an elliptic contact is the circular contact which occurs when the reduced radii of curvature in both principal directions are equal.

1.3 EHL Review

One of the major developments in the field of tribology in the mid-twentieth century must be a recognition and understanding of elasto-hydrodynamic lubrication. It revealed the existence of a previously unsuspected regime of lubrication in highly stressed and non-conformal machine elements. Much of the early interest was based on hydrodynamic lubrication. The understanding of hydrodynamic lubrication began with the classical experiments of Tower (1885) [96] in which the existence of a film was detected from measurements of pressure within the lubricant. This was also the conclusion of Petrov (1883) [81] from his friction measurements. This work was closely followed by Reynolds' (1886) [86] celebrated analytical paper in which he used a reduced form of Navier-Stokes equation to generate a second-order differen-

tial equation, known as the Reynolds equation, for pressure in a narrow converging gap between the bearing surfaces. Besides presenting the differential equation for hydrodynamic lubrication, Reynolds also presented a comparison between his theoretical prediction and the experimental results of Tower [96].

Following Reynolds' theoretical contribution and the successful application of his theory to journal and thrust bearings, Martin (1916) [71] began looking at the more complicated problem of gear lubrication. Martin examined theoretically the operation of gears almost without wear as observed in practice and the suggestion that a hydrodynamic film separated the opposing teeth in gears. Martin considered two rigid circular cylinders and an incompressible, isoviscous lubricant. Martin's solution of the Reynolds equation for a lubricating film between two rigid circular cylinders presented a useful beginning to theoretical studies. The film thicknesses predicted from Martin's work were very small compared to the known surface irregularities of gear teeth and this concluded that gears could not be lubricated by hydrodynamic action. This discouraging result probably accounts for the long time interval of about 20 years before the next significant flurry of theoretical work on gear lubrication. Meldahl (1941) [72] considered the effect of local elastic distortion on the predictions of hydrodynamic theory. Although his work failed to demonstrate the full significance of elastic effects, he did point the way for future investigations.

A major development in the history of elasto-hydrodynamic lubrication was reported theoretically by Grubin (1949) [41] who gave an excellent account of the physical mechanism of elasto-hydrodynamic lubrication. Grubin successfully implemented the combined effects of high pressure on the lubricant and the solids forming the contact. By assuming that the shape of the elastically deformed solids in a highly loaded lubricated contact was the same as the shape produced in a dry contact, Grubin was able to examine the generation of pressure in the inlet region and to determine the required separation of the solids within the Hertzian [51] contact zone. The analysis allowed for the effect of pressure upon viscosity as proposed by Barus (1893) [6]. The most valuable result from this analysis was the film thickness equation for highly loaded elastic contacts. This equation predicted film thicknesses which were one or two orders of magnitude greater than Martin's

prediction for similar conditions and consistent with the formation of satisfactory fluid films in gear contacts. Besides the analysis of the inlet region, Grubin concluded that the pressure curve would exhibit a rather spectacular second maximum near the outlet end of the Hertzian zone.

The characteristics of an elasto-hydrodynamic contact predicted by Grubin were confirmed by Petrusevich (1951) [82] when he obtained solutions which simultaneously satisfied the governing elastic and hydrodynamic equations. The three main features of the solution are now recognised as general characteristics of highly loaded elasto-hydrodynamic lubrication contacts. These features, shown in figure (1.1), are as follows:

- An almost parallel oil film in the central region of the contact with a local restriction near the outlet.
- A near-Hertzian pressure curve over most of the contact region.
- A very local second pressure maximum of considerable height near the outlet end of the contact region.

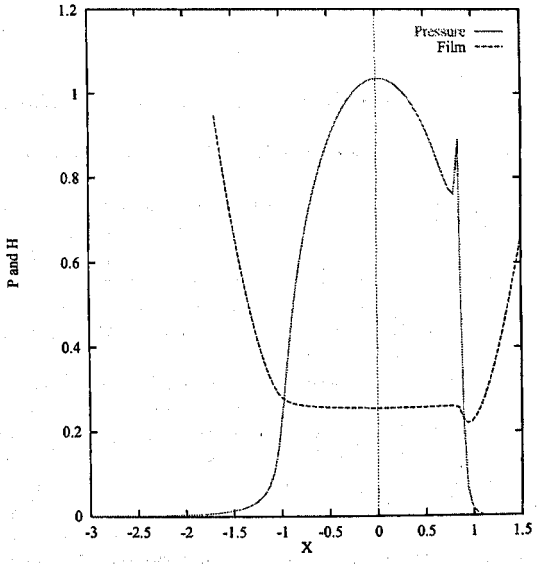

Figure 1.1: Features of pressure and film thickness.

Following the pioneering work of Petrusevich, several numerical solutions of isothermal elasto-hydrodynamic lubrication contact problems have been presented. Weber and Saalfeld (1954) [103] presented solutions which considered both

constant and pressure dependent viscosities but the solutions were limited to small deformations and could not distinguish between the near Hertzian solutions which occur in most real contacts.

A new approach to elasto-hydrodynamic lubrication theory was presented by Dowson and Higginson [29] (1959). By introducing the inverse method, Dowson and Higginson were able to solve elasto-hydrodynamic lubrication line contact problems. The close agreement between the theoretical minimum film thickness predictions and the experimental results obtained by Crook (1958) [27] and Sibley (1961) [93], demonstrated that the gap between theory and experiment had been largely closed. It was only in the 1970's that complete numerical solutions to isothermal elasto-hydrodynamic lubrication point contact problems began to emerge. Cheng (1970) [24] proposed a Grubin type inlet analysis for elliptical contacts. Hamrock and Dowson (1974) [44] presented an elasticity model in which the computational domain is divided into rectangles and a uniform pressure is assumed to act over each rectangle. They also presented extensive results on isothermal elasto-hydrodynamic lubrication point contact problems [45, 46, 47, 48]. In 1981 Evans and Snidle [35] employed the inverse method to solve highly loaded point contact problems.

Alternative methods began to emerge in the 80's. The first method to emerge was the Newton-Raphson method which was used by Okamura (1982) [79] and Houpert and Hamrock (1986) [54]. The Newton-Raphson method was mainly used to solve lightly loaded line contact problems. This was followed by the introduction of the multigrid method. Lubrecht [65] used the Gauss-Seidel scheme together with the multigrid method to accelerate convergence. Lubrecht was able to solve both line [67] and point [68] contact problems but still had difficulties in solving highly loaded problems due to numerical instabilities. Further reduction in computational times was achieved by Lubrecht and Ioannides [66] who made use of the multilevel multi-integration scheme [15, 16] to evaluate the elastic deformation. In 1989 Chang et al. developed an algorithm that combined the Newton-Raphson and the multigrid method to solve line contact problems.

A major contribution was made by Venner et al. in 1990 [101] when

they developed a relaxation scheme for solving lightly to highly loaded elasto-hydrodynamic line and point contact problems. They employed their relaxation scheme together with the multigrid method and the multilevel multi-integration method [15, 16]. The problem of instability was no longer an issue and highly loaded problems could now be solved routinely. Due to the pressure dependent viscosity, which varies by several orders of magnitude over the computational domain, the relaxation scheme they developed was based on the values of pressure. More recently, this relaxation scheme was also employed by Ehret (1996) [33]. Other new methods include that of Wang (1994) [102] who has developed a scheme based on the Newton method. A more recent method is the homotopy method [4] which is used by Scales [75] to solve elasto-hydrodynamic lubrication problems.

Over the past decade, the interest in elasto-hydrodynamic lubrication has moved on from steady-state problems to time-dependent (or transient) problems. Much of the earlier work on transient problems was based on the line contact problems [23, 21, 80, 100]. It is only over the last three to four years that the point contact problems have been considered [3, 2, 99] but this is still very limited. However, experimental work studying the effects of surface features using optical interferometry dates back to 1979 [104]. More recent experimental work includes that of Kaneta [58] and Kaneta et al.[59, 60].

1.4 Overview of Contents

The aim of this work is to present an efficient, robust and general purpose numerical solver for isothermal (Newtonian) steady-state and time-dependent (transient) elasto-hydrodynamic lubrication circular contact problems. The solver for elasto-hydrodynamic lubrication problems will be based on the FDMG Multigrid Software [92] and a new relaxation scheme which will be developed in this work. These problems are very important in engineering applications and by developing a general purpose multigrid solver, mainly for industrial applications, engineers will be able to solve a wide range of these problems under different operating conditions.

Having presented above an introduction to two regimes of lubrication and

an overview of the developments in elasto-hydrodynamic lubrication in Sections 1.1, 1.2 and 1.3, we will now present an outline of the contents of the rest of this thesis.

Chapter 2 will describe the mathematical model of isothermal (Newtonian) Elasto-Hydrodynamic Lubrication (EHL) circular contact problems. The model is highly non-linear consisting of coupled integro-differential equations. The governing equations of the model will also be presented in their dimensionless and discretised forms.

Chapter 3 will outline an overview of different iterative schemes used to date to solve elasto-hydrodynamic lubrication problems. This will include the inverse method and the direct iteration methods, namely the Gauss-Seidel and the Newton-Raphson methods. Also presented in this chapter will be the effective influence Newton method of Wang [102], the homotopy method which is used by Scales [75] and the relaxation schemes of Venner [97] and Ehret [33]. Based on the analysis of the governing Reynolds' equation of the elasto-hydrodynamic lubrication model, a new relaxation scheme for solving these problems will be presented in this chapter. In order to show the efficiency of the new relaxation scheme, a local Fourier analysis will also be presented. This chapter will be concluded with a test problem solved on a single grid using different numerical methods.

Chapter 4 will give a general description of the multigrid method together with an overview of its use in solving elasto-hydrodynamic lubrication problems. Also presented in this chapter will be a multigrid solver for elasto-hydrodynamic lubrication problems based on the FDMG Multigrid Software [92] and the new relaxation scheme of the previous chapter.

Chapter 5 will present test problems on steady-state elasto-hydrodynamic lubrication circular contact problems. The solutions obtained using the multigrid solver for elasto-hydrodynamic lubrication problems, developed in the previous chapter, will be compared with those obtained using other numerical methods which will include the relaxation schemes of Venner [101] and Ehret [33], the effective influence Newton method of Wang [102] and the homotopy method [4] used by Scales [75].

Chapter 6 will deal with time-dependent (or transient) problems based

on the backward Euler method and the governing equations will be presented as a system of differential algebraic equations. Also presented will be the local error estimates, convergence criterion and time stepping associated with these problems. The employed convergence criterion will be a novel concept when solving transient elasto-hydrodynamic lubrication problems. This new technique is used to solve differential algebraic equations and was originally developed by Shampine [90] for ordinary differential equations. This chapter will be concluded with test problems based on zero and reversal entrainments showing the effectiveness of the convergence criterion. A comparison will also be made between solutions obtained using fixed and variable time step methods.

Chapter 7 will draw this work to a close by making some conclusions regarding the effectiveness of the approach adopted in this thesis.

Chapter 2

GOVERNING EQUATIONS AND DISCRETISATION

This chapter describes the mathematical model of Elasto-Hydrodynamic Lubrication (EHL) [30, 40] employed in this work. This mathematical model [30, 97, 102], describing the isothermal (Newtonian) elasto-hydrodynamic lubrication circular contact problem, is made up of three equations and is highly non-linear, consisting of coupled integro-differential equations:

- The Reynolds equation, which relates the pressure in the lubricant film to the geometry of the gap and the velocities of the running surfaces.
- The film thickness equation, which defines the elastic distortion of the surfaces caused by the pressures in the film.
- The force balance equation, which makes sure that the integral over the pressure balances the externally applied load.

In addition, the variation of viscosity and density with pressure must also be taken into account due to the high pressures in the lubricant film. Hence, the relationships describing the variation of viscosity and density with pressure are also

presented. The equations in the model are non-dimensionalised using the Moes [73] and the Hertzian [51] parameters. For the sake of generality, the Hamrock-Dowson [47] dimensionless parameters are also presented, together with their relationship with the Moes parameters.

Since it is not possible to find exact analytic solutions of elasto-hydrodynamic lubrication problems, numerical methods must be employed in order to find approximate solutions using a discretisation scheme. The widely used finite difference discretisation method is employed in this work. This chapter is concluded by presenting the governing equations in their discretised form as a non-linear system of equations.

2.1 The Reynolds Equation

The differential equation governing the pressure distribution in fluid film lubrication is known as the Reynolds equation. This equation was derived by Reynolds in 1886 and it was presented in a paper [86] which contained not only the basic differential equation of fluid (incompressible) film lubrication but also a comparison between his theoretical prediction and the experimental results of Tower [96]. The Reynolds equation allows the pressure distribution in the domain to be obtained according to the kinematics and the geometry of the surfaces and is of the form

$$\frac{\partial}{\partial x}\left(\frac{\rho h^3}{\eta}\frac{\partial p}{\partial x}\right)+\frac{\partial}{\partial y}\left(\frac{\rho h^3}{\eta}\frac{\partial p}{\partial y}\right)=6u_s\frac{\partial(\rho h)}{\partial x}+6\rho h\frac{\partial u_s}{\partial x}+12\frac{\partial(\rho h)}{\partial t} \qquad (2.1)$$

where,

p is the pressure,

h is the film thickness,

η is the viscosity,

ρ is the density,

t is the time,

x and y are Cartesian coordinates

and $u_s = u_1 + u_2$ denotes the sum of the velocities of the running surfaces as shown in Figure (2.1).

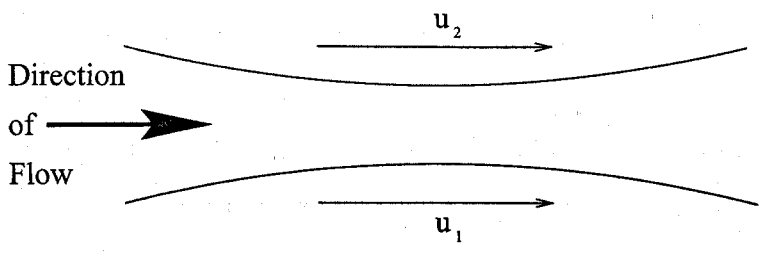

Figure 2.1: Fluid flow between two moving surfaces.

The two left hand side terms of equation (2.1) are the Poiseuille terms and they describe the net flow rates due to the pressure gradients in the lubricant film. The right hand side of equation (2.1) is made up of three terms and they represent three different effects that account for the pressure generation in the lubricant film. The first two terms are referred to as the Couette terms and they describe the net entraining flow rates due to the surface velocities. The Couette terms lead to two distinct effects: the *wedge* and the *stretch* effects. The wedge effect is extremely important and is the main device for pressure generation. The stretch effect considers the rate at which the surface velocity changes in the sliding direction. The third term on the right hand side of equation (2.1) represents the *squeeze* effect which, describes the net flow rates due to the squeezing motion.

In this work, both steady state and time dependent (transient) problems will be considered. The stretch effect will not be taken into account in either the steady state or the transient problems. However, when solving steady state problems, the contribution from the squeeze effect will be zero.

The boundary conditions for the Reynolds equation (2.1) are $p = 0$ sufficiently far upstream and on each side of the contact. In the outlet region, which is a free boundary, $p = \frac{\partial p}{\partial x} = 0$.

2.1.1 Viscosity

When studying elasto-hydrodynamic lubrication, one of the effects that can not be overlooked is the increase of viscosity with increasing pressure. One of the most widely used viscosity-pressure relations is the Barus equation [6], which is given by

$$\eta(p) = \eta_0 \, exp(\alpha \, p) \tag{2.2}$$

where, η_0 is the viscosity at ambient pressure, α is the pressure viscosity coefficient and p is the pressure.

Though equation (2.2) is a very simple relation, it is only accurate for low pressures. However, a more accurate viscosity-pressure relation is the Roelands equation [87] which is given by

$$\eta(p) = \eta_0 \, exp\left\{(ln(\eta_0) + 9.67)\left[-1 + \left(1 + \frac{p}{p_0}\right)^z\right]\right\} \tag{2.3}$$

where, η_0 is the viscosity at ambient pressure, p_0 is a constant equal to 1.98×10^8, z is a pressure viscosity parameter and p is the pressure.

If the pressure viscosity coefficient, α, is defined as

$$\alpha = \frac{1}{\eta_0}\left(\frac{\partial \eta}{\partial p}\right)_{p=0} \tag{2.4}$$

then, from equation (2.3), we get the following relationship

$$\frac{\alpha \, p_0}{z} = ln(\eta_0) + 9.67\,, \tag{2.5}$$

which relates z to α and η_0. When substituted into equation (2.3), equation (2.5) gives the following form of Roelands equation

$$\eta(p) = \eta_0 \, exp\left\{\frac{\alpha \, p_0}{z}\left[-1 + \left(1 + \frac{p}{p_0}\right)^z\right]\right\}. \tag{2.6}$$

Throughout this work, we have used equation (2.6) to represent the viscosity-pressure relationship. Although equation (2.5) defines a specific value of z based upon a study of typical mineral lubricating oil, it is better in general to consider z as an independent parameter. The typical value $z = 0.68$ has been used throughout this work unless stated otherwise.

2.1.2 Density

In the analysis of elasto-hydrodynamic lubrication, the compressibility of the fluid at high pressures can not be neglected. The change of density with pressure is given by the Dowson and Higginson relation [30]

$$\rho(p) = \rho_0\left(1 + \frac{5.8 \times 10^{-10} \, p}{1 + 1.7 \times 10^{-9} \, p}\right) \tag{2.7}$$

where, p is the pressure and ρ_0 is the density at ambient pressure. This was also obtained from experimental measurements on typical mineral oils.

2.1.3 Cavitation condition

Elasto-hydrodynamic lubrication is normally associated with non-conformal contacts where the surface contacts have non-conforming geometry as described in Chapter 1. Hence, elasto-hydrodynamic lubrication contacts are open systems with plenty of air in the surrounding area. This means that when the contact geometry is diverging, the film breaks up resulting in viscous fingering of the oil and the surrounding air fills in the space. This behaviour is commonly known as cavitation. In elasto-hydrodynamic lubrication, this occurs in the outlet region of the contact where the gap is widening. The Reynolds equation of our model is not designed to cope with this phenomenon. Hence, the Reynolds equation (2.1) of our model is not valid over the entire computational domain since cavitation is assumed to take place at some point in the outlet region where the gap is widening. In these regions, negative pressures are predicted by the Reynolds equation (2.1). In our model, this is overcome by imposing a cavitation boundary condition $p \geq 0$, which is a common practice [97]. Hence, at all points in the cavitation region, pressures are set to zero during the iteration process. In some sense, the outlet boundary of the pressurised region becomes a free boundary.

An alternative method of dealing with the cavitation condition is to employ the *penalty method* [106].

2.1.3.1 Penalty method

The penalty method for the analysis of the free boundary in elasto-hydrodynamic lubrication was introduced by Wu [106] who made use of the finite element method. Wu was also able to show that the pressure gradients in elasto-hydrodynamic lubrication problems are continuous even though there is a rapid change in the pressure near the outlet of the contact region. The basic idea when using the penalty method is to add on to the discrete Reynolds equation an extra term

$$\gamma p \tag{2.8}$$

whenever the pressure is negative. The parameter γ is a large positive constant which must be chosen in a heuristic way.

2.2 The Film Thickness Equation

When studying elasto-hydrodynamic contacts, it is not necessary to consider the often rather complex geometry of the contacting elements [40]. Since the size of the contact width is small compared to the local radii of curvature of the surfaces, the geometry of the curves, describing the undeformed surfaces close to and within the boundary region of pressure, can be accurately approximated locally by paraboloids. For a two dimensional elasto-hydrodynamic lubrication point contact, the lubricant film geometry is of the form shown in Figure (2.2).

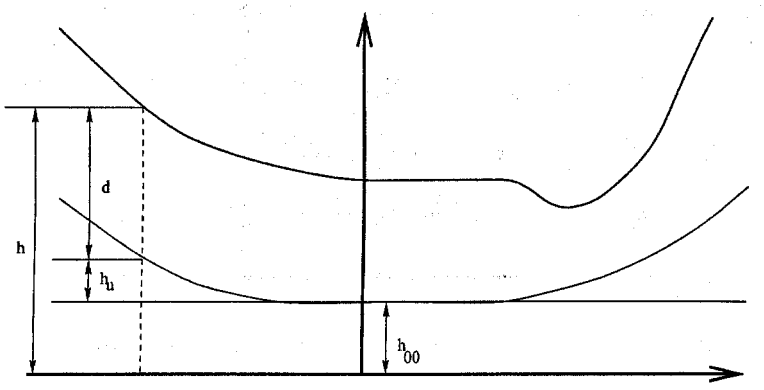

Figure 2.2: The representation of the lubricant film geometry.

The film thickness equation of such a point contact can be written as

$$h(x,y) = h_{00} + h_u(x,y) + d(x,y)\,, \tag{2.9}$$

where the three right hand terms can be described as follows:

The first term h_{00} is a constant representing the film thickness at the origin had the surfaces been undeformed.

The second term $h_u(x,y)$ represents the geometry of the undeformed surface. It is defined by paraboloids in both x and y directions and is given by

$$h_u(x,y) = \frac{x^2}{2R_x} + \frac{y^2}{2R_y} \tag{2.10}$$

where, R_x is the reduced radius of curvature in the x-direction,

$$R_x^{-1} = R_{1x}^{-1} + R_{2x}^{-1}\,,$$

R_y is the reduced radius of curvature in the y-direction,

$$R_y^{-1} = R_{1y}^{-1} + R_{2y}^{-1}\,.$$

The reduced radii of curvature, R_x, is shown in Figure (2.3) which shows the contact of two surfaces and their reduced geometries.

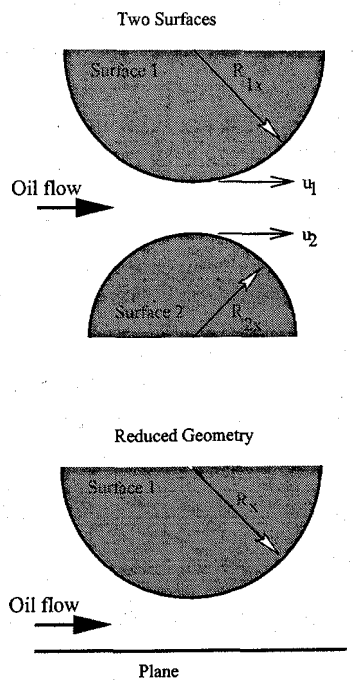

Figure 2.3: Contact geometry of two surfaces and their reduced geometries.

The third and the final term is $d(x,y)$ which represents the elastic deformation. The elastic deformation modifies the film geometry and hence plays a major part in the formation of lubrication films in elasto-hydrodynamic lubrication. By considering that the elastic deformations are small compared to the radius of curvature of the undeformed surfaces, we can assume that the surfaces in the contact are elastic semi-infinite. The material of the surfaces in contact are also assumed to be homogeneous (isotropic) and to obey linear elasticity theory. The elastic deformation $d(x,y)$ due to the pressures is obtained by summation of the deformation of the two surfaces and is given by

$$d(x,y) = \frac{2}{\pi E'} \int_{-\infty}^{\infty} \int_{-\infty}^{\infty} \frac{p(x',y')\,dx'\,dy'}{\sqrt{(x-x')^2 + (y-y')^2}} \tag{2.11}$$

where, E' is the reduced modulus of elasticity and is defined by

$$\frac{2}{E'} = \frac{1-v_1^2}{E_1} + \frac{1-v_2^2}{E_2} \tag{2.12}$$

where, E_1 and E_2 are the modulus of elasticities of the two surfaces in contact and v_1 and v_2 are the Poisson coefficients of the two surfaces in contact.

2.3 The Force Balance Equation

The applied contact load must be balanced by the pressures generated in the contact. Hence, the integral over the pressures in the lubricant must equal the applied load and is given by

$$\int_{-\infty}^{\infty}\int_{-\infty}^{\infty} p(x,y)\,dx\,dy \;=\; F \tag{2.13}$$

where F is the external load.

2.4 Non-Dimensionalisation

The governing equations of our mathematical model are non-dimensionalised using Hertz's theory [51] which gives the pressure profile, the geometry of the contact region and the elastic deformation of the surfaces in contact. This is for the case of a loaded contact between two parabolically shaped elastic bodies. For circular contact problems, the Hertzian pressure profile is given by

$$p(x,y) = \begin{cases} p_h\sqrt{1-(x/a)^2-(y/a)^2} & \text{if } x^2+y^2 < a^2 \\ 0 & \text{otherwise} \end{cases} \tag{2.14}$$

where, p_h is the maximum Hertzian pressure given by

$$p_h = \frac{3F}{2\pi\, a^2} \tag{2.15}$$

and a is the radius of the Hertzian contact circle given by

$$a = \left(\frac{3FR_x}{2E'}\right)^{\frac{1}{3}} \tag{2.16}$$

where, F is the external contact force, R_x is the reduced radius of curvature in the x-direction and E' is the reduced elastic modulus of the contacting bodies.

The dimensional Reynolds equation of a two dimensional time-dependent circular contact problem without the stretch effect is given by

$$\frac{\partial}{\partial x}\left(\frac{\rho h^3}{\eta}\frac{\partial p}{\partial x}\right) + \frac{\partial}{\partial y}\left(\frac{\rho h^3}{\eta}\frac{\partial p}{\partial y}\right) - 6u_s\frac{\partial(\rho h)}{\partial x} - 12\frac{\partial(\rho h)}{\partial t} = 0 \tag{2.17}$$

with $p = 0$ on the boundaries and $p \geq 0$ on the entire computational domain.

Equation (2.17) is made dimensionless using the following set of variables:

$$X = \frac{x}{a}, \qquad Y = \frac{y}{a}, \qquad P = \frac{p}{p_h}, \qquad H = \frac{h}{h_h},$$

$$\overline{\rho} = \frac{\rho}{\rho_0}, \qquad \overline{\eta} = \frac{\eta}{\eta_0} \qquad \text{and} \qquad T = \frac{t u_s}{2a}$$

where, p_h and a are as defined by equations (2.15) and (2.16) respectively and h_h is the maximum Hertzian deformation which is given by

$$h_h = \frac{a^2}{R_x}. \tag{2.18}$$

Hence, the dimensionless Reynolds equation is of the form

$$\frac{\partial}{\partial X}\left(\frac{\overline{\rho} H^3}{\overline{\eta}} \frac{\partial P}{\partial X}\right) + \frac{\partial}{\partial Y}\left(\frac{\overline{\rho} H^3}{\overline{\eta}} \frac{\partial P}{\partial Y}\right) - \lambda \frac{\partial (\overline{\rho} H)}{\partial X} - \lambda \frac{\partial (\overline{\rho} H)}{\partial T} = 0 \tag{2.19}$$

with $P = 0$ on the boundaries and $P \geq 0$ on the entire computational domain. The dimensionless parameter λ is given by

$$\lambda = \frac{6 \eta_0 u_s R_x^2}{a^3 p_h}. \tag{2.20}$$

The dimensionless viscosity $\overline{\eta}$ and density $\overline{\rho}$ are obtained from equations (2.6) and (2.7) respectively. The dimensional film thickness equation is of the form

$$h(x,y) = h_{00} + \frac{x^2}{2R_x} + \frac{y^2}{2R_y} + \frac{2}{\pi E'} \int_{-\infty}^{\infty} \int_{-\infty}^{\infty} \frac{p(x',y')\, dx'\, dy'}{\sqrt{(x-x')^2 + (y-y')^2}} \tag{2.21}$$

which can be written in non-dimensional form by substituting the dimensionless parameters used in non-dimensionalising the Reynolds equation (2.17). The resulting non-dimensional film thickness equation is of the form

$$H(X,Y) = H_{00} + \frac{X^2}{2} + \frac{Y^2}{2} + \frac{2}{\pi^2} \int_{-\infty}^{\infty} \int_{-\infty}^{\infty} \frac{P(X',Y')\, dX'\, dY'}{\sqrt{(X-X')^2 + (Y-Y')^2}}. \tag{2.22}$$

The dimensional force balance equation is given by

$$\int_{-\infty}^{\infty} \int_{-\infty}^{\infty} p(x,y)\, dx\, dy = F \tag{2.23}$$

which in non-dimensional form is

$$\int_{-\infty}^{\infty} \int_{-\infty}^{\infty} P(X,Y)\, dX\, dY = \frac{2\pi}{3}. \tag{2.24}$$

The minimum film thickness is

$$h_m = min(h(x,y)) \tag{2.25}$$

which in non-dimensional form is given by

$$H_m = min(H(X,Y)). \tag{2.26}$$

2.4.1 Moes and Hertzian dimensionless parameters

The above dimensionless analysis shows that if the lubricant is assumed to be compressible and if the Barus equation (2.2) is used to represent the viscosity pressure relationship, then the elasto-hydrodynamic lubrication model is characterised as a two parameter problem. All the solutions can be characterised in terms of $\overline{\alpha}$ and λ which are given by

$$\overline{\alpha} = \alpha p_h \tag{2.27}$$

and

$$\lambda = \frac{6\eta_0 u_s R_x^2}{a^3 p_h}. \tag{2.28}$$

These two parameters are related to the Moes [73] load parameter M and the materials parameter L as follows:

$$\overline{\alpha} = \frac{L}{\pi}\left(\frac{3M}{2}\right)^{1/3} \tag{2.29}$$

and

$$\lambda = \frac{4\pi}{M}\left(\frac{2}{3M}\right)^{1/3}. \tag{2.30}$$

The non-dimensional minimum film thickness, H_m, given by equation (2.26) is related to the Moes dimensionless minimum film thickness parameter, H_{min}, as follows

$$H_{min} = H_m\sqrt{\frac{6\pi}{\lambda}}. \tag{2.31}$$

Although all the numerical solutions obtained in this work are based on the Roelands equation (2.6) to represent the viscosity-pressure relationship, the above characterisation is still valid. However, besides the pressure viscosity coefficient α, either

the viscosity at ambient pressure η_0 or the pressure viscosity parameter z, which are parameters required in the Roelands equation (2.6), must also be given. For lubricants that are mineral oils, the parameters α and z do not vary too much. The pressure viscosity coefficient α is normally of the order 10^{-8} and the pressure viscosity parameter z normally lies in the range $0.5 \leq z \leq 0.8$. Unless stated otherwise, $z = 0.68$ is employed throughout this work.

2.4.2 Hamrock-Dowson's dimensionless parameters

Hamrock and Dowson [47] defined the following set of three dimensionless parameters to describe circular contact problems:

$$W = \frac{F}{E' R_x^2}, \tag{2.32}$$

$$G = \alpha E' \tag{2.33}$$

and

$$U = \frac{\eta_0 u_s}{2E' R_x} \tag{2.34}$$

where W, U and G are the load, material and speed parameters respectively. The Hamrock-Dowson's dimensionless minimum film thickness is defined as

$$H_m^{hd} = \frac{h_m}{R_x}. \tag{2.35}$$

2.4.3 Relationship between Moes and Hamrock-Dowson's parameters

The Moes parameters M and L can be expressed in terms of the Hamrock-Dowson's parameters W, G and U by taking U to be a free parameter. This relationship is of the form

$$M = W(2U)^{-3/4} \tag{2.36}$$

and

$$L = G(2U)^{1/4}. \tag{2.37}$$

The relationship between the Moes dimensionless film thickness, H_m, and the Hamrock-Dowson's minimum film thickness, H_m^{hd} is of the form

$$H_{min} = H_m^{hd}(2U)^{-1/2}. \tag{2.38}$$

Throughout this work, we have used either the Moes or the Hamrock-Dowson's dimensionless parameters. However, both forms will be presented on every occasion.

2.5 Discretisation

The use of mathematical models to simulate and analyse complicated systems in engineering and science reduces the need for expensive and time consuming experimental tests. The equations associated with the mathematical model take the form of differential and integral equations and in general it is not possible to find their exact analytic solutions. Hence, numerical methods must be employed in order to find their approximate solutions. This involves using methods such as finite difference, finite element, finite volume, spectral and boundary elements [55, 57, 85, 105] in order to find the numerical solutions of the governing equations. The basic idea in any numerical method is to discretise the continuous problem to obtain a discrete problem with many degrees of freedom often representing physical quantities at points in space.

To this date, the finite difference [55, 105] and finite element [57, 85] methods have been used to solve elasto-hydrodynamic lubrication problems with greater emphasis on the use of the finite difference approach perhaps due to its ease of coding.

The finite element method is a numerical technique for obtaining approximate solutions to a wide variety of boundary value problems. The main concept of this method is that the computational domain can be approximated by replacing it with discrete elements which can be arranged in a variety of ways and used to represent any complex shapes. The finite element discretisation reduces the problem to one of a finite number of unknowns by dividing the domain into spatial elements and then expressing the unknown field variables within each element in terms of spatial *basis functions*. The elements are inter-connected at a finite num-

ber of points called *nodes* or *nodal points.* These nodes normally lie on the element boundary where adjacent elements are connected. The interpolation functions are defined in terms of the field variables at each nodal point. For any element, the nodal values and their corresponding basis functions define the behaviour of the field variables within the element. Basis functions are normally chosen such that the field variables and their derivatives are continuous across adjoining element boundaries. Very few authors [94, 78] have used the finite element method to solve elasto-hydrodynamic lubrication problems. One important exception is that of Wu and Oden [107, 108] who have done extensive analysis in using the finite element method to solve elasto-hydrodynamic problems.

The main concept of finite difference schemes [55, 105] is to approximate the derivatives at a point by replacing the derivatives with linear combinations of discrete function values. The two most common finite difference operators are the forward and the backward difference [55] operators. These two operators are defined as follows:

Suppose a one dimensional computational domain is defined by

$$G = \{x \in \Re : x = x_j = jh_x,\ j = 0, 1, \ldots, n,\ h_x = 1/n\}$$

then the forward difference operator is given by

$$\Delta u_j = \frac{u_{j+1} - u_j}{h_x} \tag{2.39}$$

and the backward difference operator is given by

$$\nabla u_j = \frac{u_j - u_{j-1}}{h_x} \tag{2.40}$$

where, u_j is the function value at the point x_j and h_x is the mesh spacing.

2.6 Finite Difference Discretisation of Governing Equations

The governing equations (the Reynolds equation, the film thickness equation and the force balance equation) of a Newtonian steady state isothermal elasto-hydrodynamic

lubrication circular contact problem are discretised on a regular mesh over the computational domain

$$\{(X,Y) \in \Re^2 : X_a \leq X \leq X_b \ \ and \ \ -Y_a \leq Y \leq Y_a\}.$$

The governing equations are discretised with the direction of flow in the X-direction and mesh spacings h_x and h_y in the X and Y directions respectively. Due to symmetry, only half the domain is used in the Y-direction.

The dimensionless Reynolds equation (2.19), without the squeeze term, is of the form

$$\frac{\partial}{\partial X}\left(\epsilon\frac{\partial P}{\partial X}\right) + \frac{\partial}{\partial Y}\left(\epsilon\frac{\partial P}{\partial Y}\right) - \frac{\partial(\overline{\rho}H)}{\partial X} = 0 \tag{2.41}$$

which, when discretised at each non-boundary mesh point (i,j), $[(i-1)h_x+X_a, (j-1)h_y+Y_a]$, using the central and the first order backward difference scheme gives the equation

$$L_{i,j} = h_x^{-2}(\epsilon_{i-\frac{1}{2},j}(P_{i-1,j} - P_{i,j}) + \epsilon_{i+\frac{1}{2},j}(P_{i+1,j} - P_{i,j})) + h_y^{-2}(\epsilon_{i,j-\frac{1}{2}}(P_{i,j-1} - P_{i,j}) + \epsilon_{i,j+\frac{1}{2}}(P_{i,j+1} - P_{i,j})) - h_x^{-1}(\overline{\rho}_{i,j}H_{i,j} - \overline{\rho}_{i-1,j}H_{i-1,j}) = 0 \tag{2.42}$$

where, $\epsilon_{i+\frac{1}{2},j}$, $\epsilon_{i-\frac{1}{2},j}$, $\epsilon_{i,j+\frac{1}{2}}$ and $\epsilon_{i,j-\frac{1}{2}}$, $(i = 2,\ldots,m_x-1\ ;\ j = 2,\ldots,n_y-1)$, denote the values of $\epsilon = \frac{\overline{\rho}H^3}{\overline{\eta}\lambda}$ at the intermediate locations midway between the mesh points and m_x and n_y are the maximum number of points in X and Y directions respectively. As an example

$$\epsilon_{i-\frac{1}{2},j} = \frac{\epsilon_{i,j} + \epsilon_{i-1,j}}{2}$$

where,

$$\epsilon_{i,j} = \frac{\overline{\rho}(P_{i,j})\,H_{i,j}^3}{\overline{\eta}(P_{i,j})\,\lambda}. \tag{2.43}$$

Alternatively, a harmonic average [105] can be used, that is

$$\epsilon_{i-\frac{1}{2},j} = \frac{2\epsilon_{i,j}\epsilon_{i-1,j}}{\epsilon_{i-1,j} + \epsilon_{i,j}}.$$

As mentioned above, the density $\overline{\rho}$ is given by the Dowson and Higginson relation [30] which is given by

$$\overline{\rho}(P_{i,j}) = 1 + \frac{5.8\times10^{-10}\,p_h\,P_{i,j}}{1+1.7\times10^{-9}\,p_h\,P_{i,j}}, \tag{2.44}$$

the viscosity $\overline{\eta}$ is given by the Roelands equation [87] which is given by

$$\overline{\eta}(P_{i,j}) = exp\left\{\frac{\alpha\, p_0}{z}\left[-1+\left(1+\frac{p_h\, P_{i,j}}{p_0}\right)^z\right]\right\} \tag{2.45}$$

where $p_0 = 1.98 \times 10^8$ and $z = 0.68$ and

$$\lambda = \frac{4\,\pi}{M}\left(\frac{2}{3M}\right)^{1/3} = \frac{8\,\pi\, U}{W}\left(\frac{2}{3W}\right)^{1/3}.$$

The dimensionless film thickness equation (2.22)

$$H(X,Y) = H_{00} + \frac{X^2}{2} + \frac{Y^2}{2} + \frac{2}{\pi^2}\int_{-\infty}^{\infty}\int_{-\infty}^{\infty}\frac{P(X',Y')\,dX'\,dY'}{\sqrt{(X-X')^2+(Y-Y')^2}} \tag{2.46}$$

discretised at a point (i,j) is given by

$$H_{i,j} = H_{00} + \frac{X_{i,j}^2}{2} + \frac{Y_{i,j}^2}{2} + d_{i,j} \tag{2.47}$$

where, H_{00} is a constant and $d_{i,j}$ is the discretised elastic deformation of the material due to the pressures in the film. The discretisation of the elastic deformation will be explained in detail in Section 2.6.1.

Finally, the dimensionless force balance equation (2.24)

$$\int_{-\infty}^{\infty}\int_{-\infty}^{\infty} P(X,Y)\,dX\,dY = \frac{2\,\pi}{3} \tag{2.48}$$

in discretised form is given by

$$h_x\, h_y \sum_{i=1}^{m_x}\sum_{j=1}^{n_y} P_{i,j} - \frac{2\,\pi}{3} = 0 \tag{2.49}$$

where m_x and n_y are the maximum number of points in X and Y directions respectively.

When solving elasto-hydrodynamic lubrication problems, the force balance equation (2.49) is used to update the film thickness constant H_{00} in the following way:

$$H_{00} = H_{00} - c\left(\frac{2\,\pi}{3} - h_x\, h_y \sum_{i=1}^{m_x}\sum_{j=1}^{n_y} P_{i,j}\right) \tag{2.50}$$

where, c is a damping factor.

2.6.1 Elastic deformation

The elastic deformation at any point (X, Y) on a surface subjected to a pressure distribution is based on Boussinesq's solution [95]

$$d(X,Y) = \frac{2}{\pi^2} \int_{-\infty}^{\infty} \int_{-\infty}^{\infty} \frac{P(X',Y')\, dX'\, dY'}{\sqrt{(X-X')^2 + (Y-Y')^2}}. \tag{2.51}$$

There are two difficulties associated with equation (2.51). The first is the issue of singularity at the points $x = x'$ and $y = y'$. The second is the amount of work required in evaluating the numerical integral of equation (2.51). The amount of work required is an issue because when the elastic deformation is evaluated at any point, the entire computational domain must be integrated. This problem becomes more apparent when the numerical solution of elasto-hydrodynamic lubrication problem is obtained by means of an iterative scheme. Hence, the deformation at every node of the computational domain must be evaluated for each iteration and this can be very expensive computationally.

These two difficulties are overcome by approximating the pressure distribution using a polynomial function [28] which enables the deformation integral to be obtained analytically. Dowson and Hamrock [28] divided the pressure distribution into equidistant rectangular grids and assumed the pressure on each grid to be of a constant value and at the centre of the grid. A similar scheme is also employed by Chang [20] who divided the domain into non-equidistant rectangular grids. Like Dowson and Hamrock [28], Chang [20] assumed that the pressure is of a constant value but this value is the mean of the pressure values at the four corner points of the grid. For both these methods, rectangular blocks of uniform pressure are used to approximate the pressure distribution. Other schemes include that of Ranger et al. [84] who divided the contact area into non-equidistant rectangular grids and replaced the pressure by overlapping pressure pyramids where the pressure is assumed to be linear in both the X and Y directions and Biswas and Snidle [11] who proposed a scheme where a biquadratic polynomial is used to approximate the pressure for elements with singularity and the Simpson's rule is employed to approximate the pressure for elements without singularity. Other methods include that of Hou et al. [53], Jen et al. [56] and Liu et al. [69] who respectively employed

biquadratic polynomial, paraboloidal polynomial and elliptic paraboloid surface to approximate the pressure function.

The scheme devised by Dowson and Hamrock [28] is employed throughout this work and based on the observation that the elastic deformation at a point (X, Y), as shown in Figure (2.4), due to a uniform pressure P over the rectangular area $2a \times 2b$ is given by

$$d(X,Y) = \frac{2\,P}{\pi^2} \int_{-b}^{b} \int_{-a}^{a} \frac{dX_1\, dY_1}{\sqrt{(X - X_1)^2 + (Y - Y_1)^2}}. \tag{2.52}$$

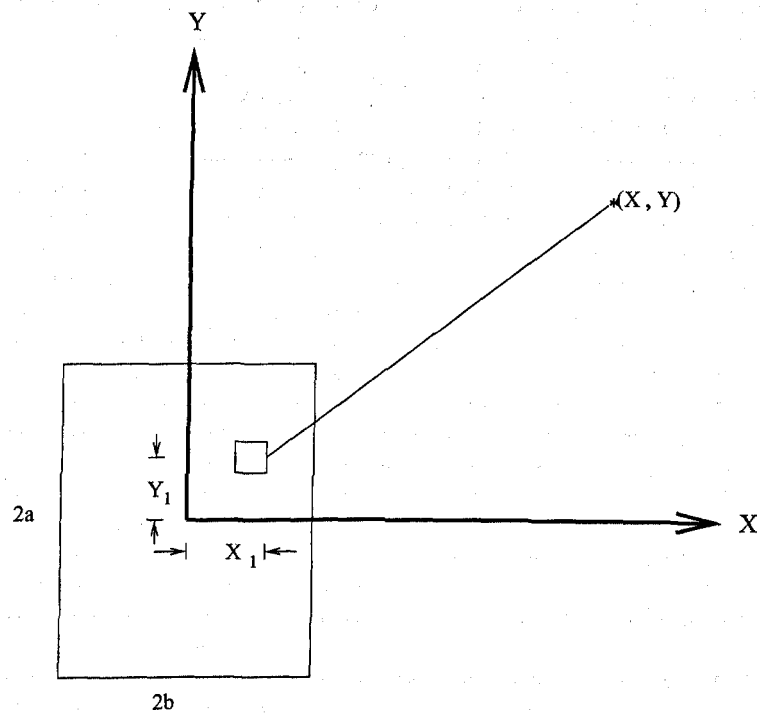

Figure 2.4: Elastic deformation at a point (X, Y) due to pressure at (X_1, Y_1).

If the entire computational domain is divided into equal rectangular areas, then from Dowson and Hamrock [28], the discretisation of the elastic deformation $d_{i,j}$ at a point (i, j) due to the contribution of all rectangular areas of uniform pressure is given by

$$d_{i,j} = \frac{2}{\pi^2} \sum_{k=1}^{m_x} \sum_{l=1}^{n_y} K_{i,k,j,l}\, P_{k,l} \tag{2.53}$$

where, m_x and n_y are the maximum number of mesh points in the X and Y direc-

tions respectively. The coefficient $K_{i,k,j,l}$ is given by

$$K_{i,k,j,l} = |X_p| \ln \left(\frac{Y_p + \sqrt{(X_p)^2 + (Y_p)^2}}{Y_q + \sqrt{(X_p)^2 + (Y_q)^2}} \right) + |Y_q| \ln \left(\frac{X_q + \sqrt{(Y_q)^2 + (X_q)^2}}{X_p + \sqrt{(Y_q)^2 + (X_p)^2}} \right) +$$

$$|X_q| \ln \left(\frac{Y_q + \sqrt{(X_q)^2 + (Y_q)^2}}{Y_p + \sqrt{(X_q)^2 + (Y_p)^2}} \right) + |Y_p| \ln \left(\frac{X_p + \sqrt{(Y_p)^2 + (X_p)^2}}{X_q + \sqrt{(Y_p)^2 + (X_q)^2}} \right) \qquad (2.54)$$

which can be rewritten as

$$K_{m,n} = |X_p| \ln \left(\frac{\frac{Y_p}{X_p} + \sqrt{1 + \left(\frac{Y_p}{X_p}\right)^2}}{\frac{Y_q}{X_p} + \sqrt{1 + \left(\frac{Y_q}{X_p}\right)^2}} \right) + |Y_q| \ln \left(\frac{\frac{X_q}{Y_q} + \sqrt{1 + \left(\frac{X_q}{Y_q}\right)^2}}{\frac{X_p}{Y_q} + \sqrt{1 + \left(\frac{X_p}{Y_q}\right)^2}} \right) +$$

$$|X_q| \ln \left(\frac{\frac{Y_q}{X_q} + \sqrt{1 + \left(\frac{Y_q}{X_q}\right)^2}}{\frac{Y_p}{X_q} + \sqrt{1 + \left(\frac{Y_p}{X_q}\right)^2}} \right) + |Y_p| \ln \left(\frac{\frac{X_p}{Y_p} + \sqrt{1 + \left(\frac{X_p}{Y_p}\right)^2}}{\frac{X_q}{Y_p} + \sqrt{1 + \left(\frac{X_q}{Y_p}\right)^2}} \right) \qquad (2.55)$$

where,

$$m = |i - k| + 1 \quad , \quad n = |j - l| + 1 \, ,$$

$$X_p = X_i - X_k + \tfrac{h}{2} \quad , \quad X_q = X_i - X_k - \tfrac{h}{2} \, ,$$

$$Y_p = Y_j - Y_l + \tfrac{h}{2} \quad \text{and} \quad Y_q = Y_j - Y_l - \tfrac{h}{2} \, .$$

One advantage of a regular mesh is that the $m_x \times n_y$ coefficients need only be calculated once and stored. In contrast, on an irregular mesh it is necessary to store the $m_x \times n_y$ coefficients for each mesh point. Hence, for a domain with $n \times n$ mesh points, the total storage cost for n^2 coefficients on regular and irregular meshes are respectively of the order n^2 and n^4. However, the complexity of evaluating the elastic deformation on the entire domain, for both regular and irregular meshes, using equation (2.53) is of the order n^4.

2.7 Conclusion

The mathematical model describing the isothermal steady state elasto-hydrodynamic lubrication circular contact problem is made up of three non-dimensional equations

with a pressure dependent density and viscosity. The three governing equations are the Reynolds equation

$$\frac{\partial}{\partial X}\left(\epsilon\frac{\partial P}{\partial X}\right)+\frac{\partial}{\partial Y}\left(\epsilon\frac{\partial P}{\partial Y}\right)-\frac{\partial(\overline{\rho}H)}{\partial X}=0 \tag{2.56}$$

where

$$\epsilon_{i,j}=\frac{\overline{\rho}(P_{i,j})\,H_{i,j}^{3}}{\overline{\eta}(P_{i,j})\,\lambda}, \tag{2.57}$$

the film thickness equation

$$H(X,Y)=H_{00}+\frac{X^2}{2}+\frac{Y^2}{2}+\frac{2}{\pi^2}\int_{-\infty}^{\infty}\int_{-\infty}^{\infty}\frac{P(X',Y')\,dX'\,dY'}{\sqrt{(X-X')^2+(Y-Y')^2}} \tag{2.58}$$

and the force balance equation

$$\int_{-\infty}^{\infty}\int_{-\infty}^{\infty}P(X,Y)\,dX\,dY=\frac{2\,\pi}{3}. \tag{2.59}$$

The density $\overline{\rho}$ is assumed to depend on the pressure according to the Dowson and Higginson relation

$$\overline{\rho}(P_{i,j})=1+\frac{5.8\times10^{-10}\,p_h\,P_{i,j}}{1+1.7\times10^{-9}\,p_h\,P_{i,j}} \tag{2.60}$$

and the viscosity $\overline{\eta}$ is given by the Roelands equation

$$\overline{\eta}(P_{i,j})=exp\left\{\frac{\alpha\,p_0}{z}\left[-1+\left(1+\frac{p_h\,P_{i,j}}{p_0}\right)^{z}\right]\right\} \tag{2.61}$$

where, $p_0=1.98\times10^8$ and $z=0.68$ unless stated otherwise..

The governing equations of the elasto-hydrodynamic lubrication model are highly non-linear consisting of a complex system of coupled integro-differential equations with a cavitation boundary condition $P\geq 0$. Hence, it is not possible to obtain solutions analytically and a numerical method must be employed. This can be achieved by discretising the governing equations at every point on the computational domain. Throughout this work, a finite difference discretisation scheme is employed on a rectangular computational domain. For a steady state isothermal elasto-hydrodynamic lubrication circular contact problem, the discretised equations employed in this work include the discretised Reynolds equation

$$\begin{aligned}L_{i,j}=h_x^{-2}(\epsilon_{i-\frac{1}{2},j}(P_{i-1,j}-P_{i,j})+\epsilon_{i+\frac{1}{2},j}(P_{i+1,j}-P_{i,j}))+h_y^{-2}(\epsilon_{i,j-\frac{1}{2}}(P_{i,j-1}-\\ P_{i,j})+\epsilon_{i,j+\frac{1}{2}}(P_{i,j+1}-P_{i,j}))-h_x^{-1}(\overline{\rho}_{i,j}H_{i,j}-\overline{\rho}_{i-1,j}H_{i-1,j})=0\,,\end{aligned} \tag{2.62}$$

the discretised film thickness equation

$$H_{i,j} = H_{00} + \frac{X_{i,j}^2}{2} + \frac{Y_{i,j}^2}{2} + \frac{2}{\pi^2} \sum_{k=1}^{m_x} \sum_{l=1}^{n_y} K_{i,k,j,l}\, P_{k,l} \tag{2.63}$$

where the kernel $K_{i,k,j,l}$ is given by equation (2.54) and the discretised force balance equation

$$h_x\, h_y \sum_{i=1}^{m_x} \sum_{j=1}^{n_y} P_{i,j} - \frac{2\,\pi}{3} = 0\,. \tag{2.64}$$

Having created a system of discretised equations representing all the grid points on the computational domain, it must now be solved using an iterative scheme. On a computational domain with $n \times n$ mesh points, the complexity of evaluating the elastic deformation at any mesh point on the computational domain is of the order n^2. Hence, the overall complexity of evaluating the elastic deformation at every point on the computational domain is of the order n^4. When discretising the Reynolds equation, this must be taken into account since the Couette term of the Reynolds equation involves the differential of the film thickness. This implies that for a large n, which is essential especially when solving highly loaded problems (the maximum Hertzian pressure p_h is large) found in practice, the computational costs can be very large. This means that obtaining solutions using iterative schemes is the only means of getting efficient solutions. The next chapter will describe different iterative schemes employed to date to solve elasto-hydrodynamic lubrication problems.

Chapter 3

SINGLE GRID ITERATIVE METHODS

Due to the extreme complexity of the equations associated with elasto-hydrodynamic lubrication problems, as outlined in the previous chapter, it is not possible to obtain their solutions analytically. Hence, numerical methods must be employed. Up to this date, various numerical methods have been used to solve elasto-hydrodynamic lubrication problems with greater emphasis on the use of single grid iterative methods [25, 36, 45, 84]. This chapter gives an overview of the different numerical schemes employed to solve elasto-hydrodynamic lubrication problems. This includes the *inverse method*, which was the earliest successful method employed by Dowson and Higginson [30] to obtain solutions to the elasto-hydrodynamic lubrication line contact problem, and the *direct iteration methods*, which includes the Gauss-Seidel and the Newton-Raphson methods [55, 105]. These methods were mainly used to solve line contact and lightly loaded problems due to the computational costs and numerical instabilities associated with point contact and highly loaded problems [97] found in practice. The point contact problems, which are two dimensional, are not easy to solve mainly due to the elastic deformation integral. However, new

methods are constantly being developed in order to solve these problems more efficiently and overcome the huge computational costs. These new methods include the *effective influence Newton method* [102] of Wang, the *homotopy method* [4] which is employed by Scales [75] and the *multigrid method* [13, 18, 105] which is used by [33, 64, 97]. The multigrid method greatly reduces the computational costs as is shown by Lubrecht [68]. The multigrid method increases the rate of convergence and problems which were previously unsolvable can now be solved routinely without any large computational costs.

Besides the issue of the computational costs, the issue of instability is an important entity when solving elasto-hydrodynamic lubrication problems. Most of the numerical schemes can not cope with heavily loaded point contact problems because the employed relaxation schemes can not deal with the heavy load due to the sensitivity of viscosity to pressure which may lead to instability [101]. This problem of instability can be looked into by analysing the governing equations of elasto-hydrodynamic lubrication problems and then developing a relaxation scheme that will be able to cope with a wide range of loads. Hence, an analysis of the coefficients of the Reynolds equation is presented in this chapter and based on this analysis a new relaxation scheme developed in this work is presented together with the relaxation schemes of Venner [97] and Ehret [33]. The relaxation schemes of Venner and Ehret are also developed from the analysis of the Reynolds equation of the elasto-hydrodynamic lubrication model. This chapter is concluded by presenting a test problem solved on a single grid using different numerical methods.

3.1 Iterative Methods

The mathematical model of Elasto-Hydrodynamic Lubrication (EHL) employed in this work as described in Chapter 2 consists of three equations: the Reynolds equation (2.19), the film thickness equation (2.22) and the force balance equation (2.24). The solution for the pressure (P) and the film thickness (H) must simultaneously satisfy the three equations. Besides this, all the pressures in the lubricant should be greater than or equal to zero. This is referred to as the *cavitation condition*

[30, 40] and is described in detail in Section (2.1.3) of Chapter 2. Since the model is highly non-linear and is made up of a complex system of integro-differential equations, numerical methods must be used to obtain solutions. However, the solution of elasto-hydrodynamic lubrication problems can be difficult to calculate due to numerical instability of the numerical schemes employed and computational intensity arising from the calculation of the elastic deformation integral. This is especially true for transient and highly loaded problems found in practice. Since the late 1960's, many researchers have been engaged in developing more effective numerical algorithms. The overall effectiveness of numerical algorithms for solving elasto-hydrodynamic lubrication problems can be evaluated based on numerical stability, accuracy, efficiency, robustness and programmability. These numerical algorithms can be classified into the following three categories:

- Inverse method: Dowson and Higginson [29], Evans and Snidle [35, 37] and Kweh [61].
- Direct-iteration methods: Hamrock and Dowson [45], Ranger [84], Evans and Snidle [36], Chittenden [25], Zhu and Chang [109] and Wang [102].
- *Multigrid method:* Ai [1], Cheng [22], Ehret [33], Lubrecht [68] and Venner [97].

The inverse method, the earliest method used, and the direct-iteration methods, which are the most straightforward methods for solving elasto-hydrodynamic lubrication problems will be considered in the next few sections. The two most common direct-iteration methods employed to solve these problems are the Gauss-Seidel and the Newton-Raphson schemes. The multigrid method, which was first employed to solve elasto-hydrodynamic lubrication problems in the late 1980's, will be covered in the next chapter.

3.1.1 Inverse method

This, the earliest successful method, was introduced by Ertel [34] and used by Dowson and Higginson [29] to obtain solutions of the elasto-hydrodynamic lubrication

line contact problem. Dowson and Higginson obtained solutions for a wide range of loads, speeds and material properties and derived a formula for predicting the minimum film thickness [30, 47] which is widely used up to this date. Following Dowson and Higginson's work, Evans and Snidle [35, 37] used the inverse method to solve point contact problems.

In the inverse method, the Reynolds equation of the elasto-hydrodynamic lubrication model is used to solve for the film profile, say $H1$, corresponding to a given pressure distribution, say P, that balances the applied load. $H1$ is then compared with the film profile, say $H2$, obtained by solving the elasticity equation with the given pressure distribution P. The differences between these two film profiles are then used to adjust the pressure profile, P. This sequence is repeated until the discrepancy between $H1$ and $H2$ is sufficiently small.

Although this method can produce a solution through a small number of pressure adjustments and can solve problems with relatively heavy loads, an accurate solution is difficult to obtain due to the relative insensitivity of the film profile to pressure variations [22]. Furthermore, since the procedure of pressure adjustments relies on experience, the algorithm can not be easily automated.

3.1.2 Gauss-Seidel method

A Gauss-Seidel scheme [55, 105] may be employed to solve for the pressure from the Reynolds equation of the elasto-hydrodynamic lubrication model. The idea is to treat the discretised Reynolds equation as a linear equation for pressures. The first step is to compute the film profile and the lubricant viscosity and density corresponding to a given pressure distribution. Then the linearised Reynolds equation is used to solve for the new pressure distribution. With the new pressure distribution, the film thickness constant is adjusted using the force balance equation as shown by equation (2.50). This is repeated until the pressure distribution and the film profile have reached a desired accuracy. This method has been used to obtain solutions to both point [25, 45, 109] and line [50] contact problems. It is easy to implement and use but it is unstable for highly loaded problems due to the sensitivity of viscosity to pressure [65, 97]. For the large number of mesh points required for point contact

problems, this scheme is expensive in terms of the computational time. However, it is not expensive in terms of the computational storage and the implementation of the cavitation condition is straightforward. For a system with n grid points, at least $O(n)$ relaxations are required to obtain a converged solution and the evaluation of the elastic deformation requires $O(n^2)$ operations [97]. Hence, the complexity of this scheme is at least $O(n^3)$.

3.1.3 Newton-Raphson method

The use of this method to solve elasto-hydrodynamic lubrication problems was first presented in a paper by Okamura [79]. Based on the algorithm presented by Okamura, Houpert and Hamrock [54] employed the Newton-Raphson method to solve a line contact problem.

Houpert and Hamrock [54] used the Newton-Raphson method to solve simultaneously the discretised forms of the Reynolds, film thickness (which includes the elasticity equation) and force balance equations. These discretised equations are linearised, which involves the computation of a full Jacobian matrix which is made up of the derivatives of all the discrete equations with respect to the variable pressure. When solving the elasto-hydrodynamic lubrication problems, a full Jacobian matrix is required because the elastic deformation at one point is determined by the pressure distribution over the entire grid. For a mesh of $m_x \times n_y$ points, this results in an often prohibitively large dense system of $m_x n_y$ equations. Hence, it is essential to seek computationally less expensive methods. Having obtained the Jacobian matrix, it is inverted and then used to obtain a new approximation to the solution. This process is repeated until the solution simultaneously satisfies the three governing equations.

Besides being expensive both in terms of the computational time and storage, especially for point contact problems, this method is not very efficient in dealing with the cavitation condition [65, 97]. Since the governing equations are solved simultaneously and the free boundary cavitation region is not known in advance, the implementation of the cavitation condition is not easy especially for point contact problems [68, 65, 97]. This is why this method is mainly used to solve

line contact problems [26, 64]. Due to the elastic deformation, the inversion of the full Jacobian matrix requires $O(n^3)$ operations and the overall complexity of the Newton-Raphson method is also $O(n^3)$ [65, 97] where n represents the number of mesh points in the X and Y directions. One big advantage of this method is that the convergence close to the solution is very rapid and it is achieved in only a few iterations [40, 97].

In general, the Newton-Raphson method can be described as follows: Suppose $\underline{\tilde{P}}$ is an approximation to the true solution $\underline{P}$, then at a point (i,j), $\tilde{L}_{i,j} = L(\tilde{P}_{i,j}) \neq 0$ and $L_{i,j} = L(P_{i,j}) = 0$. Taylor's theorem gives

$$L_{i,j} = \tilde{L}_{i,j} + \sum_{l=1}^{n_y} \sum_{k=1}^{m_x} \frac{\partial \tilde{L}_{i,j}}{\partial \tilde{P}_{k,l}} \Delta P_{k,l} + O((\Delta P)^2) \tag{3.1}$$

where, $\tilde{L}_{i,j}$ is the discretised Reynolds equation at the point (X_i, Y_j) and m_x and n_y are the number of mesh points in the X and Y directions respectively.

In recent years, modifications have been made to Newton's method in order to overcome some of the above difficulties. Nowadays, the system of equations is solved using Gaussian elimination or an iterative scheme. Gaussian elimination may be used in order to solve a system of linearised equations if the dimension of the coefficient matrix (Jacobian matrix) of the linear system is sufficiently small, e.g., in line contact problems. Chang et al. [22] reduced the complexity to $O(n^2)$ by ignoring most of the terms that reflect the relation between the film thickness and the pressure in the elastic deformation. This resulted in a tridiagonal Jacobian matrix instead of the original full matrix. Some other modified schemes have been presented by Oh [77], Houpert and Hamrock [54] and Wang [102]. One example of a more recent modified scheme is the *Effective Influence Newton Method* (EINM) of Wang [102].

3.1.3.1 Effective influence Newton method

The effective influence Newton method, developed by Wang [102] to solve elasto-hydrodynamic lubrication problems, uses a variant of Newton's method for solving non-linear equations. The method employs the notion of an effective influence region to determine the contribution from the elastic deformation in the solution

of a set of approximate linear equations used in the Newton formulation of elasto-hydrodynamic lubrication problems. The elastic deformation at a point (i,j) is, and must be, determined by the pressure distribution over the entire computational domain, though the contribution decreases radially outwards [102]. However, when obtaining the solution of the linearised Reynolds equation, Wang's Newton method ignores pressures not close to the point (i,j).

The elastic deformation at a point (i,j) due to a rectangular area of uniform pressure at some point k,l is strongly influenced by the distance between the two points, as can be seen from equation (2.54). This enables us to define an effective influence region such that only the pressures within this region are considered when solving the approximate linearised Reynolds equation and this results in a banded instead of a full Jacobian matrix. Thus, the number of elements and the computational costs involved in the elasto-hydrodynamic lubrication calculations are greatly reduced. The effective influence Newton method can be described as follows:

If (m_i) and (n_j) are the number of effective points from the point (i,j) in the X and Y directions respectively, then the effective influence Newton's formula is of the form

$$\sum_{l=j-n_j}^{j+n_j} \sum_{k=i-m_i}^{i+m_i} \frac{\partial \tilde{L}_{i,j}}{\partial \tilde{P}_{k,l}} \Delta P_{k,l} + \tilde{L}_{i,j} = 0 \,. \tag{3.2}$$

The simplest form of the effective influence Newton's method make use of five adjacent nodal points in linearising the original Reynolds equation. This is the method employed by Dowson and Wang [31] in solving elasto-hydrodynamic lubrication problems. The resulting equation is of the form

$$\frac{\partial \tilde{L}_{i,j}}{\partial \tilde{P}_{i-1,j}} \Delta P_{i-1,j} + \frac{\partial \tilde{L}_{i,j}}{\partial \tilde{P}_{i,j}} \Delta P_{i,j} + \frac{\partial \tilde{L}_{i,j}}{\partial \tilde{P}_{i+1,j}} \Delta P_{i+1,j} = -\tilde{L}_{i,j} - \frac{\partial \tilde{L}_{i,j}}{\partial \tilde{P}_{i,j-1}} \Delta P^{new}_{i,j-1} - \frac{\partial \tilde{L}_{i,j}}{\partial \tilde{P}_{i,j+1}} \Delta P^{old}_{i,j+1} \,. \tag{3.3}$$

For a constant j, equation (3.3) results in a tridiagonal system of equations which is solved simultaneously using I-line relaxation, provided that $\Delta P^{new}_{i,j-1}$ and $\Delta P^{old}_{i,j+1}$ are known. On every iteration the correction term $\Delta P_{i,j}$ is evaluated on the entire grid. Having obtained $\Delta \underline{P}$, a new approximation $\overline{P}$ to $\tilde{P}$ is computed at

every point on the entire grid using

$$\overline{P}_{i,j} = \tilde{P}_{i,j} - w\,\Delta P_{i,j} \tag{3.4}$$

where w is a damping factor.

After a complete sweep, the new values of pressure are used to recalculate the elastic deformation and the pressure dependent viscosity and density. Results obtained on a single grid using the effective influence Newton method will be presented at the end of this chapter in Section (3.3).

3.1.4 Homotopy method

The concept of a homotopy method is simple in that one problem is deformed into another by the continuous variation of a single parameter. This parameter maybe part of the problem specification and therefore have some physical significance, or it maybe artificial. The key point here is that one of the problems will be easy to solve, and this will be continuously deformed into one that is hard to solve. In practice, the deformation process must be discretised and a sequence of intermediate problems solved. However, by allowing the changes to be sufficiently small at each stage, it can always be arranged that the solution of one intermediate problem will lie within the domain of convergence of some locally convergent algorithm for the next. In this way, solving a series of locally convergent problems can provide a route to global convergence. This process is termed *continuation* [4].

Consider the problem of finding a root $\underline{q}^*$ of the non-linear equation system given by

$$\underline{F}(\underline{q}) = \underline{0}\,. \tag{3.5}$$

A homotopy function $\underline{S}(\underline{q}, \beta)$ is a function for which $\beta \in [0, 1]$ such that the following conditions hold:

$$\underline{S}(\underline{q}, 0) = \underline{Q}(\underline{q}) \quad \textit{and} \quad \underline{S}(\underline{q}, 1) = \underline{F}(\underline{q})\,. \tag{3.6}$$

The function $\underline{S}(\underline{q}, \beta)$ (assumed to be continuous though not necessarily differentiable with respect to β) represents a continuous deformation of $\underline{Q}(\underline{q})$ into $\underline{F}(\underline{q})$ as β varies

(not necessarily monotonically) from 0 to 1. If the problem of finding $\underline{q}_0$ satisfying

$$\underline{Q}(\underline{q}_0) = \underline{S}(\underline{q}_0, 0) = \underline{0} \tag{3.7}$$

is one that can be solved, and a continuous solution path exists connecting $(\underline{q}_0, 0)$ to $(\underline{q}^*, 1)$ along which $\underline{S}(\underline{q}, \beta) = \underline{0}$, then continuously tracking the solution path is a globally convergent method for solving the system (3.5) [4].

Artificially parametrised homotopy functions can be constructed in many ways, but those most usually encountered are convex linear homotopies of the form

$$\underline{S}(\underline{q}, \beta) = \beta \underline{F}(\underline{q}) + (1 - \beta)\underline{Q}(\underline{q}), \tag{3.8}$$

such as the fixed point homotopy

$$\underline{S}_f(\underline{q}, \beta) = \beta \underline{F}(\underline{q}) + (1 - \beta)(\underline{q} - \underline{q}_0) \tag{3.9}$$

where $\underline{q}_0$ can be viewed as an initial estimate of $\underline{q}^*$.

Consider the problem of finding a root of

$$\underline{S}(\underline{q}, \beta) = \underline{0} \tag{3.10}$$

for $\beta = 1$, where $\underline{q}$ represents the basic independent variables of the problem and one or more parameters a_i are defined in terms of β by (usually linear) relationships of the form $a_i = \varphi_i(\beta)$. The problem is assumed to have been easily solved for the root $\underline{q}_0$ corresponding to $\beta = 0$ (e.g. using a Newton-type method). The parametrised problem form is in the homotopy form but the dependence upon β is no longer necessarily linear.

An efficient homotopy technique for the robust, simultaneous solution of elasto-hydrodynamic lubrication point contact equations is one based upon physical parametrisation, using the pressure coefficient of viscosity α as the underlying parameter:

$$\alpha = \alpha_0 + \beta(\alpha^* - \alpha_0). \tag{3.11}$$

When $\beta = 0$, $\alpha = \alpha_0$ (typically 5×10^{-9}, representing a near isoviscous case) and when $\beta = 1$, $\alpha = \alpha^*$ (the desired value for the oil in question is typically 2×10^{-8} or more). Non-dimensionalisation of the governing equations is carried out

once and for all using the final value of p_h (maximum Hertzian pressure) which is computed from the final value of α. Viscosity and density are computed from the local continuation values of alpha and p_h. This enables the continuation process to be carried out without changing the size of the domain, but the intermediate problems do not correspond obviously to meaningful physical problems. The initial problem is easy to solve using a Newton type method, and working with α has the added advantage that the same mesh can be used throughout (the computational domain size does not have to change as it would were load used as a parameter, for example).

The kinds of numerical algorithm that can be used to solve this problem are surveyed in reference [4]. Points satisfying equation (3.10) map out a curve in $(\underline{q}, \beta)$-space, the zero curve, as β varies. The predictor-corrector algorithm starts from one point on this curve and takes a predictor step along the tangent there. The step size is adaptive, and the algorithm tries to maintain it as large as possible. The step direction is also chosen to make doubling back along the path impossible. A series of corrector steps is then taken with the intention of converging to a point further along the zero curve. Failing that, a new predictor with a reduced step size is undertaken. A purely locally convergent projected Newton method is used for the corrector steps. It should be noted that the Jacobian matrix is full and so a dense linear equation solver is used. To save on Jacobian evaluations, the Jacobian is only updated at points on the zero curve. In practice, the zero curve does not have to be tracked with high accuracy, since accumulation of discretisation errors such as occurs, for example, in the integration of ODE systems, does not arise here [4]. This algorithm allows the tracking of zero curves with rapid changes of arc length and non-monotonicity with respect to β. Such situations cause the failure of simple continuation techniques where the β values are explicitly prescribed and monotonic.

For methods such as that just outlined, cavitation is often perceived as difficult to handle because it is not possible to arbitrarily set components of the pressure to zero without compromising convergence by introducing discontinuities. Penalty functions [106] can be used to resolve the cavitation problem. The basic

idea is to add on to the discrete Reynolds equation a term

$$\psi(P) = \gamma P^2 \tag{3.12}$$

for some positive constant γ, wherever the pressure is negative. In this way, the equation can not be satisfied unless negative pressures are driven towards zero (squaring the pressure keeps the problem continuous in first derivatives). The larger γ is, the more this will be the case, but also the more sudden will be changes in curvature of the problem functions. For this reason we achieve greater robustness by deriving γ continually from the homotopy parameter according to

$$\gamma = \beta\gamma^* \tag{3.13}$$

where γ^* is the target value (typically 1000).

In order to be able to cater for the very hardest problems, the γ continuation is sometimes carried out as a separate phase following completion of the α continuation. For many problems, though, the two can be merged quite satisfactorily.

The homotopy method is very robust and can be used to solve both lightly and highly loaded point contact problems but at the expense of large computational times. However, the CPU times can be reduced by using iterative methods for the linear equation solution rather than the Gaussian elimination methods employed at this stage. This is an area of present research [89]. Solutions obtained using this method will be presented in Chapter 5 where they will be compared with those obtained using other methods.

3.2 Single Grid Relaxation Schemes

As described above, various numerical relaxation schemes have been used in order to solve elasto-hydrodynamic lubrication line and point contact problems, but these schemes are restrictive in one form or another. This includes the limitations in solving highly loaded point contact problems found in practice and the limitations in the use of a large number of mesh points due to large CPU times. In order to understand why these schemes may not be very robust or flexible, an analysis of

the governing equations of the elasto-hydrodynamic lubrication model described in Chapter 2 is necessary.

Consider the Reynolds equation (2.41) of a steady state elasto-hydrodynamic lubrication model. For convenience, this equation is of the form

$$\frac{\partial}{\partial X}\left(\epsilon\frac{\partial P}{\partial X}\right)+\frac{\partial}{\partial Y}\left(\epsilon\frac{\partial P}{\partial Y}\right)-\frac{\partial(\overline{\rho}H)}{\partial X}=0 \tag{3.14}$$

which is highly non-linear and the coefficient ϵ is given by

$$\epsilon=\frac{\overline{\rho}(P)H^3}{\overline{\eta}(P)\lambda}. \tag{3.15}$$

The coefficient ϵ varies several orders of magnitude over the computational domain as shown in Figure (3.1). In the contact region, the coefficient ϵ is extremely small, as small as 10^{-15} for highly loaded problems. In this region, the film thickness H is small, the viscosity $\overline{\eta}$ is large and lies in the range 10 to 10^{15} as shown in Figure (3.2) and the density $\overline{\rho}$ is greater than one. In the non-contact region (inlet and outlet regions), the coefficient $\epsilon >> 1$ and is of the order 10^4. In this region, the film thickness H is large and the viscosity $\overline{\eta}$ and the density $\overline{\rho}$ are close to one. In general, the minimum viscosity and density is one and this occurs when the pressure is zero.

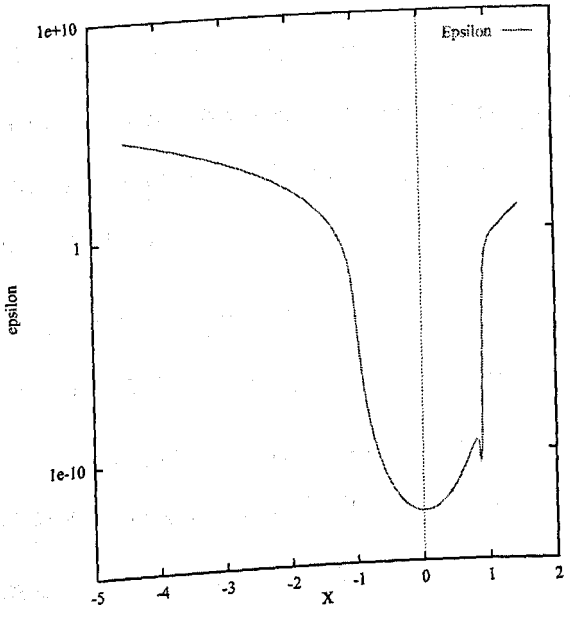

Figure 3.1: Profile of the coefficient ϵ along the X axis.

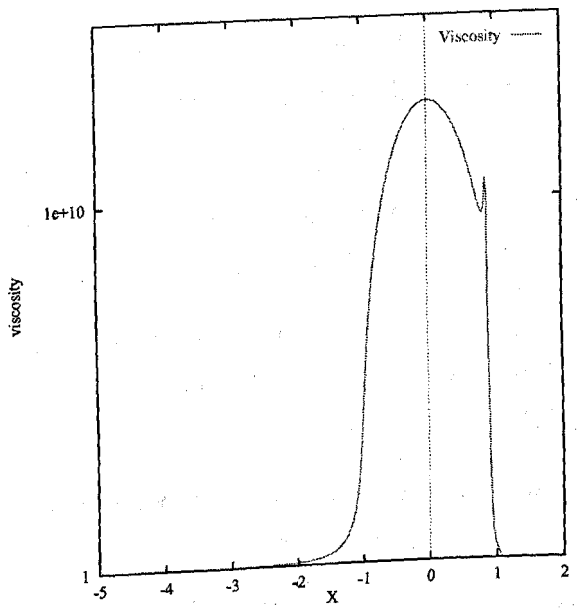

Figure 3.2: Profile of viscosity $\overline{\eta}$ along the X axis.

The coefficient ϵ can be summarised as follows: In both the inlet and the outlet regions of the computational domain, the coefficient $\epsilon >> 1$ whereas in the contact region, the coefficient ϵ is very close to zero.

When the coefficient ϵ is small, the Reynolds equation (3.14) described in Chapter 2 is approximated by the Couette term

$$\frac{\partial(\overline{\rho}\,H)}{\partial X} \approx 0 \tag{3.16}$$

which is a relation in the X-direction only. Consequently, when discretised, there is no direct coupling via pressure between adjacent grid points in the Y-direction.

When the coefficient ϵ is large, the Couette term $\frac{\partial(\overline{\rho}H)}{\partial X}$ in the Reynolds equation (3.14) is small compared to the remaining terms. Thus the Reynolds equation (3.14) has the form of a 2-d Poisson-type equation and is approximated by the Poiseuille terms

$$\frac{\partial}{\partial X}\left(\epsilon\frac{\partial P}{\partial X}\right) + \frac{\partial}{\partial Y}\left(\epsilon\frac{\partial P}{\partial Y}\right) \approx 0\,. \tag{3.17}$$

The above analysis of the Reynolds equation (3.14) gives an insight into the nature of this equation which depends very much on the coefficient ϵ. Due to the extreme values of the coefficient ϵ over the computational domain, the character of the problem changes. This means that whichever relaxation scheme is employed to

solve elasto-hydrodynamic lubrication problems, it must be able to cope with both large and small values of the coefficient ϵ. Hence, the coefficient ϵ plays an important role in deciding which relaxation process to employ in order to obtain the solution pressure P of the discretised Reynolds equation (2.42). The relaxation process employed must be a stable error smoother over the entire domain and must be able to cope with the extreme values of the coefficient ϵ which is highly non-linear and depends on pressure. The general approach taken in the relaxation schemes employed by Venner [97] and Ehret [33] and also in the new relaxation scheme developed in this work is to make the choice of the relaxation scheme dependent on the coefficient ϵ.

When the coefficient ϵ of the Reynolds equation (3.14) is large, (a Poisson-type problem), a *point Gauss-Seidel* [13, 55, 105] relaxation scheme provides good error smoothing and stability as is shown by Lubrecht [65] and Venner [97]. However, the performance of the point Gauss-Seidel relaxation scheme begins to deteriorate as the coefficient ϵ decreases [97]. Firstly the relaxation becomes unstable - low frequency error components are amplified and the relaxation process diverges. Secondly, due to the loss of coupling in the Y-direction, the relaxation becomes ineffective in reducing high frequency error components in the Y-direction [97].

From the above analysis of the Reynolds equation, the problem of instability can be overcome by using a relaxation scheme that can cope with the extreme values of the coefficient ϵ, which is smaller in the contact region than the non-contact region of the computational domain. The variation in the values of the coefficient ϵ is more evident in the highly loaded problems, which are normally not easy to solve as discussed above is Section 3.1. Hence, the problem of instability can be resolved by using different relaxation schemes in the different regions of the computational domain. This means that the relaxation schemes employed in the contact and non-contact regions of the computational domain must be different. This concept is employed by Venner [97], Ehret [33] and Nurgat and Berzins [74] in their respective relaxation schemes for solving elasto-hydrodynamic lubrication point contact problems. The relaxation schemes employed by Venner and Ehret and the new relaxation scheme employed by Nurgat and Berzins will be presented

later in this chapter.

The problem of loss of coupling can be overcome by making use of a *line relaxation scheme* [13, 55, 105] instead of a point relaxation scheme. This implies that instead of visiting the grid points one by one in some order, e.g. lexicographic order, and solving the discrete equation at each grid point, a system of discrete equations on a line of points is solved simultaneously. This must be done on a line which is in the direction of strong coupling.

For elasto-hydrodynamic lubrication point contact problems, there is strong coupling in the X-direction. Hence, a line relaxation scheme in the X-direction, commonly known as *I-Line relaxation* is employed as shown in Figure (3.3), that is on a line $Y = j$ $(j = 1, \ldots, n_y)$, where n_y is the maximum number of points in the Y-direction. However, due to symmetry, only half the domain is used as shown in Figure (3.3).

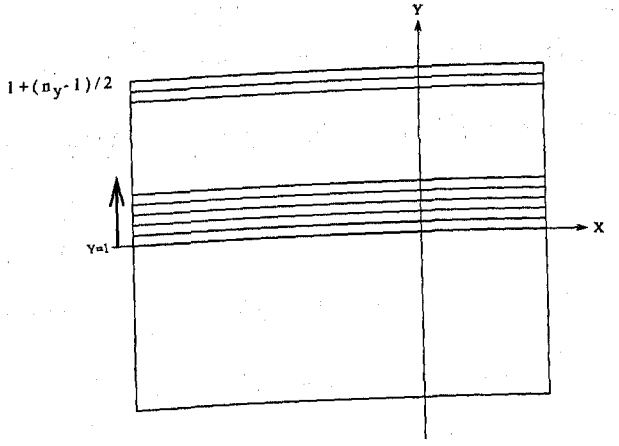

Figure 3.3: Representation of domain for I-line relaxation.

3.2.1 Relaxation schemes of Venner and Ehret

The relaxation schemes employed by both Venner [97] and Ehret [33] are very similar except for the order in which the pressures $\underline{P}$ and the film thicknesses $\underline{H}$ are calculated. Venner solves for the solutions pressure $\underline{P}$ and film thickness $\underline{H}$ simultaneously using the Reynolds and the film thickness equations. Ehret first solves for $\underline{P}$ using the Reynolds equation and then the new obtained pressures are used to update the film thickness $\underline{H}$. As mentioned in the previous section, they have

employed a relaxation scheme which depends on the coefficient ϵ of the Reynolds equation and different relaxation schemes are employed on the computational domain. The relaxation scheme employed by both Venner [97] and Ehret [33] make use of the point Gauss-Seidel relaxation, the Gauss-Seidel line relaxation and the Jacobi distributive line relaxation schemes depending on the value of pressure on the computational domain. In a standard Gauss-Seidel relaxation scheme, the new updated solution gets used immediately in relaxing subsequent equations whereas in a standard Jacobi relaxation, the new updated solution replaces the old one at the end of a complete sweep. The relaxation scheme of Venner and Ehret can be described as follows: The point Gauss-Seidel scheme is employed in the regions around the cavitation boundary whereas in the regions of the computational domain where the pressure is small, the Gauss-Seidel line relaxation scheme is employed. In the regions where the pressure is small, the coefficient ϵ of the Reynolds equation (3.14) is large and the Reynolds equation (3.14) is approximated by the Poiseuille terms (a Poisson-type problem). The Jacobi distributive line relaxation scheme is employed in the remaining parts of the domain where the pressure is large. Hence, the coefficient ϵ is small and the Reynolds equation (3.14) is approximated by the Couette term which is dominated by the elastic considerations.

3.2.1.1 Point Gauss-Seidel relaxation scheme

A point relaxation scheme implies visiting grid points one by one in some order, e.g. lexicographic order, and solving the discrete equation at each grid point on the computational domain. A point Gauss-Seidel relaxation scheme employed around the cavitation boundary region by Venner [97] and Ehret [33] can be described as follows: Given an approximation $\tilde{P}_{i,j}$ and the associated approximation $\tilde{H}_{i,j}$ to the pressure $P_{i,j}$ and the film thickness $H_{i,j}$ respectively at a point (i,j), a new pressure approximation $\overline{P}_{i,j}$ is computed using

$$\overline{P}_{i,j} = \tilde{P}_{i,j} + \left(\frac{\partial \tilde{L}_{i,j}}{\partial \tilde{P}_{i,j}}\right)^{-1} r_{i,j} \tag{3.18}$$

where, $\tilde{L}_{i,j} = L(\tilde{P}_{i,j})$ is given by equation (2.42), $\frac{\partial \tilde{L}_{i,j}}{\partial \tilde{P}_{i,j}}$ is given by

$$\frac{\partial \tilde{L}_{i,j}}{\partial \tilde{P}_{i,j}} = -h_{xy}^{-2}\left(\epsilon_{i-\frac{1}{2},j} + \epsilon_{i+\frac{1}{2},j} + \epsilon_{i,j-\frac{1}{2}} + \epsilon_{i,j+\frac{1}{2}}\right) - \frac{2}{\pi^2 h_{xy}}\left(\overline{\rho}_{i,j}K_{i,i,j,j} - \overline{\rho}_{i-1,j}K_{i-1,i,j,j}\right), \tag{3.19}$$

h_{xy} denotes the mesh spacings in the X and Y directions with $h_x = h_y$ and $r_{i,j}$, the residual at the point (i,j), is given by

$$r_{i,j} = h_{xy}^{-1}(\overline{\rho}_{i,j}\tilde{H}_{i,j} - \overline{\rho}_{i-1,j}\tilde{H}_{i-1,j}) - h_{xy}^{-2}\left(\epsilon_{i-\frac{1}{2},j}(\overline{P}_{i-1,j} - \tilde{P}_{i,j}) + \epsilon_{i+\frac{1}{2},j}(\tilde{P}_{i+1,j} - \tilde{P}_{i,j}) + \epsilon_{i,j-\frac{1}{2}}(\overline{P}_{i,j-1} - \tilde{P}_{i,j}) + \epsilon_{i,j+\frac{1}{2}}(\tilde{P}_{i,j+1} - \tilde{P}_{i,j})\right) + \delta H. \tag{3.20}$$

The correction term δH in equation (3.20) is approximated by

$$\delta H = \frac{2}{\pi^2 h_{xy}}\left(\overline{\rho}_{i,j}\sum_{k=i-1}^{i+1}\sum_{l=j-1}^{j+1}K_{i,k,j,l}\delta P_{k,l} - \overline{\rho}_{i-1,j}\sum_{k=i-2}^{i}\sum_{l=j-1}^{j+1}K_{i-1,k,j,l}\delta P_{k,l}\right) \tag{3.21}$$

where,

$$\delta P_{k,l} = \begin{cases} \overline{P}_{k,l} - \tilde{P}_{k,l} & \text{if } ((l<j) \text{ or } ((k<i) \text{ and } (l=j))) \\ 0 & \text{otherwise.} \end{cases} \tag{3.22}$$

In general, it is very expensive to update the film thickness at every point on the computational domain during the relaxation process due to the elastic deformation. However, an improved approximation of the film thickness , denoted by δH, is used when evaluating the residual $r_{i,j}$ as can be seen from equation (3.20). At any point (i,j), an improved approximation of the film thickness δH is computed using the correction terms δP which are close to the point (i,j) as shown in equation (3.21). Wang [102] has shown that it is not necessary to obtain the exact representation of the film thickness at a point (i,j) since the kernel K decreases with the distance $|i-k|$. After a complete sweep, the film thickness at any point on the computational domain where the point Gauss-Seidel relaxation scheme is employed is computed using the new solution pressure.

3.2.1.2 Gauss-Seidel line relaxation scheme

The Gauss-Seidel line relaxation scheme employed by Venner [97] in the regions of the computational domain where the values of pressure are small (the coefficient ϵ is

large) can be described as follows: Given an old and a new pressure approximation $\tilde{P}_{i,j}$ and $\overline{P}_{i,j}$ respectively to $P_{i,j}$, then the correction terms $\Delta P_{i,j}$ and the new film thickness $\overline{H}_{i,j}$ on the line $Y = j$ are solved simultaneously using a system of equations which involves two equations per grid point i and only points (i, j) where the coefficient ϵ is large are considered. The two equations at the grid point (i, j) are of the form

$$\overline{H}_{i,j} - \frac{2}{\pi^2} \sum_{k=1}^{n_x-1} K_{i,k,j,j} \Delta P_{k,j} = f_{i,j} + \tilde{w}_{i,j} \tag{3.23}$$

and

$$\begin{aligned} h_{xy}^{-2} \Big\{ & \epsilon_{i-\frac{1}{2},j} \left(\tilde{P}_{i-1,j} + \Delta P_{i-1,j} \right) + \epsilon_{i+\frac{1}{2},j} \left(\tilde{P}_{i+1,j} + \Delta P_{i+1,j} \right) + \\ & \epsilon_{i,j+\frac{1}{2}} \tilde{P}_{i,j+1} + \epsilon_{i,j-\frac{1}{2}} \overline{P}_{i,j-1} + \left(\epsilon_{i,j-\frac{1}{2}} + \epsilon_{i,j+\frac{1}{2}} + \epsilon_{i+\frac{1}{2},j} + \epsilon_{i-\frac{1}{2},j} \right) \\ & \left(\tilde{P}_{i,j} + \Delta P_{i,j} \right) \Big\} - h_{xy}^{-1} \left(\overline{\rho}_{i,j} \overline{H}_{i,j} - \overline{\rho}_{i-1,j} \overline{H}_{i-1,j} \right) = 0 \end{aligned} \tag{3.24}$$

where, $\tilde{w}_{i,j}$ denotes the discretised elastic deformation, $f_{i,j}$ denotes the right hand side and h_{xy} denotes the mesh spacings in the X and Y directions with $h_x = h_y$.

Having computed the correction terms $\Delta P_{i,j}$ and $\overline{H}_{i,j}$ on the line $Y = j$ and before moving on to the line $Y = j + 1$, the new pressure approximation $\overline{P}_{i,j}$ is computed using

$$\overline{P}_{i,j} = \tilde{P}_{i,j} + \Delta P_{i,j} \,. \tag{3.25}$$

An alternative Gauss-Seidel line relaxation scheme is employed by Ehret [33]. Instead of computing $\Delta \underline{P}$ and $\underline{\overline{H}}$ simultaneously, the correction terms $\Delta P_{i,j}$ on the line $Y = j$, but only at the grid points where the coefficient ϵ is large, are first computed using the following system of equations

$$a_{i-1,j} \, \Delta P_{i-1,j} + a_{i,j} \, \Delta P_{i,j} + a_{i+1,j} \, \Delta P_{i+1,j} = r_{i,j} \tag{3.26}$$

where,

$r_{i,j}$ is given by (3.20),

$a_{i-1,j} = \frac{1}{h_{xy}^2} \epsilon_{i-\frac{1}{2},j} + \frac{2}{\pi^2 h_{xy}} \overline{\rho}_{i-1,j} \, K_{i-1,i-1,j,j}$,

$a_{i,j} = -\frac{1}{h_{xy}^2} \left(\epsilon_{i-\frac{1}{2},j} + \epsilon_{i+\frac{1}{2},j} + \epsilon_{i,j-\frac{1}{2}} + \epsilon_{i,j+\frac{1}{2}} \right) - \frac{2}{\pi^2 h_{xy}} \overline{\rho}_{i,j} K_{i,i,j,j}$ and

$a_{i+1,j} = \frac{1}{h_{xy}^2}\epsilon_{i+\frac{1}{2},j}$.

On the line $Y = j$, equation (3.26) results in a tridiagonal system of equations which is solved simultaneously for the correction terms $\Delta P_{i,j}$. Having computed the correction terms $\Delta P_{i,j}$ on the line $Y = j$ and before moving on to the line $Y = j + 1$, the new pressure approximation $\overline{P}_{i,j}$ is computed using equation (3.25).

After a complete sweep, that is when all the lines $Y = j$ $(j = 1, \ldots, n_y)$ have been visited, the new pressure approximation $\underline{\overline{P}}$ obtained using the Gauss-Seidel line relaxation scheme is used to recalculate the new film thickness $\underline{\overline{H}}$.

3.2.1.3 Jacobi distributive line relaxation scheme

The distributive relaxation scheme was introduced by Brandt and Dinar [14] and was first employed by Lubrecht and Ioannides [66] to solve elasto-hydrodynamic lubrication problems. Lubrecht and Ioannides showed that the stability of elasto-hydrodynamic lubrication problems is improved if the employed relaxation scheme is based on the distribution of pressure variations. The distributive relaxation is a scheme where instead of changing the approximation at only one point, changes are also applied to one or more adjacent points.

The Jacobi distributive line relaxation scheme employed by Venner [97] and Ehret [33] works on the principle that the pressure at a point (i, j) depends on the variation of pressures in the neighbourhood of the point (i, j). This scheme is only employed in the regions of the computational domain where the pressure is large. Hence, the value of the coefficient ϵ is small and the solution is dominated by the Couette term of the Reynolds equation (3.14). The Jacobi distributive line relaxation employed by Venner [97] can be described as follows: Given an approximation $\tilde{P}_{i,j}$ and the associated approximation $\tilde{H}_{i,j}$ to the pressure $P_{i,j}$ and the film thickness $H_{i,j}$ respectively at a point (i, j), a new pressure approximation $\overline{P}_{i,j}$ is computed at the end of a complete sweep, that is after all the interior lines $Y = j$ $(j = 1, \ldots, n_y)$ have been visited, using

$$\overline{P}_{i,j} = \tilde{P}_{i,j} + \delta P_{i,j} \tag{3.27}$$

where,

$$\delta P_{i,j} = \Delta P_{i,j} - \frac{1}{4}(\Delta P_{i-1,j} + \Delta P_{i+1,j} + \Delta P_{i,j-1} + \Delta P_{i,j+1}) \,. \tag{3.28}$$

The correction terms $\Delta P_{i,j}$ and the new film thickness $\overline{H}_{i,j}$ on the line $Y = j$ are solved simultaneously using a system of equations that involves two equations per grid point (i,j) and only points where the coefficient ϵ is small are considered. The two equations per grid point (i,j) are of the form

$$\overline{H}_{i,j} - \frac{2}{\pi^2}\sum_{k=1}^{n_x-1} \Delta K_{i,k,j,j}\Delta P_{k,j} = f_{i,j} + \tilde{w}_{i,j} \tag{3.29}$$

and

$$\begin{aligned} h_{xy}^{-2} \Bigg\{ & \epsilon_{i-\frac{1}{2},j}\left(\tilde{P}_{i-1,j} - \frac{\Delta P_{i-2,j}}{4} + \Delta P_{i-1,j} - \frac{\Delta P_{i,j}}{4}\right) + \\ & \epsilon_{i+\frac{1}{2},j}\left(\tilde{P}_{i+1,j} - \frac{\Delta P_{i,j}}{4} + \Delta P_{i+1,j} - \frac{\Delta P_{i+2,j}}{4}\right) + \\ & \epsilon_{i,j+\frac{1}{2}}\left(\tilde{P}_{i,j+1} - \frac{\Delta P_{i,j}}{4}\right) + \epsilon_{i,j-\frac{1}{2}}\left(\tilde{P}_{i,j-1} - \frac{\Delta P_{i,j}}{4}\right) - \\ & \left(\epsilon_{i,j-\frac{1}{2}} + \epsilon_{i,j+\frac{1}{2}} + \epsilon_{i+\frac{1}{2},j} + \epsilon_{i-\frac{1}{2},j}\right)\left(\tilde{P}_{i,j} - \frac{\Delta P_{i-1,j}}{4} + \right. \\ & \left. \Delta P_{i,j} - \frac{\Delta P_{i+1,j}}{4}\right) \Bigg\} - h_{xy}^{-1}\left(\overline{\rho}_{i,j}\overline{H}_{i,j} - \overline{\rho}_{i-1,j}\overline{H}_{i-1,j}\right) = 0 \end{aligned} \tag{3.30}$$

where, $\tilde{w}_{i,j}$ denotes the discretised elastic deformation, $f_{i,j}$ denotes the right hand side, h_{xy} denotes the mesh spacings in the X and Y directions with $h_x = h_y$ and $\Delta K_{i,k,j,j} = \Delta K_{i,k,j,j} - \frac{1}{4}(\Delta K_{i,k-1,j,j} + \Delta K_{i,k+1,j,j} + \Delta K_{i,k,j,j-1} + \Delta K_{i,k,j,j+1})$.

Since $\Delta K_{i,k,j,j}$ decreases with increasing distance $|i-k|$ [97, 102], only the three largest terms of the summation in equation (3.29) are employed when computing $\Delta P_{i,j}$ and $\overline{H}_{i,j}$ using equations (3.29) and (3.30). These terms include $\Delta K_{i,i-1,j,j}$, $\Delta K_{i,i,j,j}$ and $\Delta K_{i,i+1,j,j}$. After a complete sweep, that is after all the interior lines ($j = 1\,,\, n_y$) have been visited, the new pressure approximation $\underline{\overline{P}}$ in the regions of the computational domain where the Jacobi distributive line relaxation scheme has been employed is obtained using the correction terms $\Delta\underline{P}$, which are applied distributively, as can be seen from equation (3.27).

An alternative Jacobi distributive line relaxation scheme is employed by Ehret [33]. As before, a new pressure approximated $\overline{P}_{i,j}$ at a point (i,j) is obtained

using equation (3.27). However, instead of computing $\Delta P_{i,j}$ and $\overline{H}_{i,j}$ simultaneously, the correction terms $\Delta P_{i,j}$ on the line $Y = j$, but only at the grid points where the coefficient ϵ is small, are first computed using the following system of equations

$$a_{i-2,j}\,\Delta P_{i-2,j} + a_{i-1,j}\,\Delta P_{i-1,j} + a_{i,j}\,\Delta P_{i,j} + a_{i+1,j}\,\Delta P_{i+1,j} + a_{i+2,j}\,\Delta P_{i+2,j} = r_{i,j} \tag{3.31}$$

where,

$\tilde{L}_{i,j} = L(\tilde{P}_{i,j})$ is given by equation (3.30) ,

$a_{i-2,j} = -\frac{1}{4\,h_{xy}^2}\,\epsilon_{i-\frac{1}{2},j} - \frac{2}{\pi^2\,h_{xy}}\,\Delta K_{i,i-2,j,j}$,

$a_{i-1,j} = \frac{1}{h_{xy}^2}\,\epsilon_{i-\frac{1}{2},j} + \frac{1}{4\,h_{xy}^2}\left(\epsilon_{i-\frac{1}{2},j} + \epsilon_{i+\frac{1}{2},j} + \epsilon_{i,j-\frac{1}{2}} + \epsilon_{i,j+\frac{1}{2}}\right) - \frac{2}{\pi^2\,h_{xy}}\,\Delta K_{i,i-1,j,j}$,

$a_{i,j} = \frac{-5}{4\,h_{xy}^2}\left(\epsilon_{i-\frac{1}{2},j} + \epsilon_{i+\frac{1}{2},j} + \epsilon_{i,j-\frac{1}{2}} + \epsilon_{i,j+\frac{1}{2}}\right) - \frac{2}{\pi^2\,h_{xy}}\,\Delta K_{i,i,j,j}$,

$a_{i+1,j} = \frac{1}{h_{xy}^2}\,\epsilon_{i+\frac{1}{2},j} + \frac{1}{4\,h_{xy}^2}\left(\epsilon_{i-\frac{1}{2},j} + \epsilon_{i+\frac{1}{2},j} + \epsilon_{i,j-\frac{1}{2}} + \epsilon_{i,j+\frac{1}{2}}\right) - \frac{2}{\pi^2\,h_{xy}}\,\Delta K_{i,i+1,j,j}$,

$a_{i+2,j} = -\frac{1}{4\,h_{xy}^2}\,\epsilon_{i+\frac{1}{2},j} - \frac{2}{\pi^2\,h_{xy}}\,\Delta K_{i,i+2,j,j}$,

$\Delta K_{i,k,j,l} = \overline{\rho}_{i,j}\,K_{i,k,j,l} - \overline{\rho}_{i-1,j}\,K_{i-1,k,j,l} - \frac{1}{4}\left((\overline{\rho}_{i,j}\,K_{i,k-1,j,l} - \overline{\rho}_{i-1,j}\,K_{i-1,k-1,j,l}) + (\overline{\rho}_{i,j}\,K_{i,k+1,j,l} - \overline{\rho}_{i-1,j}\,K_{i-1,k+1,j,l}) + (\overline{\rho}_{i,j}\,K_{i,k,j,l-1} - \overline{\rho}_{i-1,j}\,K_{i-1,k,j,l-1}) + (\overline{\rho}_{i,j}\,K_{i,k,j,l+1} - \overline{\rho}_{i-1,j}\,K_{i-1,k,j,l+1})\right)$

and $r_{i,j}$, the residual at the point (i,j), is given by equation (3.20).

After a complete sweep, that is when all the lines $Y = j$ $(j = 1, \ldots, n_y)$ have been visited, the new pressure approximation $\underline{\overline{P}}$ in the regions of the computational domain where the Jacobi distributive line relaxation scheme has been employed is obtained using equation (3.27). The new pressure approximation $\underline{\overline{P}}$ is then used to recalculate the new film thickness $\underline{\overline{H}}$.

3.2.2 A new relaxation scheme

A new relaxation scheme has been developed and employed in this work in order to solve elasto-hydrodynamic lubrication point contact problems. The main aim of this work is to derive a scheme that is simple and easy to understand and implement. It differs from the scheme of Venner in the sense that, though Venner's scheme has proved to be very effective, it is difficult to understand due to its complexity. Besides this, it is also quite difficult for others to implement because it has not been

described in its entirety [97]. The new relaxation scheme developed and employed in this work employs the same general philosophy used by Venner [97] and Ehret [33] in that either the Gauss-Seidel or the Jacobi line relaxation schemes are used in the different regions of the computational domain. The choice of the relaxation scheme depends very much on the coefficient ϵ of the Reynolds equation (3.14). The coefficient ϵ is very close to zero in the contact region whereas in the non-contact region of the computational domain the coefficient $\epsilon >> 1$. Hence, in this new relaxation scheme, the Jacobi and the Gauss-Seidel line relaxation schemes are respectively employed in the contact and non-contact regions of the computational domain. This new relaxation scheme can be described as follows:

The discretised Reynolds equation (2.42) of a steady state elasto-hydrodynamic lubrication point contact problem can be rewritten as

$$L_{i,j} = \epsilon_{i-\frac{1}{2},j}(P_{i-1,j} - P_{i,j}) + \epsilon_{i+\frac{1}{2},j}(P_{i+1,j} - P_{i,j}) + h_x^2 h_y^{-2}(\epsilon_{i,j-\frac{1}{2}}(P_{i,j-1} - P_{i,j}) + \epsilon_{i,j+\frac{1}{2}}(P_{i,j+1} - P_{i,j})) - h_x(\overline{\rho}_{i,j}H_{i,j} - \overline{\rho}_{i-1,j}H_{i-1,j}) = 0 \qquad (3.32)$$

where, $\epsilon_{i+\frac{1}{2},j}$, $\epsilon_{i-\frac{1}{2},j}$, $\epsilon_{i,j+\frac{1}{2}}$ and $\epsilon_{i,j-\frac{1}{2}}$, $(i = 2,\ldots,m_x-1\ ;\ j = 2,\ldots,n_y-1)$, denote the values of ϵ at the intermediate locations midway between the mesh points and h_x and h_y are mesh spacings in the X and Y directions respectively. The coefficient ϵ is given by equation (2.43) and the density $\overline{\rho}$ is given by equation (2.44).

The scope of the new relaxation scheme involves employing both the Gauss-Seidel and the Jacobi line relaxation schemes on the same grid, but without any overlap, depending on the position of the grid point (i,j) on the computational domain. The two relaxation schemes are employed as follows:

Given an approximation $\tilde{P}_{i,j}$ and the associated approximation $\tilde{H}_{i,j}$ to the pressure $P_{i,j}$ and the film thickness $H_{i,j}$ respectively, a new approximation $\overline{P}_{i,j}$ is computed using

$$\overline{P}_{i,j} = \tilde{P}_{i,j} + w\Delta P_{i,j} \qquad (3.33)$$

where w is a damping factor, which is critical to ensure convergence of the method.

On the line $Y = j$, the correction terms $\Delta P_{i,j}$ $(i = 1,\ldots,m_x)$ are solved simultaneously using a system of equations created at each grid point (i,j). Depending on the position of the grid point (i,j), either the Gauss-Seidel or the

Jacobi schemes are employed. If the grid point (i,j) lies in the non-contact region of the computational domain, then the Gauss-Seidel scheme is employed and the equation at this grid is given by

$$\frac{\partial \tilde{L}_{i,j}}{\partial \tilde{P}_{i-1,j}}\Delta P_{i-1,j} + \frac{\partial \tilde{L}_{i,j}}{\partial \tilde{P}_{i,j}}\Delta P_{i,j} + \frac{\partial \tilde{L}_{i,j}}{\partial \tilde{P}_{i+1,j}}\Delta P_{i+1,j} = r_{i,j} \tag{3.34}$$

where,

$\tilde{L}_{i,j} = L(\tilde{P}_{i,j})$ is given by equation (3.32) ,

$\frac{\partial \tilde{L}_{i,j}}{\partial \Delta P_{i-1,j}} = \epsilon_{i-\frac{1}{2},j} - \frac{2h_x}{\pi^2}\left(\overline{\rho}_{i,j}\, K_{i,i-1,j,j} - \overline{\rho}_{i-1,j}\, K_{i-1,i-1,j,j}\right)$,

$\frac{\partial \tilde{L}_{i,j}}{\partial \Delta P_{i,j}} = -(\epsilon_{i-\frac{1}{2},j} + \epsilon_{i+\frac{1}{2},j}) - \frac{h_x^2}{h_y^2}(\epsilon_{i,j-\frac{1}{2}} + \epsilon_{i,j+\frac{1}{2}}) - \frac{2h_x}{\pi^2}\left(\overline{\rho}_{i,j}\, K_{i,i,j,j} - \overline{\rho}_{i-1,j}\, K_{i-1,i,j,j}\right)$,

$\frac{\partial \tilde{L}_{i,j}}{\partial \Delta P_{i+1,j}} = \epsilon_{i+\frac{1}{2},j} - \frac{2h_x}{\pi^2}\left(\overline{\rho}_{i,j}\, K_{i,i+1,j,j} - \overline{\rho}_{i-1,j}\, K_{i-1,i+1,j,j}\right)$

and $r_{i,j}$, the residual at the point (i,j), is given by

$$\begin{aligned} r_{i,j} = {} & \epsilon_{i-\frac{1}{2},j}(\tilde{P}_{i-1,j} - \tilde{P}_{i,j}) + \epsilon_{i+\frac{1}{2},j}(\tilde{P}_{i+1,j} - \tilde{P}_{i,j}) + h_x^2\, h_y^{-2}(\epsilon_{i,j-\frac{1}{2}}(\overline{P}_{i,j-1} - \\ & \tilde{P}_{i,j}) + \epsilon_{i,j+\frac{1}{2}}(\tilde{P}_{i,j+1} - \tilde{P}_{i,j})) - h_x(\overline{\rho}_{i,j}\tilde{H}_{i,j} - \overline{\rho}_{i-1,j}\tilde{H}_{i-1,j})\,. \end{aligned} \tag{3.35}$$

However, if the grid point (i,j) lies in the contact region of the computational domain, then the Jacobi scheme is employed and the equation at this grid point is as given by equation (3.34) except for the residual $r_{i,j}$ which is now of the form

$$\begin{aligned} r_{i,j} = {} & \epsilon_{i-\frac{1}{2},j}(\tilde{P}_{i-1,j} - \tilde{P}_{i,j}) + \epsilon_{i+\frac{1}{2},j}(\tilde{P}_{i+1,j} - \tilde{P}_{i,j}) + h_x^2\, h_y^{-2}(\epsilon_{i,j-\frac{1}{2}}(\tilde{P}_{i,j-1} - \\ & \tilde{P}_{i,j}) + \epsilon_{i,j+\frac{1}{2}}(\tilde{P}_{i,j+1} - \tilde{P}_{i,j})) - h_x(\overline{\rho}_{i,j}\tilde{H}_{i,j} - \overline{\rho}_{i-1,j}\tilde{H}_{i-1,j})\,. \end{aligned} \tag{3.36}$$

For a constant j, that is on the line $Y = j$, equation (3.34) results in a tridiagonal system of equations which is solved simultaneously for the correction term $\Delta\underline{P}$. Having obtained $\Delta\underline{P}$ using I-Line relaxation on the line $Y = j$ and before moving on to the line $Y = j+1$, at every point on the line $Y = j$ which lies in the non-contact region, as shown in Figure (3.4), a new approximation $\overline{P}_{i,j}$ to $\tilde{P}_{i,j}$ is computed using equation (3.33) with the damping factor w lying in the range 0.3 to 0.9. Besides this, all the correction terms $\Delta\underline{P}$ in the contact region on the line $Y = j$ are saved in order to update the solution in the contact region after a complete sweep, that is after all the lines $Y = j$ $(j = 1, \ldots, n_y)$ have been visited.

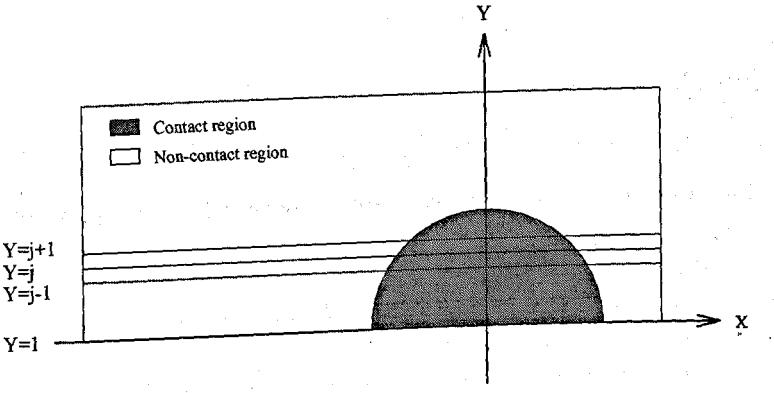

Figure 3.4: Contact and non-contact regions of the computational domain.

After all interior lines j ($j = 1, \ldots, n_y$) have been visited, that is after a complete sweep, a new approximation $\overline{P}_{i,j}$ to $\tilde{P}_{i,j}$ is computed on the entire grid at every point which lies only in the contact region of the computational domain. This new approximation $\overline{P}_{i,j}$ is computed using equation (3.33) but this time the damping factor w is chosen to be 0.1. Thus the saved values of the corrections $\Delta\underline{P}$ for the portions of each of the lines in the contact region of the computational domain, shown as shaded region in Figure (3.4), are added en-masse at the end of the iteration. Having updated all the pressure values on the entire grid, the elastic deformation and the pressure dependent viscosity and density at every point on the entire grid are recalculated using the new pressure values.

The choice of the damping factor w in the non-contact region of the computational domain is critical and depends very much on the load of the problem. For highly loaded problems, a value close to 0.3 is recommended, whereas for lightly loaded problems, any value in the range 0.3 to 0.8 is suitable but in order to achieve a faster rate of convergence, a value close to 0.8 is better. However, if the problem is highly loaded and a large damping factor close to 0.8 is used, then the solution will diverge.

3.2.3 Differences between Venner's relaxation scheme and the new relaxation scheme

Venner's relaxation scheme differs in many ways from the new relaxation scheme developed in this work. We will now describe the differences between these two

relaxation schemes.

Venner's relaxation scheme employs respectively the Jacobi distributive and the Gauss-Seidel line relaxation schemes in the contact and non-contact regions of the computational domain whereas the new relaxation scheme makes use of the Jacobi and the Gauss-Seidel line relaxation schemes in the contact and non-contact regions of the computational domain respectively. Besides this, Venner's relaxation scheme also makes use of the point Gauss-Seidel scheme in and around the cavitation region. In Venner's relaxation scheme, regions of the domain where the Jacobi distributive line relaxation scheme is employed, the correction terms at the points (i,j), $(i \pm 1, j)$ and $(i, j \pm 1)$ are used to update the solution at the point (i,j) as shown in equation (3.27) whereas in the remaining parts of the domain, where the Gauss-Seidel line relaxation and the point Gauss-Seidel schemes are employed, the method used to update the solution is similar to the one used in the new relaxation scheme. The solution, P, at a point (i,j) in the new relaxation scheme is updated using the correction term $\Delta P_{i,j}$ as shown in equation (3.33). The correction terms in the new relaxation scheme are obtained by solving a tridiagonal system of equations as can be seen from equation (3.34) whereas in Venner's relaxation scheme, regions of domain where the Jacobi distributive line relaxation scheme is employed, the system of equations is pentadiagonal as can be seen from equation (3.30). However, in the regions where the Gauss-Seidel line relaxation scheme is employed, a tridiagonal system of equations is used. In Venner's relaxation scheme, the film thickness equation gets updated during the relaxation process as can be seen from equations (3.23) and (3.29). This is not the case in the new relaxation scheme.

The main difference between the Venner's relaxation scheme and the new relaxation scheme is in the contact region of the computational domain. This is where the Jacobi distributive line relaxation scheme is employed by the Venner's relaxation scheme and the Jacobi line relaxation scheme is employed by the new relaxation scheme. The system of equations solved in order to obtain the correction terms and the way pressures are updated at a point (i,j) are also different in the two schemes as can be seen from equations (3.27) and (3.33).

3.3 Test Problem

This test problem, which appears in Wang [102], is solved on a domain $\{(X,Y) : -3.5 \leq X \leq 1.5, -2.0 \leq Y \leq 2.0\}$ using the Effective Influence Newton method (EINM) [102], the New Relaxation Scheme (NRS), the homotopy method used by Scales [75] and the relaxation scheme of Ehret [33], which is very similar to that of Venner, on a single 65×65 grid. However, due to symmetry, only the nodes in the positive Y-direction are employed when solving using the effective influence Newton method and the new relaxation scheme. For this highly loaded problem, the Hamrock and Dowson's dimensionless parameters with the speed parameter U fixed at 5.6102×10^{-11} are $W = 3.4125 \times 10^{-6}$ and $G = 4865$. The equivalent Moes dimensionless parameters are $M = 99$ and $L = 16$. This in turn gives $\lambda = 2.3975 \times 10^{-2}$. The pressure viscosity index $\alpha = 2.2056 \times 10^{-8}$ and the maximum Hertzian pressure, p_h, at this load is $1.21\,GPa$. Hence, the value of $\overline{\alpha} = \alpha \times p_h = 27$. The maximum Hertzian pressure p_h and the dimensionless parameter $\overline{\alpha}$ indicate the load of the problem and the higher their values, the higher the load.

3.3.1 Discussion

Tables (3.1), (3.2), (3.3) and (3.4) show respectively how the numerical solution obtained using the effective influence Newton method, the new relaxation scheme, the homotopy method used by Scales [75] and the relaxation scheme of Ehret [33] changes with the number of iterations, labelled Its. The results obtained using the homotopy method used by Scales and the relaxation scheme of Ehret were communicated to us. The central, labelled Hcent, and the minimum, labelled Hmin, film thicknesses obtained using the four schemes indicate that the new relaxation scheme and the relaxation scheme of Ehret are more efficient than the effective influence Newton method. The discrepancy in the minimum and central film thicknesses obtained using the four methods is very small. However, the values obtained by Scales [75] using the homotopy method as shown in Table (3.3) are somewhat different. The discrepancies in the values obtained using the other three methods as shown in Tables (3.1), (3.2) and (3.4) are negligible and comparing these values with

the homotopy method, the discrepancies are more apparent but still comparable. The reason for this is not very clear. The number of iterations carried out when using the effective influence Newton method is much higher than the other three methods. The homotopy method, which is very robust and powerful, has the least number of iterations but this is at the expense of large computational time.

Also shown in Tables (3.1), (3.2), (3.3) and (3.4) are the Root Mean Square Residuals, labelled RMSRES, which represents the L_2-norm, that is

$$RMSRES = \sqrt{\frac{1}{m_x n_y} \sum_{i=1}^{m_x} \sum_{j=1}^{n_y} RES_{i,j}^2} \tag{3.37}$$

where, m_x and n_y are respectively the maximum number of points in the X and Y directions and $RES_{i,j}$ is the residual at the point (i,j). In terms of efficiency, the new relaxation scheme and the relaxation scheme of Ehret are very comparable and there is very little to choose between the two methods. The homotopy method has the smallest root mean square residual compared to the other methods.

Its	Hcent	Hmin	RMSRES	ΔP_s
100	0.1230	0.0684	9.162E-3	4.785E-3
500	0.1829	0.1030	5.293E-3	4.352E-5
1000	0.1882	0.1052	2.529E-3	1.011E-5
1500	0.1897	0.1057	1.097E-3	3.513E-6
2000	0.1902	0.1058	4.588E-4	1.355E-6
2900	0.1905	0.1059	9.990E-5	2.447E-7

Table 3.1: Results obtained using the effective influence Newton method.

Its	Hcent	Hmin	RMSRES	ΔP_s
100	0.1795	0.0956	4.211E-3	3.181E-3
300	0.1903	0.1059	3.149E-4	8.986E-6
400	0.1905	0.1059	7.081E-5	2.129E-6
500	0.1906	0.1059	1.565E-5	4.659E-7
600	0.1906	0.1059	3.447E-6	1.022E-7
680	0.1906	0.1059	9.968E-7	2.952E-8

Table 3.2: Results obtained using the new relaxation scheme.

Its	Hcent	Hmin	RMSRES	ΔP_s
10	0.0882	0.0481	1.672E-3	7.600E-6
15	0.0895	0.0486	1.662E-3	1.268E-3
30	0.1442	0.0746	1.111E-3	4.364E-3
40	0.1723	0.0912	6.355E-4	4.319E-3
50	0.1968	0.1087	1.155E-4	4.496E-3
53	0.2020	0.1124	2.535E-7	7.327E-4
54	0.2020	0.1124	1.701E-9	1.099E-5

Table 3.3: Results obtained using the Homotopy method.

Its	Hcent	Hmin	RMSRES
50	0.1836	0.1043	2.425E-1
300	0.1896	0.1060	1.538E-4
400	0.1896	0.1060	8.036E-6
500	0.1896	0.1060	4.299E-7
600	0.1896	0.1060	3.269E-8

Table 3.4: Results obtained using the relaxation scheme of Ehret.

The last columns, labelled ΔP_s where the subscript s indicates that it is on a single grid, in Tables (3.1) (3.2) and (3.3) show the changes in the solution pressure from one iteration to the next and it is computed using

$$\Delta P_s = \frac{\sum_{i=1}^{m_x}\sum_{j=1}^{n_y}\left|P_{i,j}^{k} - P_{i,j}^{k-1}\right|}{\sum_{i=1}^{m_x}\sum_{j=1}^{n_y} P_{i,j}^{k}} \tag{3.38}$$

where k indicates the k^{th} iteration. Though the change in the solution, ΔP_s, is commonly used [102] as a means for testing the accuracy and convergence criterion, it is really not a good practice since it can be misleading as it only indicates the change in the solution pressure at each iteration. It is possible to get very small changes and the solution might be diverging from the true solution.

3.4 Smoothing Analysis

The convergence behaviour of any numerical solver depends strongly on the relaxation scheme being employed. The employed relaxation scheme must have a good smoothing property. However, the convergence behaviour in itself does not say anything about the actual smoothing efficiency. The smoothing efficiency can be analysed using a local mode Fourier analysis [12, 105].

In order to analyse the new relaxation scheme described above in Section 3.2.2 for solving elasto-hydrodynamic lubrication problems, we need to consider the Reynolds equation (2.41) of Chapter 2. For convenience, it is of the form

$$\frac{\partial}{\partial X}\left(\epsilon\frac{\partial P}{\partial X}\right)+\frac{\partial}{\partial Y}\left(\epsilon\frac{\partial P}{\partial Y}\right)-\frac{\partial(\overline{\rho}H)}{\partial X}=0 \tag{3.39}$$

where, the first two terms are the Poiseuille terms and the third term is the Couette term. As described above in Section 3.2, the coefficient ϵ of the Reynolds equation (3.39) varies several orders of magnitude over the computational domain. In the contact region, ϵ is very close to zero whereas in both the inlet and outlet regions of the computational domain, $\epsilon >> 1$. When ϵ is very close to zero (contact region), the Reynolds equation (3.39) is approximated by the Couette term, that is

$$\frac{\partial(\overline{\rho}H)}{\partial X}\approx 0 \tag{3.40}$$

and when $\epsilon >> 1$ (remaining parts of the domain), the Couette term $\frac{\partial(\overline{\rho}H)}{\partial X}$ is small and the Reynolds equation (3.39) is approximated by the Poiseuille terms, that is

$$\frac{\partial}{\partial X}\left(\epsilon\frac{\partial P}{\partial X}\right)+\frac{\partial}{\partial Y}\left(\epsilon\frac{\partial P}{\partial Y}\right)\approx 0\,. \tag{3.41}$$

In order to carry out a local Fourier analysis of the new relaxation scheme, which depends on the coefficient ϵ, the two approximations of the Reynolds equation (3.39), that is equations (3.40) and (3.41), must be considered. The new relaxation scheme uses the Jacobi and Gauss-Seidel line relaxation schemes on the same grid depending on the value of ϵ. The Jacobi and Gauss-Seidel line relaxation schemes are respectively employed in the contact and non-contact regions of the computational domain. This means that the Jacobi line relaxation scheme is employed to solve equation (3.40) and the Gauss-Seidel line relaxation scheme is

employed to solve equation (3.41). Due to the complexity of equation (3.40), we will only consider the local Fourier analysis of the new relaxation scheme using equation (3.41).

3.4.1 Fourier analysis of the Poiseuille terms

Consider the simpler case of when $\epsilon >> 1$. Assuming that ϵ is constant, then equation (3.41) can be rewritten as

$$\frac{\partial^2 P(X,Y)}{\partial X^2} + \frac{\partial^2 P(X,Y)}{\partial Y^2} = F(X,Y) \tag{3.42}$$

which, as described in Chapter 2, is discretised using central differencing at each non-boundary mesh point (l,m), $((l-1)h_{xy} + X_a, (m-1)h_{xy} + Y_a)$ where $X, Y \in [X_a, X_b] \times [Y_a, Y_b]$ and h_{xy} is the grid mesh spacing in the X and Y directions. Equation (3.42) in discretised form can be written as

$$h_{xy}^{-2}(P_{l-1,m} + P_{l+1,m} + P_{l,m+1} + P_{l,m-1} - 4P_{l,m}) = F_{l,m} \tag{3.43}$$

where h_{xy} is the grid mesh spacing in the X and Y directions.

In the new relaxation scheme, when $\epsilon >> 1$, the Reynolds equation (3.39), when discretised, is approximated by equation (3.43) which is solved using the Gauss-Seidel line relaxation scheme. In a line relaxation scheme, instead of scanning the grid points one by one in some order, e.g. lexicographic order, and solving the discrete equation at each grid point, a system of discrete equations on a line of points are solved simultaneously. This is normally done in the direction of strong coupling. Hence, for elasto-hydrodynamic lubrication problems, I-Line relaxation scheme is employed and all the points (l,m) on the horizontal line $Y = m$ are considered.

If $\underline{\tilde{P}}$ is an approximation to $\underline{P}$, then the new approximation $\underline{\overline{P}}$ must simultaneously satisfy all the equations (3.43) on the line $Y = m$. Hence, $\overline{P}_{l,m}$ satisfies

$$h_{xy}^{-2}(\overline{P}_{l-1,m} + \overline{P}_{l+1,m} + \tilde{P}_{l,m+1} + \overline{P}_{l,m-1} - 4\overline{P}_{l,m}) = F_{l,m}\,. \tag{3.44}$$

The error at the point (l,m) before and after a relaxation is respectively given by $\tilde{v}_{l,m}$ and $\overline{v}_{l,m}$, where

$$\tilde{v}_{l,m} = P_{l,m} - \tilde{P}_{l,m} \qquad \textit{and} \qquad \overline{v}_{l,m} = P_{l,m} - \overline{P}_{l,m}\ . \tag{3.45}$$

Generally, iterative schemes have the property of reducing the non-smooth (high frequency) part of the error at a much faster rate than that of the smooth part. This fact is exploited by the multigrid method where coarser grids are employed in order to deal with the smooth part of the error. When using multigrids, the role of relaxation is not to reduce the error but to smooth it out. One way of understanding the smoothing properties of grid functions is by means of Fourier analysis [12, 105]. This is a local process and is a very good technique for analysing the true behaviour of modes with high frequencies which represents the non-smooth part of the error. However, this technique is inaccurate for modes with smaller frequencies but this can be ignored when using the multigrid method because modes with smaller frequencies can be represented on coarser grids.

Since smoothing is a local process, it can be analysed locally on a particular grid by representing the errors in terms of Fourier series. Hence, the Fourier series representation of $\tilde{v}$ and $\overline{v}$ is of the form:

$$\tilde{v}_{l,m} = \sum \tilde{A}(\theta_1,\theta_2)e^{i(\theta_1 l+\theta_2 m)} \quad and \quad \overline{v}_{l,m} = \sum \overline{A}(\theta_1,\theta_2)e^{i(\theta_1 l+\theta_2 m)}. \quad (3.46)$$

where, $\{\theta = (\theta_1,\theta_2) : -\pi \leq \theta \leq \pi\}$. Subtracting equation (3.44) from equation (3.43) gives

$$\overline{v}_{l-1,m} + \overline{v}_{l+1,m} + \tilde{v}_{l,m+1} + \overline{v}_{l,m-1} - 4\overline{v}_{l,m} = 0 \quad (3.47)$$

which, using equation (3.46), can be rewritten as

$$(e^{-i\theta_1} + e^{i\theta_1} + e^{-i\theta_2} - 4)\overline{A}(\theta_1,\theta_2) + e^{i\theta_2}\tilde{A}(\theta_1,\theta_2) = 0\,, \quad (3.48)$$

which shows the relation between the amplitudes of a Fourier component before and after relaxation. Consequently, the amplification factor $\mu(\theta)$ of the $\theta = (\theta_1,\theta_2)$ component is

$$\mu(\theta_1,\theta_2) = \frac{|\overline{A}(\theta_1,\theta_2)|}{|\tilde{A}(\theta_1,\theta_2)|} = \frac{|e^{i\theta_2}|}{|4 - 2cos\theta_1 - e^{-i\theta_2}|}. \quad (3.49)$$

Figure (3.5) shows the amplification factor as a function of $\theta = (\theta_1,\theta_2)$ for the Gauss-Seidel line relaxation scheme which is employed when the coefficient $\epsilon >> 1$. Since $\mu(\theta) \leq 1$, the scheme is stable for all values of θ. We can also see that $\mu(\theta) \to 1$ as $\theta \to 0$ which means that the low frequency (smooth) error components are not

reduced by the relaxation as effectively as the high frequency (non-smooth) error components. Since we are only interested in the smoothing effect, the reduction of the high frequency components of the error can be measured by a quantity called the *smoothing factor*, $\overline{\mu}$, [12, 105] which is defined as the maximum amplification factor for the error components that can be represented on a grid with coarser mesh, that is

$$\overline{\mu}(\theta) = max\ \mu(\theta_1, \theta_2) \tag{3.50}$$

where, $\{\theta = (\theta_1, \theta_2) : \theta_i \in [-\pi, -\frac{\pi}{2}] \cup [\frac{\pi}{2}, \pi]$ *with the subscript* $i = 1, 2\}$. The smoothing factor $\overline{\mu}$ for this problem is 0.24.

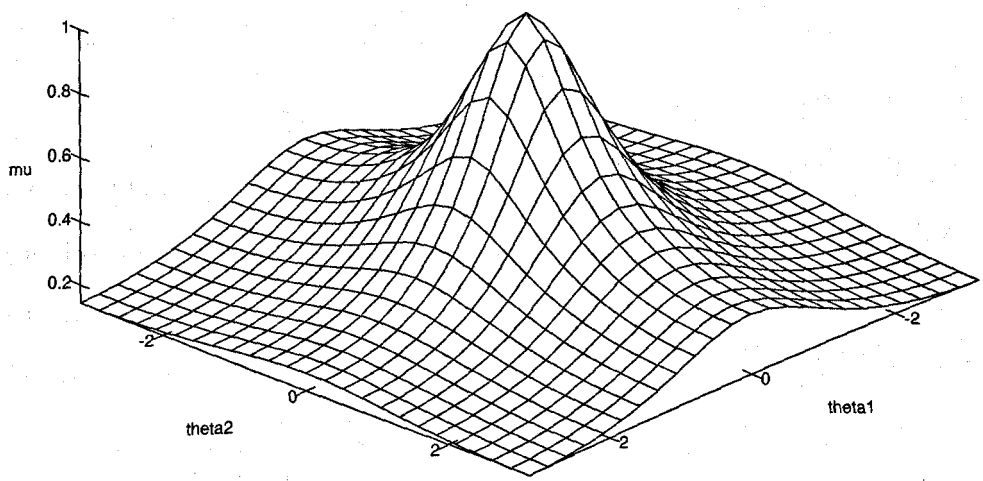

Figure 3.5: Amplification factor $\mu(\theta_1, \theta_2)$ for Gauss-Seidel line relaxation.

3.5 Conclusion

The inverse method [29, 35, 37, 61] and the direct iterative methods [25, 36, 45, 84] were the earliest methods employed to solve elasto-hydrodynamic lubrication problems. However, these methods are not ideal for solving practical problems found in industrial applications due to computational costs and numerical instabilities, especially when solving highly loaded problems [68, 97]. Solving highly loaded problems requires a large number of mesh points in order to obtain realistic solutions but, due to large CPU times, these methods are not ideal for solving these problems. Hence, these schemes are mainly used to solve line contact and lightly loaded problems.

However, new schemes have emerged recently, but they are still restrictive. One such method is Wang's [29] effective influence Newton method which is suitable for solving point contact problems, but the use of finer meshes is restricted due to large CPU times. This method seems to work as it is shown by Wang [102] but it is not as efficient as the new relaxation scheme which is developed in this work. Another method is the homotopy method [75] which is very robust but at the expense of large CPU times.

A big breakthrough in reducing CPU times was achieved by Lubrecht [68] who introduced the multigrid method in solving elasto-hydrodynamic lubrication problems. Hence, problems with a large number of mesh points could now be solved routinely. Since Lubrecht made use of the Gauss-Seidel relaxation scheme, the problem of instability was still an issue. This problem arises due to the nature of the Reynolds equation of the elasto-hydrodynamic lubrication model. The coefficient ϵ of the Reynolds equation varies several orders of magnitude over the computational domain. In the contact region, it is extremely small and it can be as small as 10^{-15} whereas in the non-contact region, $\epsilon >> 1$ and it lies in the range 10 to 10^5. Due to the extreme values of the coefficient ϵ over the computational domain, the character of the problem changes. This means that whichever relaxation scheme is employed to solve elasto-hydrodynamic lubrication problems, it must be able to cope with the extreme values of the coefficient ϵ. Hence, the coefficient ϵ plays an important role in deciding which relaxation scheme to use when solving these problems.

Following Lubrecht's work, Venner [97] employed the multigrid method and developed a relaxation scheme dependent on the coefficient ϵ. Hence, Venner was able to solve point contact problems that were previously unsolvable. More recent work involving the use of the multigrid method includes that of Ehret [33] who has also employed a relaxation scheme which is very similar to that of Venner.

The new relaxation scheme developed in this chapter also depends on the coefficient ϵ. The idea is to use different relaxation schemes on the same computational domain depending on the coefficient ϵ. In the contact region, the coefficient ϵ is very close to zero whereas in the non-contact region of the computational domain, the coefficient $\epsilon >> 1$. Hence, in the new relaxation scheme, the Jacobi and

the Gauss-Seidel line relaxation schemes are respectively employed in the contact and non-contact regions of the computational domain. The new relaxation scheme is very simple and easy to implement and understand compared to the relaxation schemes of Venner and Ehret. In the next chapter, we will present a multigrid solver for elasto-hydrodynamic lubrication problems based on the new relaxation scheme.

Chapter 4

DEVELOPING AN EHL SOLVER USING MULTIGRID

The multigrid method has been extensively used to solve various boundary value problems [12]. However, its use for solving Elasto-Hydrodynamic Lubrication (EHL) problems is relatively new. The multigrid method was introduced into the field of tribology by Lubrecht [68] who through his extensive work [65] has made it a very efficient method for solving elasto-hydrodynamic lubrication line and point contact problems. The use of the multigrid method makes it computationally less expensive to solve elasto-hydrodynamic lubrication problems using a large number of mesh points. In order to obtain better efficiency, the use of a large number of mesh points is crucial especially for highly loaded problems. The use of iterative schemes to solve highly loaded problems is very expensive computationally. Generally, the use of inappropriate iterative schemes for solving system of equations arising from the discretisation of partial or integro-differential boundary value problems may result in stalling, [13, 55], where the computational time taken to achieve a small physical effect is large. For example the error reduces by a small amount from one iteration to the next. Hence, computationally this can be very expensive.

The aim of this work is to develop a fast, robust and general purpose numerical solver for elasto-hydrodynamic lubrication point contact problems using the multigrid method. Hence, this chapter begins with a general description of the multigrid method. This includes both the Correction Scheme and the Full Approximation Scheme (FAS). The correction scheme is employed when solving linear problems and since elasto-hydrodynamic lubrication problems are non-linear the correction scheme cannot be employed and a full approximation scheme must be used. The inter-grid operators, namely the restriction and the prolongation operators, used to transfer the residuals and the corrections from one grid to another are also described. An account of different multigrid cycles, namely V and W cycles, is given together with the full-multigrid scheme. The full-multigrid scheme which instead of using coarser grids only to accelerate convergence, also uses them to generate accurate first approximations on the finest grid. Also presented in this chapter will be a general overview of the use of the multigrid method to solve elasto-hydrodynamic lubrication problems. This chapter will conclude with a description of how a multigrid solver for elasto-hydrodynamic lubrication problems (multigrid solver) employed in this work is developed. This is achieved by making use of the new relaxation scheme described in Section 3.2.2 of the previous chapter and the FDMG Multigrid Software [92]. The latter is used as a starting point for implementing the multigrid method in the multigrid solver and will be described later in this chapter. The FDMG multigrid software is a simple general purpose solver, and, in order to solve elasto-hydrodynamic lubrication point contact problems, additions and modifications are made to the FDMG multigrid software in order to deal with the complexity of the elasto-hydrodynamic lubrication model.

4.1 Multigrid Method

In general, when using the multigrid method, the governing equations are discretised on several grid levels and are approximated at each level by a system of equations. The residuals of these equations are calculated on the finer grid level and then transferred down to the coarser level where correction terms are computed. The

corrections from the coarser grid level are then used to obtain the corrections on the finer grid level. This is repeated until the residuals on the finest grid level are sufficiently small.

In order to understand the principle of multigrid fast solvers, an insight into the nature of the algebraic errors associated with the conventional iterative schemes is required. Besides this, an understanding of how these schemes reduce the errors is also required. Generally, iterative schemes have the property of reducing the non-smooth (high frequency) part of the error at a much faster rate than that of the smooth part which is associated with low frequencies. When using multigrids, the role of relaxation is not to reduce the error but to smooth it out. This is achieved by making use of a sequence of coarser grids. In a multilevel solver, which makes use of a series of coarser grids, each high frequency component of the error, which has a wavelength of the order of the mesh size, is reduced on one grid until it becomes smooth when the same procedure is applied on a coarser grid. The smooth part of the error, which is associated with lower frequency, can be adequately represented on a coarser grid. A good illustration of this is provided in the multigrid guide of Brandt [13] and the tutorial by Briggs [18].

In order to understand the multigrid method, consider the simplest case of a two grid method and consider the following problem

$$Lu = f \quad on \quad \Omega \tag{4.1}$$

where, L is the differential operator, u is the solution and f is the source term (rhs).

Discretisation of equation (4.1) on a uniform grid with mesh size h gives

$$L^h \underline{u}^h = \underline{f}^h . \tag{4.2}$$

Let $\tilde{\underline{u}}^h$ be an approximation to the true solution $\underline{u}^h$, then the error is given by

$$\underline{e}^h \equiv \underline{u}^h - \tilde{\underline{u}}^h \tag{4.3}$$

and the residual or defect is given by

$$\underline{r}^h = \underline{f}^h - L^h \tilde{\underline{u}}^h . \tag{4.4}$$

Using $L^h \underline{u}^h = \underline{f}^h$, equation (4.4) can be rewritten as

$$\underline{r}^h = L^h \underline{u}^h - L^h \tilde{\underline{u}}^h . \tag{4.5}$$

If L^h is a linear operator, then equation (4.5), using equation (4.3), reduces to

$$L^h \underline{e}^h = \underline{r}^h \tag{4.6}$$

and is called the Correction Scheme (CS).

At this point the error $\underline{e}^h$ is evaluated using equation (4.6) but after a few iterations or 'relaxations' it will be smooth compared to the mesh size. Hence, using the approximation L^H of L^h on a coarser grid with mesh size H, where $H = 2h$, the correction term $\underline{v}^H$ is calculated from

$$L^H \underline{v}^H = I_h^H \underline{r}^h \tag{4.7}$$

where, I_h^H is a restriction operator that restricts $\underline{r}^h$ to a coarser grid. The restriction operator is called the fine to coarse grid operator.

Using the obtained solution $\tilde{\underline{v}}^H$ which is an approximation of $\underline{v}^H$, the approximation $\tilde{\underline{u}}^h$ on the fine grid is corrected using

$$\overline{\underline{u}}^h = \tilde{\underline{u}}^h + I_H^h \tilde{\underline{v}}^H \tag{4.8}$$

where I_H^h is a prolongation operator. It is known as the coarse to fine grid operator or the interpolation operator.

In elasto-hydrodynamic lubrication problems, since L^h is a nonlinear operator, the correction scheme given by equation (4.6) is not applicable. Hence, an alternative coarse grid equation for the solution of the error must be derived. This can be achieved by rewriting equation (4.5) using equation (4.3) to get

$$\underline{r}^h = L^h \underline{u}^h - L^h \tilde{\underline{u}}^h = L^h(\tilde{\underline{u}}^h + \underline{e}^h) - L^h \tilde{\underline{u}}^h \tag{4.9}$$

which can be rewritten as

$$L^h(\tilde{\underline{u}}^h + \underline{e}^h) = L^h \tilde{\underline{u}}^h + \underline{r}^h \,. \tag{4.10}$$

Equation (4.10) is usually referred to as the Full Approximation Scheme (FAS) and is used to obtain an approximation of the error on the coarse grid. The FAS coarse grid representation of equation (4.10) is given by

$$L^H \hat{\underline{u}}^H = \hat{\underline{f}}^H \tag{4.11}$$

where $\underline{\hat{u}}^H$ is a coarse grid variable given by

$$\underline{\hat{u}}^H = I_h^H \underline{\tilde{u}}^h + \underline{e}^H \tag{4.12}$$

and $\underline{\hat{f}}^H$ is the FAS right hand side which is given by

$$\underline{\hat{f}}^H = L^H(I_h^H \underline{\tilde{u}}^h) + I_h^H \underline{r}^h$$

where I_h^H is a restriction operator.

Suppose $\overline{\underline{u}}^H$ is an approximation to the solution $\underline{\hat{u}}^H$ of equation (4.11), then the coarse grid approximation $\underline{\tilde{e}}^H$ of the error $\underline{e}^H$ is given by

$$\underline{\tilde{e}}^H = \overline{\underline{u}}^H - I_h^H \underline{\tilde{u}}^h . \tag{4.13}$$

Using equation (4.13), the fine grid solution $\underline{\tilde{u}}^h$ is improved using

$$\overline{\underline{u}}^h = \underline{\tilde{u}}^h + I_H^h(\overline{\underline{u}}^H - I_h^H \underline{\tilde{u}}^h) \tag{4.14}$$

where I_h^H is a restriction operator from grid h to H and I_H^h is a prolongation operator from grid H to h.

4.1.1 Restriction operator

The restriction operator, also known as the fine to coarse operator, is defined as follows: If $\underline{u}^h$ is a fine grid function, then using a restriction operator I_h^H a coarse grid function is given by $I_h^H \underline{u}^h$. The most straightforward and simplest restriction operator is straight injection. This is where the value on a coarse grid point simply takes the value from the corresponding fine grid point, that is $I_h^H \underline{u}^h = \underline{u}^h$. This can be seen from Figure (4.1), where the fine grid points are represented by F_i , $i = 1, \ldots, 9$, and the coarse grid points are represented by C_i , $i = 1, \ldots, 4$.

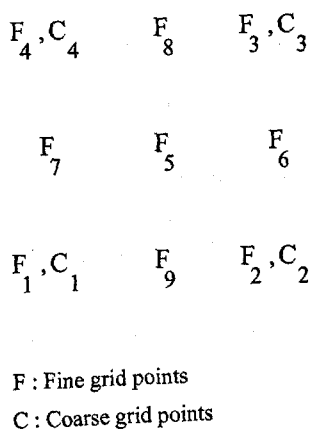

Figure 4.1: Restriction operator - Injection: $C_i = F_i$, $i = 1, \ldots, 4$.

As an alternative, the value on a non-boundary coarse grid point coinciding with the fine grid point can be obtained by taking the weighted average of the values of the fine grid point and some points adjacent to it. This can be seen from Figure (4.2), where the coarse grid point C can be represented as a weighted average of the fine grid point F_5, which coincides with the coarse grid point C, and the eight fine grid points surrounding it.

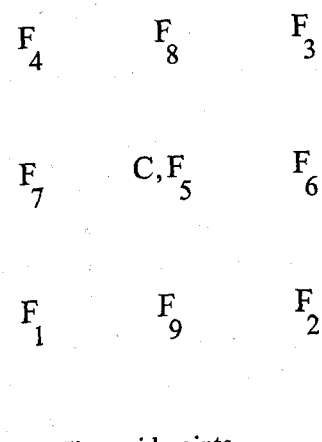

Figure 4.2: Weighted restriction operator.

A more commonly used form of a weighted restriction operator I_h^H is known as the

full weighting. In a 2-d stencil notation, it is of the form

$$I_h^H = \begin{bmatrix} \frac{1}{16} & \frac{1}{8} & \frac{1}{16} \\ \frac{1}{8} & \frac{1}{4} & \frac{1}{8} \\ \frac{1}{16} & \frac{1}{8} & \frac{1}{16} \end{bmatrix} \tag{4.15}$$

whereas in a 1-d stencil notation, it is given by

$$I_h^H = \begin{bmatrix} \frac{1}{4} & \frac{1}{2} & \frac{1}{4} \end{bmatrix}. \tag{4.16}$$

4.1.2 Prolongation operator

The prolongation or interpolation operator, also known as the coarse to fine operator, is defined as follows: If $\underline{u}^H$ is a coarse grid function, then using a prolongation operator I_H^h a fine grid function is given by $I_H^h \underline{u}^H$. The most popular prolongation operator is simple linear interpolation on a regular mesh. This is where values of all the fine grid points not coincident with the coarse grid points are obtained by taking averages of the coarse grid points. When two points are coincident, then the value on the fine grid point simply takes the value from the corresponding coarse grid point as can be seen from Figure (4.3).

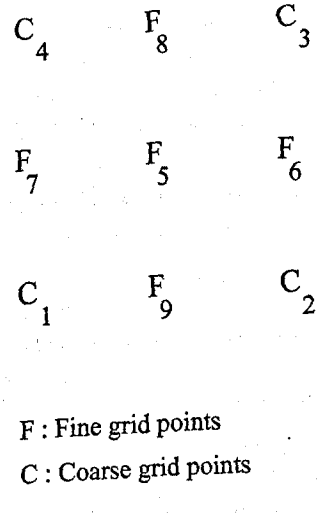

Figure 4.3: Prolongation operator - Linear Interpolation.

In Figure (4.3), the fine grid point F_5 is obtained using the average of the four coarse grid points C_1, C_2, C_3 *and* C_4 whereas the intermediate fine grid points F_6, F_7, F_8 *and* F_9 are obtained by taking the average of their respective two

adjacent coarse grid points. For example $F_7 = \frac{1}{2}(C_1 + C_4)$. The fine grid points coinciding with the coarse grid points take on the values of the corresponding coarse grid points. For example, $F_1 = C_1$. The fine grid points F_1, F_2, F_3 and F_4 are not shown in Figure (4.3).

4.1.3 Coarse grid correction cycle

If the number of nodes on a fine grid is large, then the number of nodes on a coarser grid with $H = 2h$ may still be considerable. Hence, the error on this coarse grid may still be smooth and can be represented more accurately on an even coarser grid with mesh size $2H$. Obviously this idea can be applied recursively until the coarsest grid is much smaller than the original finest grid and the equations on this coarsest grid can be solved almost exactly. The superscript k is now used to indicate the grid level. The mesh size on level k is given by $2^k + 1$ and $k = 1$ indicates the coarsest grid. The algorithm for a Coarse-Grid Correction [13] is as follows:

- Using the approximate solution compute the *residual* on the fine grid.
- *Restrict* the residual on to the coarse grid.
- Solve for the *correction* on the coarse grid.
- *Prolong* the correction on to the fine grid.
- Compute the *new approximation* to the solution.

A single relaxation may not be sufficient to reduce the non-smooth components of the error. Many relaxation schemes act as good smoothing operators where the amplitudes of non-smooth (high frequency) components are reduced by large factors on each iteration. Hence, the multigrid method is a combination of relaxation schemes and Coarse-Grid Correction. A two grid iteration is of the form

- Pre-smoothing: Perform v_1 relaxation sweeps to obtain a new approximate solution.
- Coarse-Grid Correction: Algorithm given above.

- Post-smoothing: Perform v_2 relaxation sweeps to compute a new approximation to the solution.

Using the above two grid iteration method, a multigrid method is easily obtained. Instead of solving the correction on the coarse grid, an approximate solution of the correction is obtained by introducing an even coarser grid and employing the two grid iteration method. This process can be repeated recursively down to the coarsest grid where the correction is computed exactly.

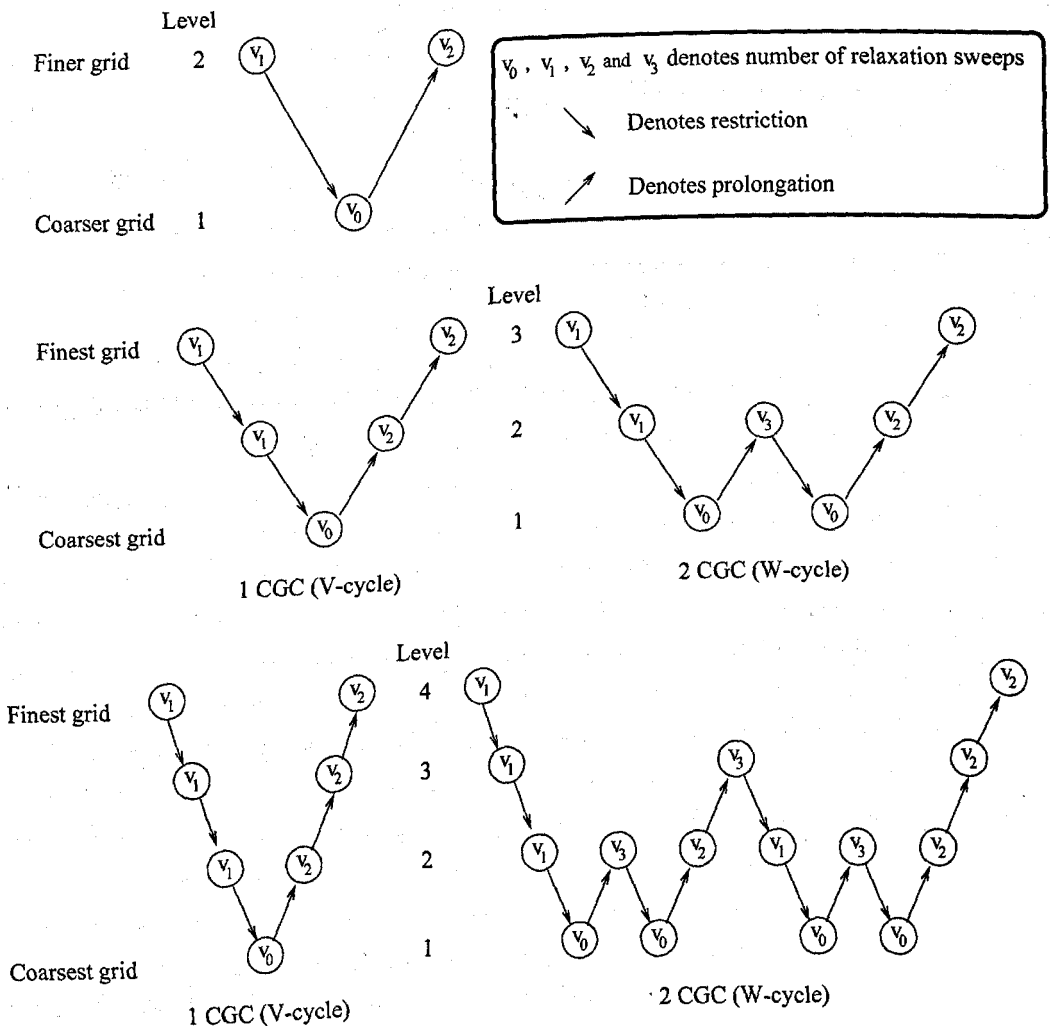

Figure 4.4: Structure of multigrid cycles.

One iteration of the multigrid method is called a cycle which starts from the finest grid to the coarsest grid and back to the finest grid. The structure of a cycle depends on the number, γ, of two grid method iterations at each intermediate

stage. A V-cycle and a W-cycle are obtained when $\gamma = 1$ and $\gamma = 2$ respectively as shown in Figure (4.4). The pre-smoothing and post-smoothing relaxations, that is v_1 and v_2 respectively, are normally of the order between 2 and 4.

4.1.4 Full-multigrid

In general, when using multigrids, coarser grids are used to accelerate convergence. However, if computations are started on the finest grid using an initial approximation, then it is possible that the algorithm might diverge due to an unfortunate choice of the initial approximation. This is unlikely to happen and the efficiency can be improved if coarser grids are used to generate an initial approximation on the finest grid. This is known as the *full-multigrid* method which is also known as *nested-iteration* [13, 105]. Hence, instead of starting with an arbitrary initial approximation on the finest grid, the first approximation is obtained by prolongation from a coarse grid solution, $\underline{u}^{k+1} = I_k^{k+1}\,\underline{u}^k$. This process can be applied recursively starting from the coarsest grid as shown in Figure (4.5).

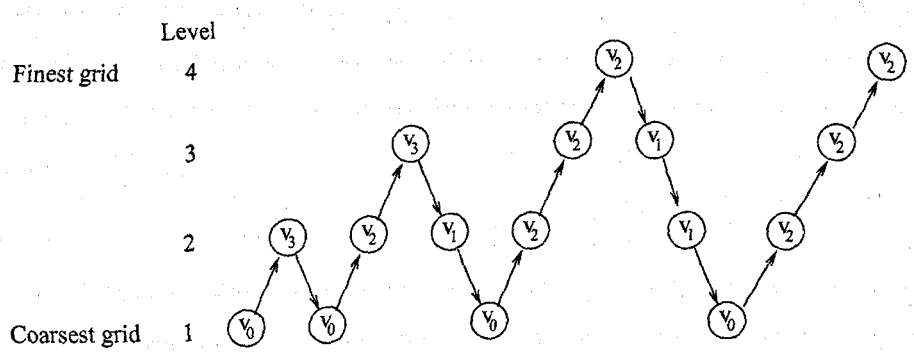

Figure 4.5: Full-multigrid with one V cycle.

4.2 Overview of the Multigrid Method for Solving EHL Problems

The computational cost of using direct linear equation solvers for elasto-hydrodynamic lubrication problems, as outlined in Chapter 3, restricts their use to small numbers of mesh points. This makes it difficult to solve problems which require larger meshes to be used to obtain a good solution. However, the use of multigrid tech-

niques [13, 18, 105] together with good relaxation schemes does help in resolving the complexity of the iteration schemes.

The multigrid method has been used extensively to solve a very wide range of boundary value problems [12] and has shown itself to be a very computationally efficient solver. This property of the multigrid methods has been exploited on various problems [13] from simple to complicated non-linear systems. This method is used extensively in the field of Computational Fluid Dynamics. This includes potential equations, Euler equations and Navier-Stokes equations with and without turbulence models. Multigrid methods are also used in conjunction with efficient grid adaptation schemes where different scales of mesh spacing are neeeded in different parts of the domain.

When solving elasto-hydrodynamic lubrication problems, Lubrecht [68, 65] developed a scheme based on the multigrid method to solve both line and point contact problems. A simple Gauss-Seidel relaxation scheme [55, 105] is used in solving the Reynolds equation of the elasto-hydrodynamic lubrication model with the multigrid method being incorporated in order to accelerate the convergence. Lubrecht [65] showed that the computing time is greatly reduced when solving line and point contact problems on a relatively large number of nodes using the multigrid method. Since Lubrecht employed the Gauss-Seidel scheme, highly loaded problems could not be solved due to the sensitivity of viscosity to pressure which may lead to instability [101]. However, by making use of the multigrid method, Lubrecht solved previously unsolvable problems due to excessive computational times, using a large number of mesh points in limited computational times and on computers with reasonable power. The multigrid method is now regarded as one of the most efficient methods for solving elasto-hydrodynamic lubrication problems.

An efficient multilevel solver requires a relaxation scheme that reduces the high frequency error components. For lightly to moderately loaded problems, a Gauss-Seidel relaxation scheme is sufficient as is shown by Lubrecht [65]. However, instability problems do arise when solving highly loaded problems using the Gauss-Seidel relaxation scheme. Following Lubrecht's work, Venner [97] used the multigrid method and developed a relaxation scheme for solving lightly to highly

loaded line and point contact problems. Hence, the problem of instability associated with highly loaded problems found in practice was no longer an issue. This relaxation scheme was later used and extended slightly by Ehret [33]. The problem of instability can also be overcome by employing the new relaxation scheme. The relaxation scheme of Venner and the new relaxation scheme are both described in detail in Chapter 3.

The multigrid solver for elasto-hydrodynamic lubrication problems makes use of the new relaxation scheme and the FDMG Multigrid Software [92]. The latter is used as a starting point for implementing the multigrid method into the multigrid solver. However, additions and modifications are made to the FDMG multigrid software due to the complexity of elasto-hydrodynamic lubrication problems. The multigrid solver for elasto-hydrodynamic lubrication problems (multigrid solver) will be described later in this chapter but we will now look at the FDMG multigrid software.

4.3 FDMG Multigrid Software

The FDMG Multigrid Software of Shaw [92] is a Full Approximation Scheme (FAS) multigrid solver for non-linear systems of partial differential equations on a finite difference mesh. It is a simple general purpose solver written in Fortran and mainly used as a teaching and research program. The software allows the user to experiment with different tools which includes the option of different relaxation schemes, restriction procedures (Injection and Full weighting) and cycling strategies (V and W cycles). The relaxation schemes include the Jacobi and the Gauss-Seidel schemes and they can be implemented either as point or line relaxation schemes. These relaxation schemes are described in detail in Chapter 3 whereas the restriction procedures and the cycling strategies of the multigrid method are described above in Section 4.1. The structure of the FDMG Multigrid Software can be divided into two parts, the *Initialisation Process* and the *Multigrid Driver*.

The *Initialisation Process* deals with the initialisation of the global arguments and the checking of the input parameters to see if they are sensible. The ini-

tialisation of the global arguments involves the setting up of various global switches which are defined using common blocks. This is achieved by analysing the chosen smoothing (relaxation) method, defining a sequence of coarser grids from the given finer grid, initialising the initial solution and setting up of all the grid geometries together with their mesh coordinates. The process of checking the input parameters involves making sure that the sequence of grids are suitable for multigrid, checking that the chosen smoothing (relaxation) method is compatible with the damping factor chosen by the user and making sure that the arrays are dimensioned sufficiently large to cope with the number of points being used to solve the elasto-hydrodynamic lubrication problem.

The *Multigrid Driver* is the main body of the FDMG multigrid software and its function is to carry out the multigrid cycles (iterations) which can either be a V-cycle or a W-cycle. These cycles are described above in Section 4.1.3. The structure of the *Multigrid Driver* is made up of Pre-smoothing, Coarsest Grid Solution and Post-smoothing as shown in Figure (4.6). The restriction and the prolongation inter-grid operators are employed respectively in between Pre-smoothing and Coarsest Grid Solution and Coarsest Grid Solution and Post-smoothing as can be seen from Figure (4.6). The concepts of pre-smoothing, coarsest grid solution, post-smoothing, restriction and prolongation are associated with the multigrid method and are described above in Section 4.1. The main subroutine calls made from the *Multigrid Driver*, as shown in Figure (4.6), are to the subroutines *SMOOTH*, *CRHS* and *PROL* which are part of the FDMG multigrid software. A description of these three subroutines will now be outlined starting with the subroutine *SMOOTH* which will be followed by the subroutines *CRHS* and *PROL*.

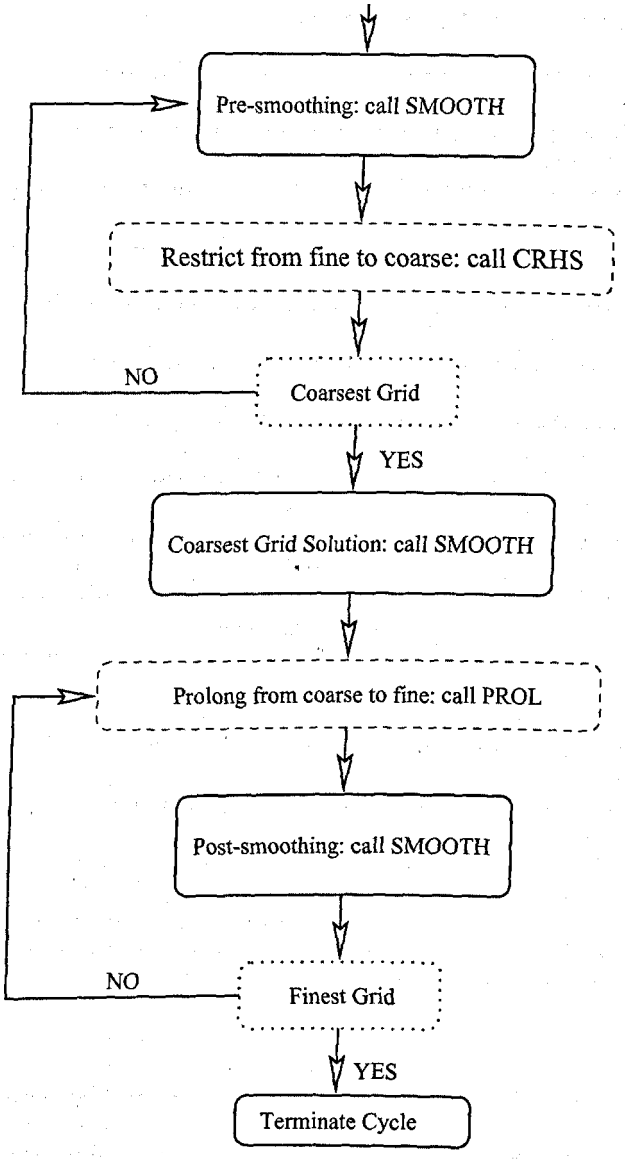

Figure 4.6: Structure of *Multigrid Driver* of the original FDMG multigrid software.

- Subroutine SMOOTH

This subroutine organises the smoothing (relaxation) method by making a subroutine call to either *POINTS*, *ILINES*, *JLINES* or *KLINES* depending on the users choice of the smoothing (relaxation) method. The subroutine *POINTS* is used to implement a standard point relaxation scheme [13, 55, 105]. The subroutines *ILINES*, *JLINES* and *KLINES* are used to implement respectively the I-line, J-line and K-line relaxation schemes. The concept of all these three relaxation schemes is to solve simultaneously a system of discrete equations on a line of points in

the direction of strong coupling. For example, if there is strong coupling in the X-direction then the I-Line relaxation scheme must be used by calling the subroutine *ILINES*. Similarly, if there is strong coupling in the Y and Z directions then the J-line and K-line relaxation schemes must be employed respectively by calling the subroutines *JLINES* and *KLINES*. The structure of the subroutines *ILINES*, *JLINES* and *KLINES* are exactly the same except for the order in which the relaxations are carried out. This can either be on the line of points in the X-direction for *ILINES*, Y-direction for *JLINES* or Z-direction for *KLINES*. In all these three subroutines, a system of block tridiagonal equations on any line of points is solved by calling the subroutine *THOMAS* which employs the widely-used Thomas' algorithm [5] (LU decomposition) to solve a block tridiagonal system of linear equations using the Gaussian elimination with partial pivoting.

- Subroutine CRHS

This routine is used to calculate the Full Approximation Scheme (FAS) coarse grid right hand side by restricting the fine grid solution and residual to the coarse grid. This process is described above in Section 4.1.

- Subroutine PROL

This routine is used to prolong from a coarser to a finer grid by adding the coarse grid correction to the fine grid solution. This is done by finding the coarse grid correction and adding it to the fine grid solution. This process is also described above in Section 4.1.

The ease of using the FDMG Multigrid Software [92] made it a good starting point for developing the multigrid solver for elasto-hydrodynamic lubrication circular contact problems.

4.4 Multigrid Solver for EHL Problems

The multigrid solver for elasto-hydrodynamic lubrication problems (multigrid solver) uses the new relaxation scheme of Chapter 3 and the above FDMG Multigrid Software [92]. The latter is used as a starting point for developing the multigrid solver.

The complexity of the elasto-hydrodynamic lubrication model, which is described in Chapter 2, means that many modifications had to be made to the FDMG multigrid software to produce the multigrid solver. The structure of the multigrid solver for elasto-hydrodynamic lubrication problems is made up of the *Driver Program*, *Modified FDMG* and *EHL Routines*. The aim is to let the user drive the multigrid solver by calling *Modified FDMG* from the *Driver Program*. *Modified FDMG* then interacts with the *EHL Routines* until convergence or the requested number of iterations have been completed. The convergence criterion used can be based on either the root mean square residual which is described in Chapter 3 (and will also be covered in Chapter 5) or the change in the pressure solution on the finest grid and the coarser grid just below it. The latter concept of checking convergence is more commonly used and will be described in Chapter 5. We will now give an outline of the *Driver Program*, *Modified FDMG* and *EHL Routines* of the multigrid solver for elasto-hydrodynamic lubrication problems (multigrid solver).

4.4.1 Driver Program

This routine is provided by the user of the multigrid solver. All the input parameters of the elasto-hydrodynamic lubrication problem to be solved must be defined in this routine. This includes the number of mesh points to be used, the computational domain on which to solve the problem, the parameters needed to define the elasto-hydrodynamic lubrication problem and the parameters required to drive the *Modified FDMG*.

4.4.2 Modified FDMG

This represents the modified version of the original FDMG Multigrid Software [92] which is described above in Section 4.3. The structure of the *Modified FDMG* is now made up of the *Initialisation Process*, *Full-multigrid* and *Multigrid Driver*.

The *Initialisation Process* is the same as before but now it also covers the initialisation of the arguments associated with elasto-hydrodynamic lubrication problems. This includes the classification of elasto-hydrodynamic lubrication problem and the calculation of the coefficient matrix K which is used to evaluate the

elastic deformation and is described in detail in Chapter 2. The coefficient matrix K is calculated and stored once on every grid.

The purpose of *Full-multigrid* is to implement the full-multigrid scheme which is described above in Section 4.1.4. Since the full-multigrid scheme is not available in the original FDMG multigrid software, it is added into the original FDMG multigrid software. The *Full-multigrid* is used after the *Initialisation Process* but prior to the application of the *Multigrid Driver*. The effectiveness of using the full-multigrid scheme will be shown below in Section 4.6 by means of an example.

The *Multigrid Driver* has an overall structure similar to that of the original FDMG multigrid software. However, extra subroutine calls are embedded into the *Multigrid Driver* in order to deal with elasto-hydrodynamic lubrication problems. All these extra subroutines are part of *EHL Routines* which will be described in the next section. Modifications are also made to the subroutines *CRHS*, *PROL*, and *ILINES* which are called from the *Multigrid Driver* and are part of the original FDMG multigrid software. These modifications are necessary in order to deal with the complexity of elasto-hydrodynamic lubrication problems and will be presented below in Section 4.5.

4.4.3 EHL Routines

These are the routines which are used specifically to deal with elasto-hydrodynamic lubrication problems. This includes the routine for evaluating the elastic deformation, the viscosity and density and the root mean square residual using respectively the subroutines *HCALC*, *EVALUATEVD* and *EVALUATERES*. These subroutine calls are made from the *Multigrid Driver* after every call to the subroutine *SMOOTH*. The calls to the subroutines *HCALC* and *EVALUATEVD* are also made after every call to the subroutines *CRHS* and *PROL*. Figure (4.7) shows how the subroutines *HCALC*, *EVALUATEVD* and *EVALUATERES* are embedded into the *Multigrid Driver* of *Modified FDMG*.

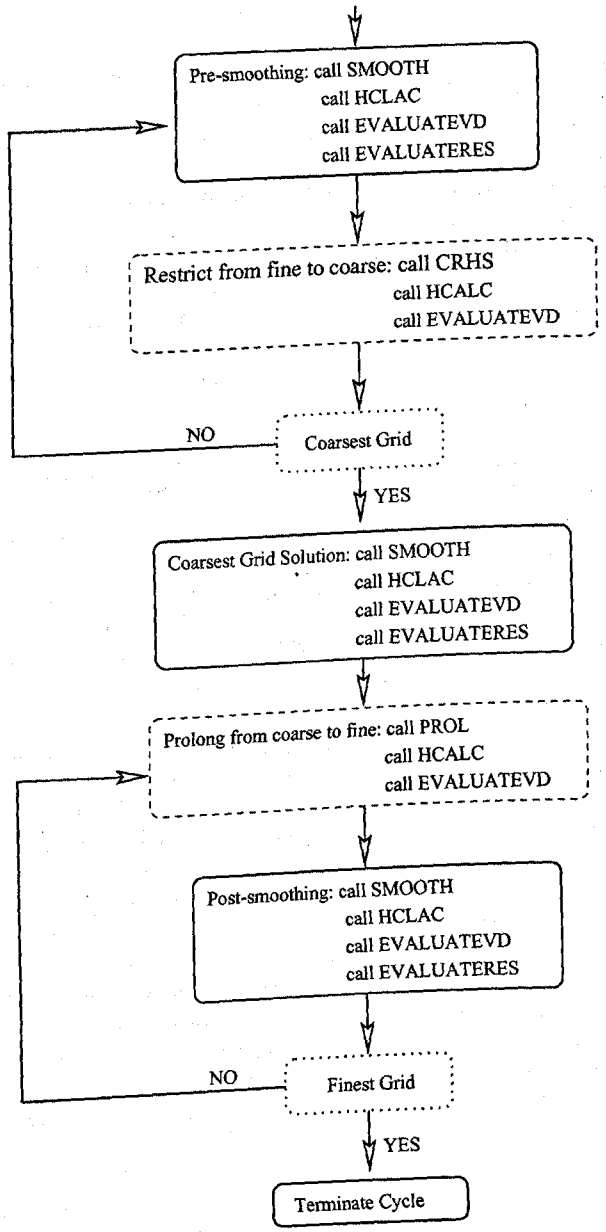

Figure 4.7: Structure of *Multigrid Driver* of the *Modified FDMG.*

Other optional subroutine calls to the *EHL Routines* from the *Multigrid Driver* at various stages of the computational run include *OUT* which is used to monitor the solution, *HMINCENT* which is used to calculate the minimum and central film thicknesses and *UERRMG* which is used to calculate the change in the pressure solution on the finest grid and the coarser grid just below it. This concept of checking the change in the pressure solution will be described in Chapter 5. When solving elasto-hydrodynamic lubrication problems, due to the strong coupling

in the X-direction, the subroutine *ILINES* is called from the subroutine *SMOOTH*. Hence, other subroutine calls to the *EHL Routines* are also made from the subroutine *ILINES*. This includes the call to the subroutines *RESID* and *SWITCH*. The subroutine *RESID* is the most widely used routine and it is employed to linearise the non-linear equations of the elasto-hydrodynamic lubrication model by discretising the governing equations at each grid point using the finite difference scheme as described in Chapter 2. It evaluates the residual at each grid point together with the entries for the system of discrete equations which is then fed into the subroutine *THOMAS* which is part of the original FDMG multigrid software and is described above in Section 4.3. The subroutine *SWITCH* is used to incorporate the cavitation condition and the new relaxation scheme to solve elasto-hydrodynamic lubrication problems. The subroutine *SWITCH* and the manner in which it handles the cavitation condition and the new relaxation scheme will be presented in the next section. The following pseudo code for the subroutine ILINES show how the subroutine calls to *RESID*, *SWITCH* and *THOMAS* are embedded into the structure of the subroutine *ILINES*.

```
      subroutine ILINES
          .
          .
      for j = 1,jmax do
C Apply nnew local Newton iterations
      for inew=1,nnew do
       for i = 1,imax do
C Assemble a tridiagonal system of equations for each line
        call RESID
C Solve the tridiagonal system of equations
      call THOMAS
        for i=1,imax do
C Update solution if Gauss-Seidel scheme
        call SWITCH
        {Apply Gauss-Seidel scheme and Cavitation Condition}

      for j=1,jmax do
      for i=1,imax do
C Update solution if Jacobi scheme
      call SWITCH
      {Apply Jacobi scheme and Cavitation Condition}
          .
          .
      return
      end
```

4.5 Modifications Made to the Original FDMG Multigrid Software

The complexity of the governing equations of the Elasto-Hydrodynamic Lubrication (EHL) model of Chapter 2 has made it necessary to modify the original FDMG Multigrid Software [92]. The implementation of the new relaxation scheme, described in Chapter 3, and the cavitation condition, described in Chapter 2, creates complications which are tackled by modifying the subroutines *CRHS*, *PROL* and *ILINES* of the original FDMG multigrid software. We will now discuss these modifications in the remainder of this section.

4.5.1 Modifications made due to the new relaxation scheme

The new relaxation scheme which is developed and employed in this work to solve elasto-hydrodynamic lubrication problems employs the Gauss-Seidel and Jacobi line relaxation schemes on the same computational domain but without any overlap. The type of relaxation scheme to be employed at any point depends very much on its position on the computational domain. As described in Chapter 3, the Gauss-Seidel and the Jacobi line relaxation schemes are respectively employed in the non-contact and contact regions of the computational domain. The new relaxation scheme is implemented in the original FDMG multigrid software by modifying the subroutine *ILINES*. This is achieved by making use of the new subroutine *SWITCH* to switch between the two relaxation schemes depending on the operating conditions. The relaxation factors associated with the two relaxation schemes are also changed during this process. The conditions required for switching between the two relaxation schemes are described in detail in Chapter 3. The pseudo code for the subroutine *ILINES* presented above in Section 4.4.3 shows how the subroutine *SWITCH* is incorporated into the subroutine *ILINES*.

4.5.2 Modifications made due to cavitation condition

One of the key features of the elasto-hydrodynamic lubrication model is the cavitation condition which is described in Section 2.1.3 of Chapter 2. In the cavitation

region, where negative pressures may be computed by the solver, the Reynolds equation (2.19) of the elasto-hydrodynamic lubrication model is not valid and the computed negative pressure must be set to zero. Hence, in the original FDMG multigrid software, the subroutine *ILINES* is modified in order to take the cavitation condition into consideration. This is done by assigning all the negative pressures to zero either after every line relaxation or after a complete sweep depending on which relaxation scheme is being employed. This uses the concept of the new relaxation scheme which employs the Gauss-Seidel and Jacobi line relaxation schemes on the same computational domain. As described in the previous section, the subroutine *SWITCH* is used to switch between the two relaxation schemes. If a negative pressure is computed at a grid point which lies in a region where the Gauss-Seidel line relaxation scheme is being employed, then the negative pressure is set to zero. However, if the grid point lies in a region where the Jacobi line relaxation is being employed, then the computed negative pressure is set to zero at the end of a complete sweep.

The other feature associated with the cavitation region is that the values of pressure in the regions of the domain adjacent to the cavitation region are very large. Hence, in the cavitation region there is a sharp drop and steep gradient in the pressure from positive values to zero. Because of this sudden sharp drop in the pressure, the cavitation boundary region must be treated as a special case when transferring the residuals from a finer grid on to a coarser grid. Hence, the injection inter-grid operator, described above in Section4.1.1, is employed in and around the regions of the cavitation when transferring the residual on to a coarser grid. In the remaining parts of the domain, the full weighting inter-grid operator, which is also described above in Section 4.1.1, is employed. This concept is implemented in the original FDMG multigrid software by modifying the subroutine *CRHS*. This is done by flagging all the grid points on all the sequence of grids into cavitation and non-cavitation regions. The flagged points are then used to choose which restriction operator to use. It is also important to make sure that the cavitation region on a particular grid does not change during a multigrid cycle. Hence, the cavitation region during restriction, also known as the fine to coarse operator, and

prolongation, also known as the coarse to fine operator, must not be altered. This means that during prolongation, when the coarse grid corrections are added to the fine grid solutions, the cavitation region must be taken into account by considering only the fine grid points which lie in the non-cavitation region. Hence, the coarse grid correction terms are only added to the fine grid points which lie in the non-cavitation region. This concept is implemented in the original FDMG multigrid software by modifying the subroutine *PROL*. This is achieved by making use of the flags assigned in the subroutine *CRHS* to indicate the cavitation and non-cavitation regions.

The cavitation condition also affects the evaluation of the root mean square residual. Since the Reynolds equation (2.19) of the elasto-hydrodynamic lubrication model, which is described in Chapter 2, is not valid in the cavitation region, the evaluation of the root mean square residual, which is given by equation (3.37), must exclude the regions of the domain where the Reynolds equation (2.19) is not valid. This is achieved by calling the subroutine *EVALUATERES*, which is part of the *EHL Routines*, after every call to the subroutine *SMOOTH*. In the original FDMG multigrid software, the root mean square residual of L_2-norm is evaluated during the relaxation process in the subroutine *ILINES*. When solving elasto-hydrodynamic lubrication problems, this is not a good practice as the new relaxation scheme described in Chapter 3 make use of the Gauss-Seidel and Jacobi line relaxation schemes on the same computational domain. The Jacobi scheme updates the solution after a complete sweep of the whole region and the root mean square residual is evaluated at the end of the complete sweep, i.e. after every call to the subroutine *SMOOTH*.

4.6 Example Showing the Effectiveness of the Full-Multigrid Scheme

The implementation of the full-multigrid scheme is described above in Section 4.4.2. The main aim of this section is to illustrate how powerful the full-multigrid scheme is compared with the standard multigrid approach when solving elasto-hydrodynamic

lubrication problems. The problem used in this illustration will be described and solved in full using the multigrid solver for elasto-hydrodynamic lubrication problems in Section 5.1 of Chapter 5. The only difference between the full-multigrid scheme and the standard multigrid approach is that the latter does not employ the full-multigrid option. In order to compare the efficiency of the full-multigrid scheme with the standard multigrid approach, consider the following two listings.

The listing shown below is the partial output for this problem from the multigrid solver which employs the full-multigrid scheme. The Root Mean Square Residual, labelled RMSRES, represents the L_2-norm and is given by equation (3.37). The listing shows the RMSRES for one complete V-cycle.

FULL-MULTIGRID SCHEME

GRID 3 RMSRES 5.312979E-3
GRID 4 RMSRES 7.321600E-4
GRID 3 RMSRES 2.992205E-4
GRID 4 RMSRES 4.163396E-5

V-CYCLE NUMBER : 1

GRID 5 RMSRES 6.310523E-4
GRID 4 RMSRES 3.567165E-4
GRID 3 RMSRES 6.211190E-6
GRID 4 RMSRES 2.593017E-4
GRID 5 RMSRES 3.677663E-4

The listing shown below is the partial output for this problem from the multigrid solver but, this time employing the standard multigrid approach. The Root Mean Square Residual, labelled RMSRES, represents the L_2-norm and is given by equation (3.37). The listing shows the RMSRES for one complete V-cycle.

STANDARD MULTIGRID APPROACH

V-CYCLE NUMBER : 1

GRID	*5*	*RMSRES*	*2.507337E-2*
GRID	*4*	*RMSRES*	*2.074723E-2*
GRID	*3*	*RMSRES*	*4.580757E-4*
GRID	*4*	*RMSRES*	*2.006475E-2*
GRID	*5*	*RMSRES*	*2.577595E-2*

After one V-cycle, the Root Mean Square Residual, labelled RMSRES, obtained with the full-multigrid scheme and the standard multigrid approach are respectively of the order 10^{-4} and 10^{-2}. An interesting point to notice is that when the full-multigrid scheme is employed, the residual on the finest grid prior to the beginning of the V-cycle is of the order 10^{-4}. This is much smaller than the root mean square residual obtained after one V-cycle when the standard multigrid approach is employed. Hence, the initial approximation of the solution on the finest grid is more accurate when the full-multigrid scheme is employed.

4.7 Conclusion

At present, although many numerical methods have been used to solve elasto-hydrodynamic lubrication point contact problems, there has been greater emphasis on the single grid iterative methods. An overview of the different iterative schemes is presented in the previous chapter. One feature of these iterative schemes is that they reduce the non-smooth part of the error at a much faster rate than that of the smooth part which is associated with low frequencies. This feature is exploited by the multigrid method where coarser grids are employed in order to deal with the smooth part of the error. When using multigrids, the role of relaxation is not to reduce the error but to smooth it out. This is achieved by making use of a sequence of coarser grids. In a multigrid method, each high frequency component

of the error, which has a wavelength of the order of the mesh size, is reduced on one grid until it becomes smooth when the same procedure is applied on a coarser grid. The smooth part of the error, which is associated with lower frequency, can be adequately represented on a coarser grid.

A major drawback of using single grid iterative methods for solving elasto-hydrodynamic lubrication point contact problems is the need for a large number of iterations and consequently large CPU times. This occurs when using a large number of mesh points or when solving transient problems. In order to obtain realistic solutions, the use of a large number of mesh points is essential especially when solving highly loaded problems found in practice. The computational costs associated with single grid methods can be overcome by making use of the multigrid method. The multigrid method increases the rate of convergence and elasto-hydrodynamic lubrication problems which were previously unsolvable can now be solved routinely. Hence, the multigrid method has proved to be very successful in solving elasto-hydrodynamic lubrication problems and we have developed in this chapter a multigrid solver for these problems. It can be used to solve both steady state and time-dependent circular contact problems. Solutions to steady state problems will be presented and compared with those obtained using other numerical methods in the next chapter whereas solutions to time-dependent problems will be presented in Chapter 6.

Chapter 5

NUMERICAL EXPERIMENTS USING A MULTIGRID SOLVER BASED ON FDMG

In this chapter, the numerical solutions of steady-state elasto-hydrodynamic lubrication circular contact problems obtained using the multigrid solver with the new relaxation scheme described in the previous chapter are compared with the solutions obtained using other numerical methods. The other numerical methods, which are described in Chapter 3, include the relaxation schemes of Venner [97] and Ehret [33], the homotopy method [4] which is used by Scales [75] and the effective influence Newton method of Wang [102]. Four cases of steady-state elasto-hydrodynamic lubrication circular contact problems are considered.

5.1 Case One

This test problem, which appears in Venner [97], is solved on a domain $\{(X,Y) : -5.0 \leq X \leq 1.2, -3.5 \leq Y \leq 3.5\}$ using the New Relaxation Scheme on a Single Grid (NRS-S-Grid) and MultiGrid (NRS-M-Grid) and the Homotopy method [4],

which is used by Scales [75], on a Single Grid (H-S-Grid). A 65×65 grid is employed when the problem is solved on a single grid using the new relaxation scheme and the homotopy method. Finest 65 by 65 and coarsest 17 by 17 grids are used when the problem is solved using the multigrid method. However, due to symmetry, only the nodes in the positive Y-direction are used when the problem is solved using the new relaxation scheme on a single grid and multigrid. For this moderately loaded problem, the parameters describing the problem are shown in Table (5.1).

Parameters	Values
Pressure viscosity index α $[Pa^{-1}]$	1.7×10^{-8}
Maximum Hertzian pressure p_h $[GPa]$	0.5818
$\overline{\alpha} = \alpha\, p_h$	10
Material parameter G	4729
Load parameter W	1.8915×10^{-7}
Speed parameter U	1.0×10^{-11}
Moes parameter M	20
Moes parameter L	10

Table 5.1: Input parameters for the problem in Case One.

5.1.1 Results and discussion

The numerical solutions and the convergence histories associated with the New Relaxation Scheme on a Single Grid (NRS-S-Grid) and MultiGrid (NRS-M-Grid) and the Homotopy method on a Single Grid (H-S-Grid) are respectively shown in Tables (5.2), (5.3) and (5.4).

If the convergence criterion is based on the Root Mean Square Residual, labelled RMSRES, then the solutions obtained using the new relaxation scheme on a single grid and multigrid and the homotopy method on a single grid are of the order 10^{-6}, 10^{-5} and 10^{-11} respectively. The root mean square residual is defined by

$$RMSRES = \sqrt{\frac{1}{m_x n_y} \sum_{i=1}^{m_x} \sum_{j=1}^{n_y} RES_{i,j}^2} \tag{5.1}$$

where m_x and n_y are the maximum number of points in the X and Y directions respectively and $RES_{i,j}$ is the residual at the point (i, j).

The discrepancy in the root mean square residual (RMSRES) obtained using the new relaxation scheme on a single grid and multigrid can be attributed to the cavitation region (see Section 2.1.3) and the nature of the Reynolds equation (2.19). In the cavitation region, the Reynolds equation is not valid and problems arise when transferring the residuals and the corrections between the grids when using the multigrid method as described in Section 4.5.2.

On a single grid, it is a common practice e.g. [102] to check the change in the pressure solution from one iteration to the next as a means for testing the convergence criterion. This is labelled as ΔP_s in Tables (5.2) and (5.4) and the subscript s indicates that it is on a single grid. Thus, the change in the pressure solution on the k^{th} iteration is given by

$$\Delta P_s = \frac{\sum_{i=1}^{m_x} \sum_{j=1}^{n_y} \left| P_{i,j}^{k} - P_{i,j}^{k-1} \right|}{\sum_{i=1}^{m_x} \sum_{j=1}^{n_y} P_{i,j}^{k}} \tag{5.2}$$

where m_x and n_y are the maximum number of points in the X and Y directions respectively.

A more commonly [97] used form for checking the convergence criterion when using the multigrid method is to compare the pressure solution on the finest grid and the coarser grid just below it with mesh sizes h and $H = 2h$ respectively. This is labelled as ΔP_m in Table (5.3) and the subscript m indicates that multigrid was being used. When the iteration has converged, we would expect to see no change in this value. This change in the pressure solution when using the multigrid method is obtained using

$$\Delta P_m = h_x h_y \sum_{i=1}^{m_x} \sum_{j=1}^{n_y} \left| \tilde{P}_{i,j}^{H} - I_h^H \tilde{P}_{i,j}^{h} \right| \tag{5.3}$$

where, h_x and h_y are respectively the mesh spacings in the X and Y directions, m_x and n_y are the maximum number of points in the X and Y directions respectively and I_h^H is the restriction operator which is described in detail in Chapter 4.

Convergence based on ΔP_s when using a single grid method and ΔP_m when using the multigrid method suggest that the solution obtained using the new relaxation scheme on a single grid might have an accuracy of the order 10^{-8} as can be seen from Table (5.2). This value is much smaller than that obtained using the other two methods which are of the order 10^{-4} and 10^{-6} as can be seen from Tables (5.3) and (5.4) respectively. Though it is a common practice to base the convergence criterion on ΔP_s and ΔP_m, this can be misleading. ΔP_s only indicates the change in the solution at each iteration and it is not a good practice to use it as a means for testing accuracy or convergence criterion. It is possible to get very small changes and the solution might be very far from the true solution. This reasoning can also apply to ΔP_m. The convergence criterion based on the root mean square residual seems to be more appropriate but it is rarely used in elasto-hydrodynamic lubrication problems.

Also shown in Tables (5.2), (5.3) and (5.4) are the central, labelled Hcent, and minimum, labelled Hmin, film thicknesses obtained using the new relaxation scheme on a single grid (NRS-S-Grid) and multigrid (NRS-M-Grid) and the homotopy method on a single grid (H-S-Grid).

Its	Hcent	Hmin	RMSRES	SumP	ΔP_s
100	0.4322	0.2914	1.1204E-02	2.0594	1.311E-03
300	0.4513	0.3048	1.9066E-03	2.0979	6.537E-05
500	0.4524	0.3054	2.5793E-04	2.0947	7.447E-06
700	0.4525	0.3054	3.3917E-05	2.0944	9.621E-07
1000	0.4525	0.3055	1.6112E-06	2.0943	4.561E-08

Table 5.2: NRS-S-Grid for M=20 & L=10.

Its	Hcent	Hmin	RMSRES	SumP	ΔP_m
1	0.4612	0.3076	1.3773E-02	2.0842	1.377E-02
5	0.4529	0.3057	1.6256E-04	2.0909	8.322E-04
10	0.4526	0.3054	7.3911E-05	2.0904	2.452E-04
15	0.4525	0.3053	4.3010E-05	2.0905	2.251E-04
20	0.4525	0.3053	3.6674E-05	2.0905	2.236E-04
25	0.4525	0.3053	3.6051E-05	2.0905	2.234E-04

Table 5.3: NRS-M-Grid for M=20 & L=10.

Its	Hcent	Hmin	RMSRES	SumP	ΔP_s	alpha
1	0.6478	0.6468	4.302E-01	2.0944	1.0000E+00	5.000E-09
7	0.2466	0.1765	1.371E-02	2.0944	4.9562E-05	5.000E-09
8	0.2468	0.1765	1.369E-02	2.0944	2.3835E-04	5.000E-09
14	0.3600	0.2440	8.178E-03	2.0944	5.6744E-02	1.096E-08
20	0.4411	0.2953	2.023E-03	2.0944	3.8711E-03	1.773E-08
23	0.4477	0.2998	1.349E-03	2.0944	4.5581E-03	1.652E-08
24	0.4372	0.2927	2.333E-03	2.0944	1.7103E-02	1.576E-08
31	0.4530	0.3034	7.721E-04	2.0944	7.2105E-03	1.733E-08
37	0.4604	0.3086	2.533E-07	2.0944	3.7252E-04	1.700E-08
38	0.4604	0.3086	9.132E-09	2.0944	2.9120E-06	1.700E-08
44	0.4605	0.3130	1.282E-07	2.0944	2.7799E-03	1.700E-08
45	0.4605	0.3130	2.762E-11	2.0944	3.3570E-06	1.700E-08

Table 5.4: H-S-Grid for M=20 & L=10.

The final values of central (Hcent) and minimum (Hmin) film thicknesses obtained using the NRS-S-Grid, the NRS-M-Grid and the H-S-Grid are summarised in Table (5.5) Also shown in Table (5.5) are the values obtained by Venner [97] and Ehret [33] who have used the multigrid method using a relaxation scheme which is described in Chapter 3. On a 65×65 domain, the discrepancy between the values of Hcent and Hmin obtained using the NRS-S-Grid, the NRS-M-Grid and the H-S-Grid is minimal. However, the discrepancy in these values compared to those obtained by Venner [97] is between 6% and 16%. Table (5.5) also shows the results obtained using the new relaxation scheme (NRS-M-Grid), the relaxation scheme of

Venner [97] and the relaxation scheme of Ehret [33]. These three schemes, that is NRS-M-Grid, Venner and Ehret, employ the multigrid method with a 257×257 finest grid using the domain $\{(X,Y) : -4.5 \leq X \leq 1.5, -3.0 \leq Y \leq 3.0\}$. These results show that the discrepancy between the results obtained using the new relaxation scheme and the relaxation scheme of Ehret is minimal while the results of Venner are some what more distant, though still comparable.

Method	Hcent	Hmin	Mesh	X-domain	Y-domain
NRS-S-Grid	0.453	0.306	65×65	[-5,1.2]	[-3.5,3.5]
NRS-M-Grid	0.453	0.305	65×65	[-5,1.2]	[-3.5,3.5]
H-S-Grid	0.460	0.313	65×65	[-5,1.2]	[-3.5,3.5]
Venner	0.489	0.355	65×65	[-4.5,1.5]	[-3.0,3.0]
NRS-M-Grid	0.443	0.304	257×257	[-4.5,1.5]	[-3.0,3.0]
Venner	0.498	0.345	257×257	[-4.5,1.5]	[-3.0,3.0]
Ehret	0.431	0.295	257×257	[-4.5,1.5]	[-3.0,3.0]

Table 5.5: Summary of Hcent and Hmin for M=20 & L=10.

Table (5.6) shows the effect of varying the computational domain on the central and minimum film thicknesses obtained using the NRS-M-Grid method on a 129×129 mesh. The domain is modified by changing the inlet boundary and as can be seen from Table (5.6), the size of the domain does have an effect on the solution.

Method	Hcent	Hmin	Mesh	X-domain	Y-domain
NRS-M-Grid	0.408	0.291	129×129	[-2.0,2.0]	[-3.0,3.0]
NRS-M-Grid	0.432	0.296	129×129	[-3.0,2.0]	[-3.0,3.0]
NRS-M-Grid	0.451	0.308	129×129	[-4.0,2.0]	[-3.0,3.0]
NRS-M-Grid	0.469	0.319	129×129	[-5.0,2.0]	[-3.0,3.0]
NRS-M-Grid	0.486	0.331	129×129	[-6.0,2.0]	[-3.0,3.0]
NRS-M-Grid	0.492	0.335	129×129	[-7.0,2.0]	[-3.0,3.0]

Table 5.6: Summary of Hcent and Hmin for M=20 & L=10 on different domains.

5.1.2 Remarks

A point to note is that when using the homotopy method, the force balance equation, labelled SumP in Table (5.4), is satisfied on every iteration but this is not the case when the new relaxation scheme is employed on a single grid or multigrid.

An interesting feature about the homotopy method is in the behaviour of the the Root Mean Square Residual (RMSRES). It does not only decrease monotonically but also has a feature of a sudden sharp drop as can be seen more clearly from Table (5.4). This may be attributed to the quadratic rate of convergence of the homotopy method close to the root. A sudden sharp decrease in ΔP_s can also be noticed in Table (5.4).

From Table (5.6), we can conclude that the solution is sensitive to the size of the computational domain. On a unifrom mesh, the number of mesh points are evenly distributed. The smaller the size of the domain, the larger the number of mesh points in the contact region and the vice versa is true on a larger domain. This might be the reason for the sensitivity of the solution to the size of the computational domain as the solution changes rapidly in the contact region. One way of overcoming this problem might be to use a non-uniform mesh where the majority of the mesh points are distributed in the contact region.

The Homotopy method is very robust but at expense of large computational time. Hence, it was not possible to use a finer mesh than 65×65. The times taken to achieve the results using the NRS-S-Grid, the NRS-M-Grid and the H-S-Grid were 13.5 minutes, 2.9 minutes and 5.73 hours respectively. An SGI R8000 was used for solutions obtained using the new relaxation scheme whereas an R10000 processor was used for the homotopy method.

5.2 CPU Times

For all the test problems to follow in this chapter, the CPU times on an SGI R8000 for solutions obtained using the new relaxation scheme on a multigrid are as follows: 1 and 15 minutes for each multigrid iteration (V-cycle) on a 129×129 and 257×257 meshes respectively. Depending on the load, the solution to each test

problem takes between 8 and 15 multigrid iterations. The CPU times for solutions obtained using the other methods were not available to the author and hence have not been specified unless stated otherwise.

5.3 Case Two

Numerical solutions of three sets of five problems are obtained using the New Relaxation Scheme (NRS) on a multigrid and the obtained minimum and central film thicknesses are compared with those obtained by Wang [102] and Ehret [33], who have respectively employed the Effective Influence Newton method (EIN) and the Multigrid Multi-Integration method (MIM). The relaxation scheme employed by Ehret is very similar to that used by Venner [97] and is described in Chapter 3. The input parameters describing these problems are shown in Table (5.7).

Parameters	Set 1	Set 2	Set 3
Viscosity index α $[Pa^{-1}]$	$[\ 2.20866 \times 10^{-8}$	to	$2.24787 \times 10^{-8}]$
Hertzian pressure p_h $[GPa]$	[0.44	to	3.68]
$\overline{\alpha} = \alpha\, p_h$	[10	to	82]
Material parameter G	[	4869	]
Load parameter W	$[0.173 \times 10^{-6}$	to	$98.19 \times 10^{-6}]$
Speed parameter U	0.089×10^{-10}	0.343×10^{-10}	5.707×10^{-10}
Moes parameter M	[20	to	500]
Moes parameter L	10	14	28

Table 5.7: Input parameters for the problems in Case Two.

The results obtained by Wang [102] using the effective influence Newton method are obtained on a single 151×81 grid with the following domains:

$$[M = 20 \Rightarrow (-6 \leq X \leq 1.5)\, and\, (-4 \leq Y \leq 4)],$$
$$[M = 50 \Rightarrow (-5 \leq X \leq 1.5)\, and\, (-2.5 \leq Y \leq 2.5)],$$
$$[M = 100 \Rightarrow (-4 \leq X \leq 1.5)\, and\, (-2.5 \leq Y \leq 2.5)],$$
$$[M = 200 \Rightarrow (-3 \leq X \leq 1.5)\, and\, (-2 \leq Y \leq 2)],$$
$$[M = 500 \Rightarrow (-2.5 \leq X \leq 1.25)\, and\, (-1.8 \leq Y \leq 1.8)].$$

The solutions obtained by Ehret [33] using the multigrid multi-integration method

employs a finest 513×513 grid and a coarsest 17×17 grid with the domain dependent on the Moes parameter M. The domains are given by

$$[M \leq 10 \Rightarrow (-7 \leq X \leq 2)\, and\, (-4.5 \leq Y \leq 4.5)],$$
$$[10 < M \leq 50 \Rightarrow (-5 \leq X \leq 2)\, and\, (-3.5 \leq Y \leq 3.5)] \text{ and}$$
$$[50 < M \leq 500 \Rightarrow (-4.5 \leq X \leq 1.5)\, and\, (-3 \leq Y \leq 3)].$$

When the solutions are obtained using the new relaxation scheme on a multigrid, different domains and mesh points are used. When the Moes parameter L is fixed at 10 and 28, a finest grid of 129×129 and a coarsest grid of 17×17 with a domain $-4.5 \leq X \leq 1.5$ and $-3 \leq Y \leq 3$ is used. However, when $L = 14$, a finest grid with 257×257 mesh points and a coarsest 17×17 grid is used and the domain employed is the same as that used by Ehret [33] in his multigrid multi-integration method.

5.3.1 Results

The minimum and central film thicknesses obtained using the three methods, the Effective Influence Newton method (EIN), the Multigrid Multi-Integration method (MIM) and the New Relaxation Scheme (NRS), are compared and the results are presented in Tables (5.9), (5.10), (5.11), (5.12), (5.13) and (5.14). A graphical representation is also shown in Figures (5.1), (5.2) and (5.3), where the Moes parameter M is plotted against the minimum and central film thicknesses using a logarithmic scale on both axes. Also shown in these tables and figures are the minimum and central film thicknesses predicted using the Hamrock and Dowson relationship (H-D) [47] which is given by

$$H_{min} = 1.79\, U^{0.68}\, W^{-0.073}\, G^{0.49} \tag{5.4}$$

and

$$H_{cen} = 1.89\, U^{0.67}\, W^{-0.067}\, G^{0.53}\ . \tag{5.5}$$

Table (5.8) shows a summary of the notation used in the Tables (5.9, 5.10, 5.11, 5.12, 5.13 and 5.14) and Figures (5.1, 5.2, 5.3, 5.4, 5.5 and 5.6).

Notation	Meaning
H-D	Hamrock and Dowson
EIN	Effective Influence Newton Method of Wang [102]
MIM	Multi-Integration Method of Ehret [33]
NRS	New Relaxation Scheme [74, 75]
Hm	Minimum film thickness
Hc	Central film thickness
P_M20	Pressure profile for M=20
H_M20	Film thickness profile for M=20

Table 5.8: Summary of notation used in the Tables and Figures to follow.

M	W	p_h	H-D	EIN	MIM	NRS
	$\times 10^{-6}$	GPa	(	$\times 10^{-6}$		)
20	0.173	0.44	10.96	11.90	12.08	12.31
50	0.433	0.60	10.25	10.06	10.26	10.64
100	0.867	0.76	9.71	8.53	8.88	8.99
200	1.733	0.96	9.26	7.21	7.43	7.40
500	4.333	1.30	8.66	5.44	5.82	5.03

Table 5.9: Minimum film thicknesses for $L = 10$, $U = 0.089 \times 10^{-10}$ and $G = 4869$.

M	W	p_h	H-D	EIN	MIM	NRS
	$\times 10^{-6}$	GPa	(	$\times 10^{-6}$		)
20	0.173	0.44	19.17	17.58	17.79	18.27
50	0.433	0.60	18.02	16.88	17.17	18.02
100	0.867	0.76	17.21	16.09	16.59	17.24
200	1.733	0.96	16.43	15.28	15.66	16.59
500	4.333	1.30	15.45	14.11	14.77	15.64

Table 5.10: Central film thicknesses for $L = 10$, $U = 0.089 \times 10^{-10}$ and $G = 4869$.

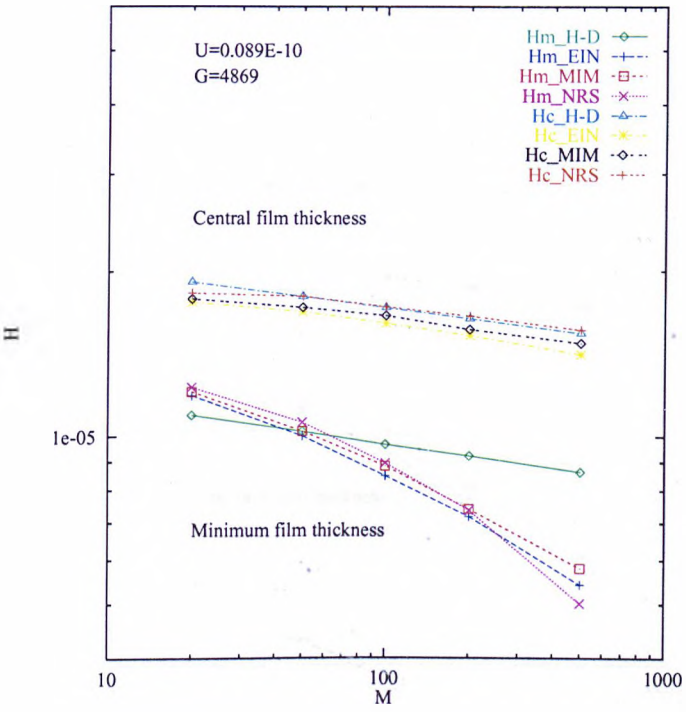

Figure 5.1: Minimum and central film thicknesses for $L = 10$.

M	W $\times 10^{-6}$	p_h GPa	H-D (	EIN $\times 10^{-6}$	MIM	NRS)
20	0.477	0.62	25.41	28.39	28.98	28.55
50	1.191	0.85	23.77	24.40	25.02	25.28
100	2.384	1.07	22.60	20.95	21.87	21.82
200	4.767	1.35	21.48	17.79	18.73	18.71
500	11.92	1.82	20.09	13.63	14.63	14.54

Table 5.11: Minimum film thicknesses for $L = 14$, $U = 0.343 \times 10^{-10}$ and $G = 4869$.

M	W $\times 10^{-6}$	p_h GPa	H-D (	EIN $\times 10^{-6}$	MIM	NRS)
20	0.477	0.62	44.13	40.86	41.54	41.03
50	1.191	0.85	41.51	39.48	40.30	41.01
100	2.384	1.07	39.62	37.77	39.13	39.25
200	4.767	1.35	37.82	36.06	37.71	38.16
500	11.92	1.82	35.57	33.47	35.19	36.82

Table 5.12: Central film thicknesses for $L = 14$, $U = 0.343 \times 10^{-10}$ and $G = 4869$.

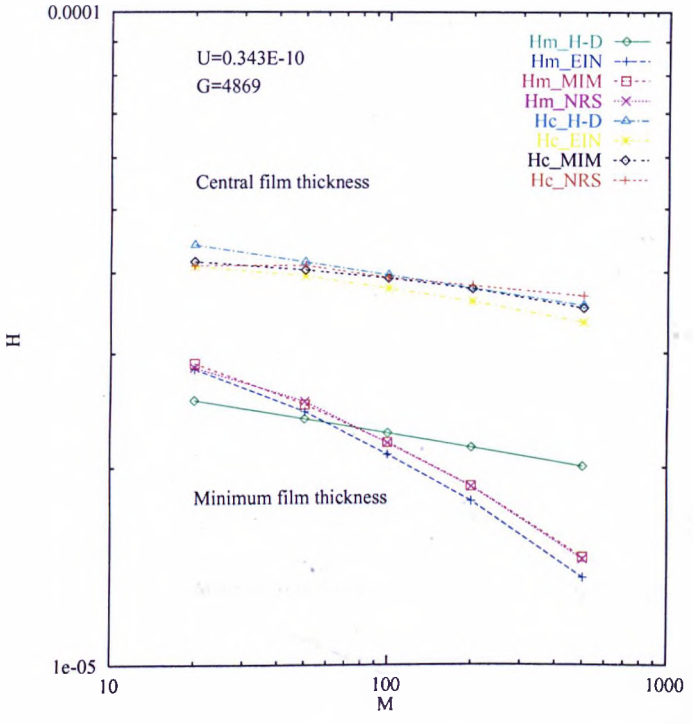

Figure 5.2: Minimum and central film thicknesses for $L = 14$.

M	W	p_h	H-D	EIN	MIM	NRS
	$\times 10^{-6}$	GPa	(	$\times 10^{-6}$		)
20	3.927	1.26	147.49	184.21	185.57	190.83
50	9.818	1.72	137.73	160.17	166.12	176.87
100	19.64	2.15	131.14	144.00	148.49	148.19
200	39.27	2.71	124.67	124.16	129.87	125.93
500	98.19	3.68	116.61	98.19	104.02	95.17

Table 5.13: Minimum film thicknesses for $L = 28$, $U = 5.707 \times 10^{-10}$ and $G = 4869$.

M	W	p_h	H-D	EIN	MIM	NRS
	$\times 10^{-6}$	GPa	(	$\times 10^{-6}$		)
20	3.927	1.26	252.19	247.05	247.82	252.94
50	9.818	1.72	236.81	242.89	245.02	255.99
100	19.64	2.15	226.41	233.52	239.56	245.61
200	39.27	2.71	216.14	225.07	233.76	241.44
500	98.19	3.68	203.27	212.93	220.54	231.18

Table 5.14: Central film thicknesses for $L = 28$, $U = 5.707 \times 10^{-10}$ and $G = 4869$.

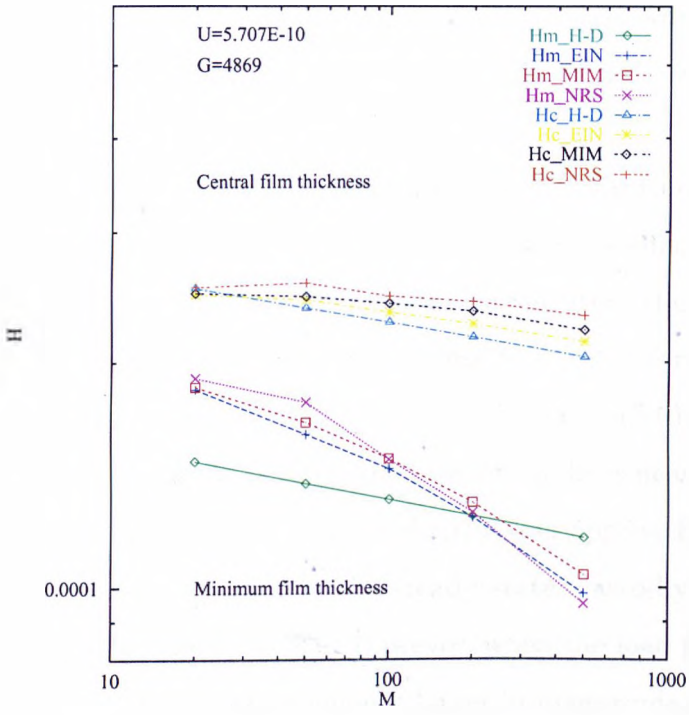

Figure 5.3: Minimum and central film thicknesses for $L = 28$.

5.3.2 Discussion

The discrepancy in the minimum and central film thicknesses predicted using the Hamrock and Dowson relationship is large when compared with the values obtained using the other three methods. This is more evident in the minimum film thicknesses. This can be attributed to the fact that the Hamrock and Dowson relationship [47] was derived not only using solutions where the maximum Hertzian pressure was less than $1\,GPa$ but also using a smaller number of grid points. The minimum and central film thicknesses obtained by Ehret [33] using the multigrid multi-integration method are sandwiched between the values obtained by Wang [102] who used the effective influence Newton method and the new relaxation scheme which is developed and used in this work. The discrepancies in the minimum and the central film thicknesses obtained using the three methods can be attributed to the use of different mesh domains and number of mesh points. When $L = 14$, the discrepancy in the minimum and central film thicknesses obtained using the new relaxation scheme is minimal when compared with those obtained by Ehret [33] using the multigrid multi-integration method. For this problem, that is when

$L = 14$, the number of mesh points employed on the finest grid when using the new relaxation scheme is 257×257 whereas for the problems when $L = 10$ and $L = 28$ a finest grid of 129×129 is used.

From the obtained results, we can conclude that the Hamrock and Dowson's load parameter W or the Moes parameter M have an effect on the elasto-hydrodynamic lubrication problems. This is more evident from the profiles of pressure and film thickness along the X axis. These profiles, that is for $L = 10$, $L = 14$ and $L = 28$, are respectively shown in Figures (5.4), (5.5) and (5.6). When the load parameter W or the parameter M is large, the pressure spike is nearer the exit zone and is smaller in magnitude and the pressure distribution approaches the Hertzian pressure profile. This is consistent with the steady state elasto-hydrodynamic lubrication analysis of Sadeghi and Sui [88]. However, when the load parameter W or the parameter M is small, the pressure spike is larger in magnitude and its position is away from the exit zone and closer to the central contact region. The pressure profile in the inlet zone decreases as the load parameter W or the parameter M increases. With regards to the film thicknesses, we can conclude that as the load parameter W or the parameter M increases, the minimum film thickness is affected more than the central film thickness and the minimum film thickness moves away from the central contact region and moves towards the exit zone.

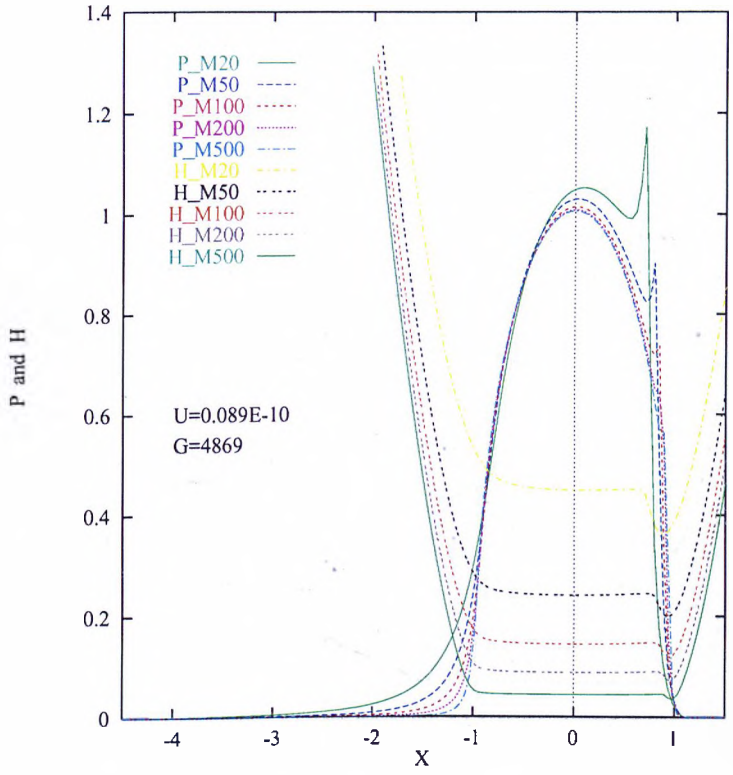

Figure 5.4: Pressure and film profiles for $L = 10$ along the X axis.

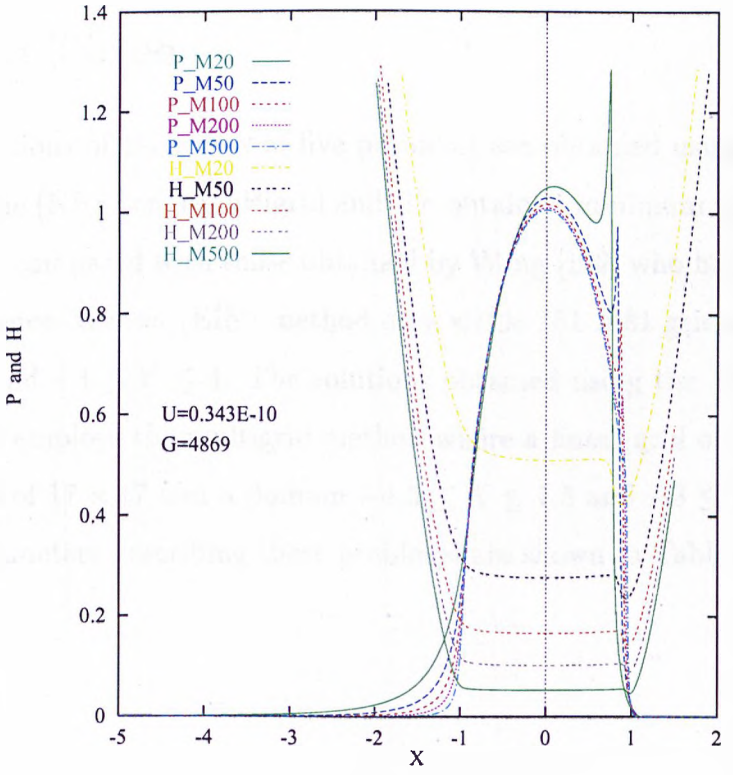

Figure 5.5: Pressure and film profiles for $L = 14$ along the X axis.

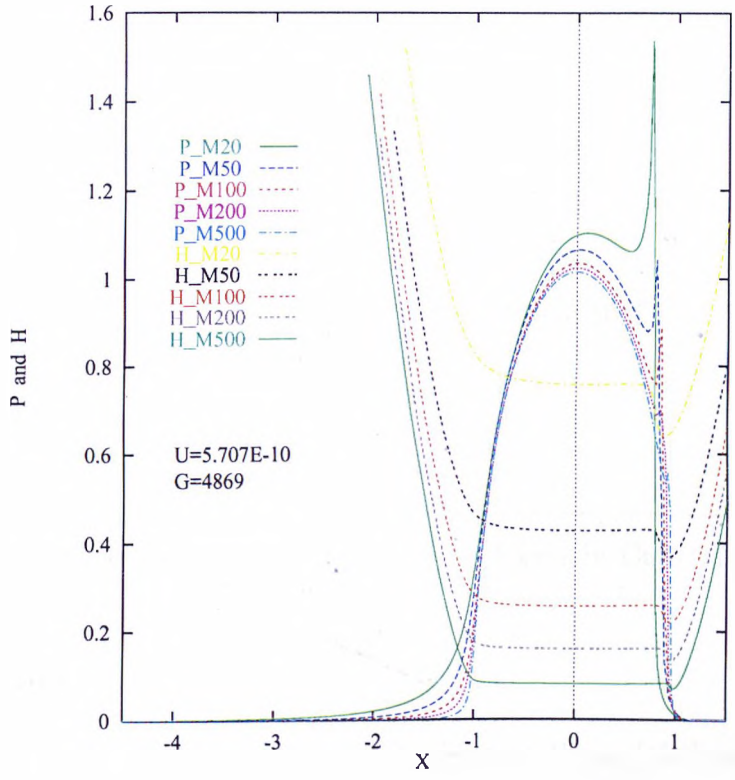

Figure 5.6: Pressure and film profiles for $L = 28$ along the X axis.

5.4 Case Three

Numerical solutions of three sets of five problems are obtained using the New Relaxation Scheme (NRS) on a multigrid and the obtained minimum and central film thicknesses are compared with those obtained by Wang [102] who has employed the Effective Influence Newton (EIN) method on a single 151×81 grid with a domain $-8 \leq X \leq 1$ and $-4 \leq Y \leq 4$. The solutions obtained using the New Relaxation Scheme (NRS) employs the multigrid method where a finest grid of 129×129 and a coarsest grid of 17×17 and a domain $-4.5 \leq X \leq 1.5$ and $-3 \leq Y \leq 3$ is used. The input parameters describing these problems are shown in Table (5.15).

Parameters	Set 1	Set 2	Set 3
Viscosity index α $[Pa^{-1}]$	2.22503×10^{-8}	2.21977×10^{-8}	2.20618×10^{-8}
Hertzian pressure p_h $[GPa]$	0.72	1.05	1.21
$\overline{\alpha} = \alpha\, p_h$	16	23	27
Material parameter G	[	4865	]
Load parameter W	0.7381×10^{-6}	2.273×10^{-6}	3.415×10^{-6}
Speed parameter U	$[0.094 \times 10^{-10}$	to	$1.87 \times 10^{-10}]$
Moes parameter M	[9	to	378]
Moes parameter L	[10	to	21]

Table 5.15: Input parameters for the problems in Case Three.

5.4.1 Results

The minimum and central film thicknesses obtained by Wang [102] using the Effective Influence Newton method (EIN) and the New Relaxation Scheme (NRS) which is developed and employed in this work are presented in Tables (5.17), (5.18), (5.19), (5.20), (5.21) and (5.22). A graphical representation is also shown in Figures (5.7), (5.8) and (5.9) where the speed parameter U is plotted against the minimum and central film thicknesses using a logarithmic scale on both axes. Also shown in these Tables and Figures are the minimum and central film thicknesses predicted using the Hamrock and Dowson relationship (H-D) [47] which is given by equations (5.4) and (5.5) respectively. The discrepancy in the minimum and central film thicknesses obtained using Effective Influence Newton method (EIN) of Wang [102] and the New Relaxation Scheme (NRS) which is developed and employed in this work increases as the speed increases and this is more evident in the minimum film thicknesses. The discrepancies can be attributed to the use of different mesh domains and number of mesh points.

Table (5.16) shows a summary of the notation used in the Tables (5.17, 5.18, 5.19, 5.20, 5.21 and 5.22) and Figures (5.7, 5.8, 5.9, 5.10, 5.11 and 5.12).

Notation	Meaning
H-D	Hamrock and Dowson
EIN	Effective Influence Newton Method of Wang [102]
NRS	New Relaxation Scheme [74, 75]
Hm	Minimum film thickness
Hc	Central film thickness
P:U=1.87E-10	Pressure profile when U=1.87E-10
H:U=1.87E-10	Film thickness profile when U=1.87E-10

Table 5.16: Summary of notation used in the Tables and Figures to follow.

M	L	U $\times 10^{-10}$	H-D (	EIN $\times 10^{-6}$	NRS)
82	10	0.094	09.23	10.18	10.16
49	12	0.187	16.33	16.31	18.06
25	15	0.468	33.92	30.40	36.03
15	18	0.935	56.91	49.70	59.35
9	21	1.870	95.88	75.29	91.09

Table 5.17: Minimum film thicknesses for $W = 0.7381 \times 10^{-6}$ and $p_h = 0.72GPa$.

M	L	U $\times 10^{-10}$	H-D (	EIN $\times 10^{-6}$	NRS)
82	10	0.094	16.78	17.95	18.54
49	12	0.187	26.90	28.56	29.84
25	15	0.468	49.58	52.77	52.96
15	18	0.935	77.64	83.95	81.19
9	21	1.870	122.66	128.51	116.61

Table 5.18: Central film thicknesses for $W = 0.7381 \times 10^{-6}$ and $p_h = 0.72GPa$.

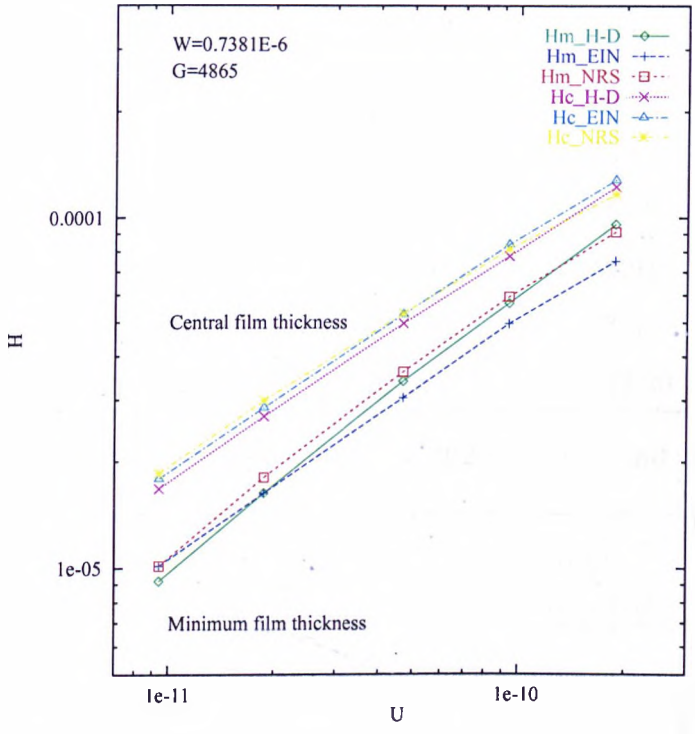

Figure 5.7: Minimum and central film thicknesses for $p_h = 0.72GPa$.

M	L	U $\times 10^{-10}$	H-D (	EIN $\times 10^{-6}$	NRS)
252	10	0.094	06.99	09.37	07.06
150	12	0.187	12.74	15.02	14.03
76	15	0.468	27.28	28.01	30.19
45	18	0.935	48.34	44.88	53.98
27	21	1.870	83.91	71.90	90.02

Table 5.19: Minimum film thicknesses for $W = 2.273 \times 10^{-6}$ and $p_h = 1.05GPa$.

M	L	U	H-D	EIN	NRS
		$\times 10^{-10}$	(	$\times 10^{-6}$	)
252	10	0.094	15.46	16.64	16.83
150	12	0.187	25.03	26.48	28.03
76	15	0.468	46.65	48.95	52.06
45	18	0.935	74.79	77.88	84.59
27	21	1.870	119.67	123.90	129.10

Table 5.20: Central film thicknesses for $W = 2.273 \times 10^{-6}$ and $p_h = 1.05GPa$.

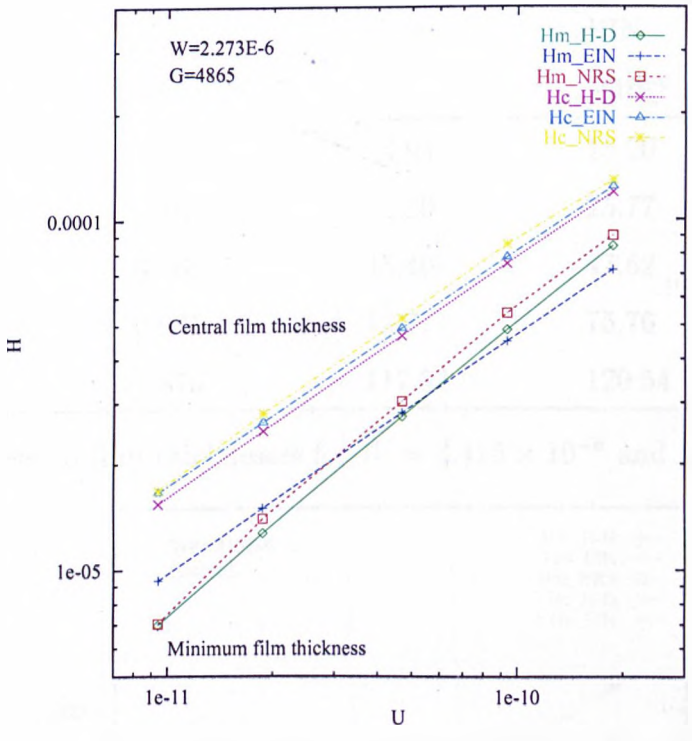

Figure 5.8: Minimum and central film thicknesses for $p_h = 1.05GPa$.

M	L	U	H-D	EIN	NRS
		$\times 10^{-10}$	(	$\times 10^{-6}$	)
378	10	0.094	06.21	09.10	6.10
226	12	0.187	11.49	14.58	11.51
113	15	0.468	25.04	27.18	27.47
68	18	0.935	44.01	43.55	47.23
40	21	1.870	78.11	69.77	86.02

Table 5.21: Minimum film thicknesses for $W = 3.415 \times 10^{-6}$ and $p_h = 1.21GPa$.

M	L	U	H-D	EIN	NRS
		$\times 10^{-10}$	(	$\times 10^{-6}$	)
378	10	0.094	14.94	16.20	16.54
226	12	0.187	24.29	25.77	26.05
113	15	0.468	45.40	47.62	50.49
68	18	0.935	72.77	75.76	77.82
40	21	1.870	117.03	120.54	129.75

Table 5.22: Central film thicknesses for $W = 3.415 \times 10^{-6}$ and $p_h = 1.21GPa$.

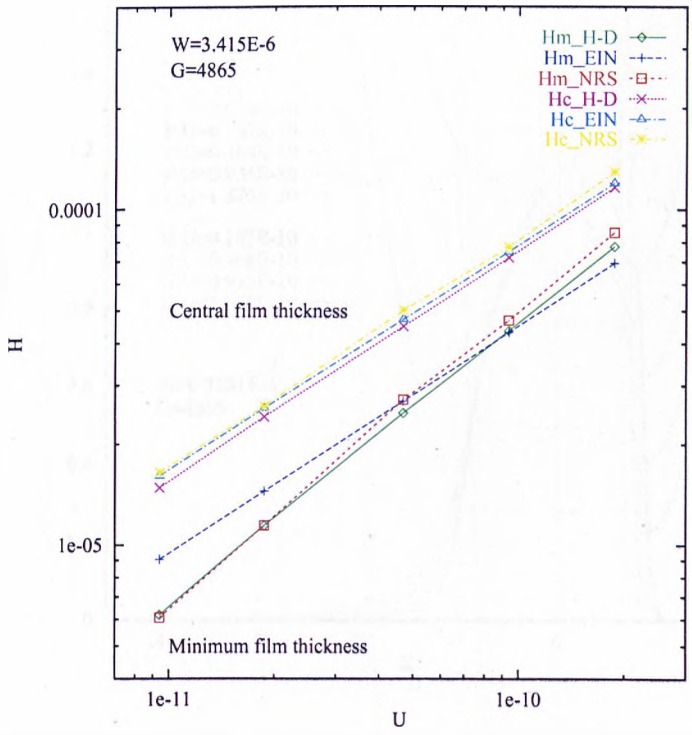

Figure 5.9: Minimum and central film thicknesses for $p_h = 1.21GPa$.

5.4.2 Discussion

From the above results, we can conclude that the Hamrock and Dowson's speed parameter U has a strong effect on the elasto-hydrodynamic lubrication problems. This is more evident from the profiles of pressure and film thickness along the X axis. These profiles, that is for $p_h = 0.72\,GPa$, $p_h = 1.05\,GPa$ and $p_h = 1.21\,GPa$, are respectively shown in Figures (5.10), (5.11) and (5.12). At low speeds, the pressure profile is very close to the Hertzian pressure profile and the pressure spike is close to the outlet region. However, at high speeds, the pressure profile distorts from the Hertzian form and the spike grows in magnitude with a sharp pointed peak which is close to the central contact region and away from the outlet region. The pressure profile in the inlet region increases gradually with speed. With regards to the film thickness, we can conclude that as the speed parameter U increases, the film thickness increases and the portion of the contact area where the two surfaces are almost parallel decreases. All these observations have been confirmed by Hamrock and Dowson [49] and also by Wang [102].

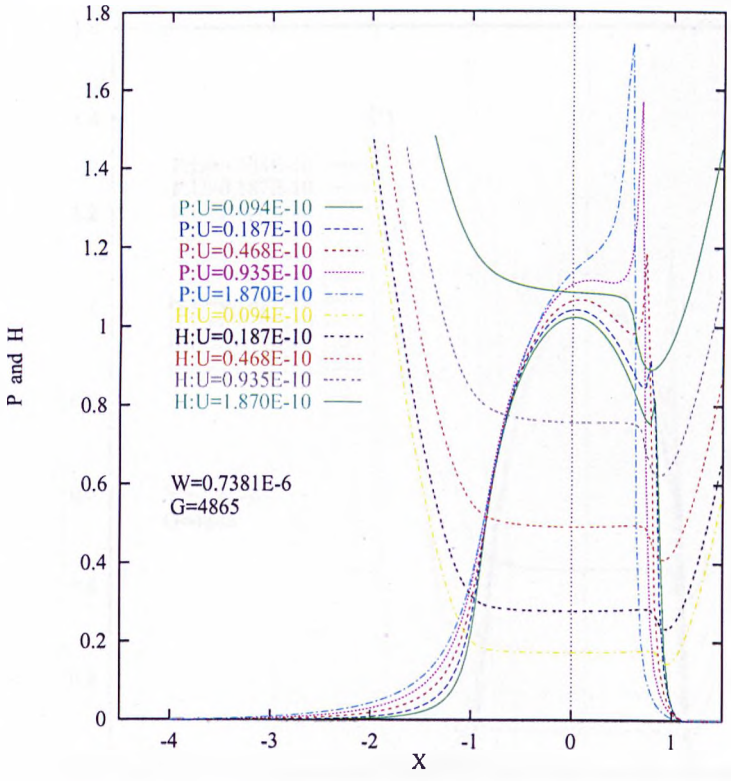

Figure 5.10: Pressure and film profiles for $p_h = 0.72\,GPa$ along the X axis.

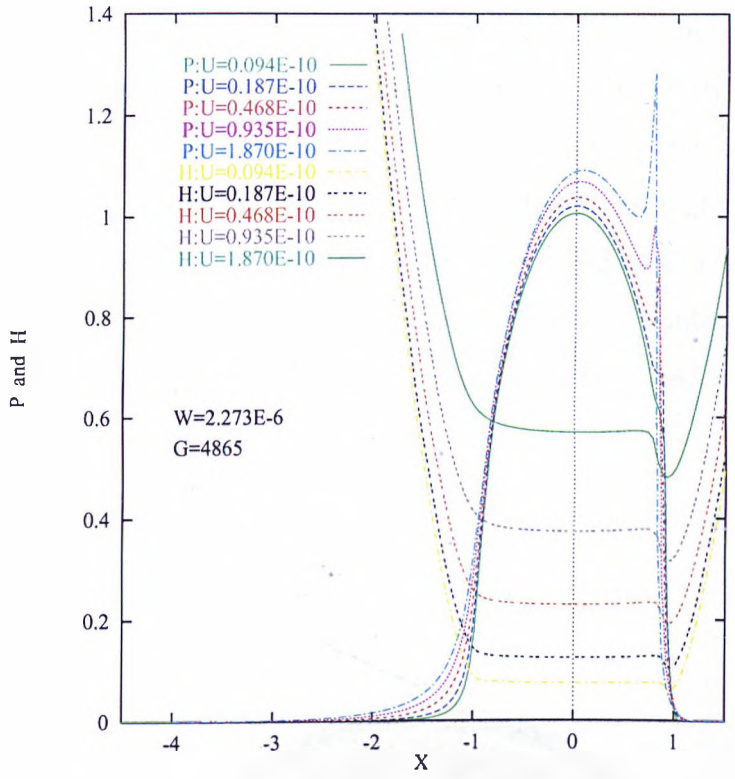

Figure 5.11: Pressure and film profiles for $p_h = 1.05\,GPa$ along the X axis.

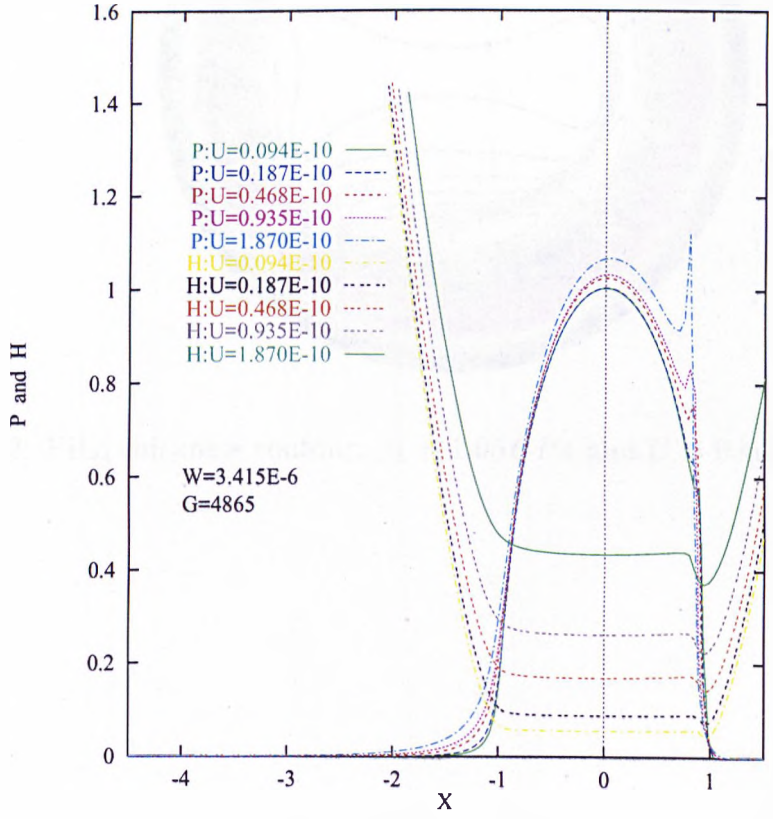

Figure 5.12: Pressure and film profiles for $p_h = 1.21\,GPa$ along the X axis.

Some of these features can also be seen in the contour and surface plots of film thickness and pressure for test problems where the maximum Hertzian pressure, p_h, is equal to $1.05\,GPa$. Figures (5.13), (5.14) and (5.15) show respectively the film thickness contour, pressure contour and pressure surface plot for when the speed parameter U is equal to $U = 0.468 \times 10^{-10}$ and Figures (5.16), (5.17) and (5.18) show respectively the film thickness contour, pressure contour and pressure surface plot for when the speed parameter U is equal to $U = 1.87 \times 10^{-10}$.

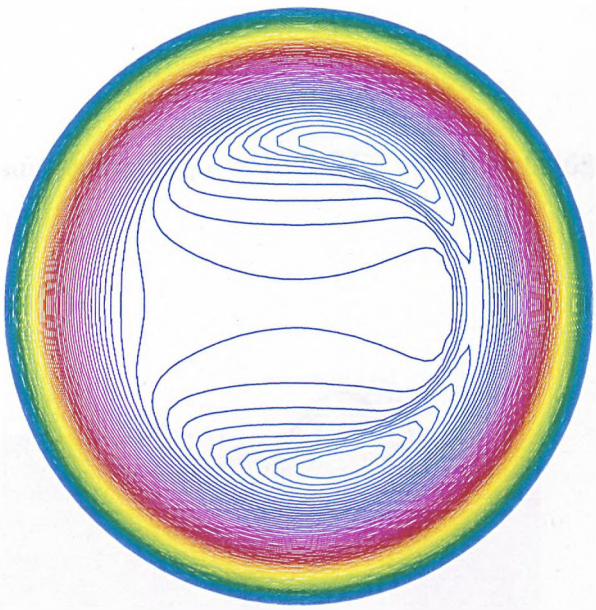

Figure 5.13: Film thickness contour: $p_h = 1.05\,GPa$ and $U = 0.468 \times 10^{-10}$.

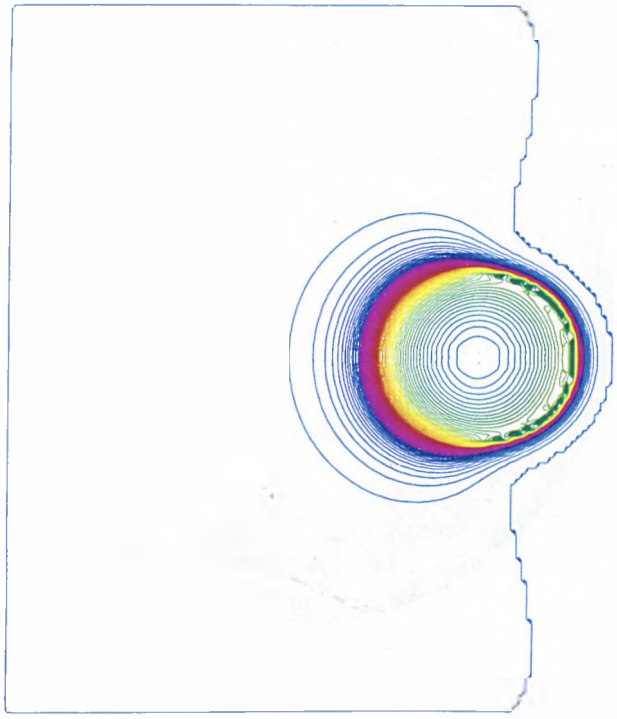

Figure 5.14: Pressure contour: $p_h = 1.05\,GPa$ and $U = 0.468 \times 10^{-10}$.

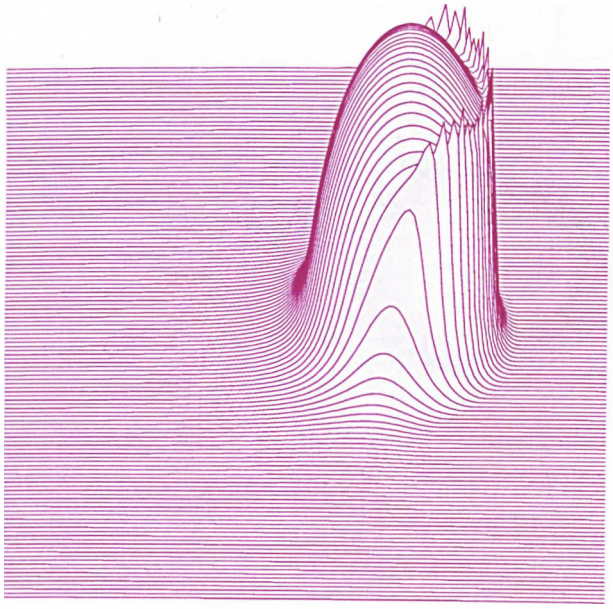

Figure 5.15: Pressure surface plot: $p_h = 1.05\,GPa$ and $U = 0.468 \times 10^{-10}$.

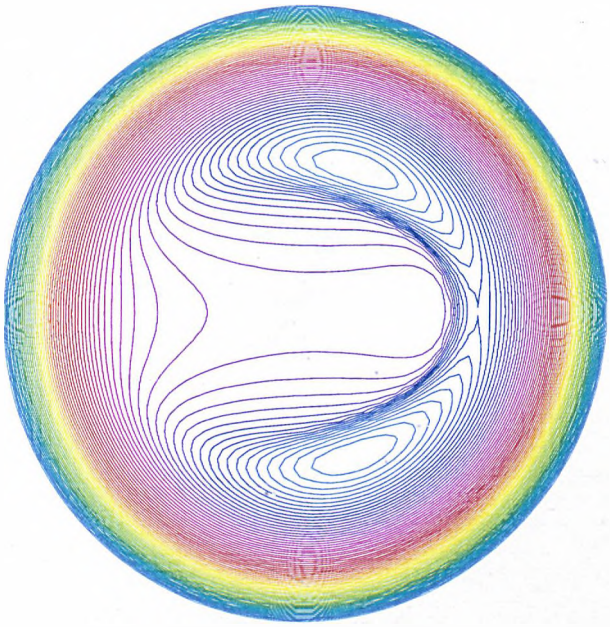

Figure 5.16: Film thickness contour: $p_h = 1.05\,GPa$ and $U = 1.87 \times 10^{-10}$.

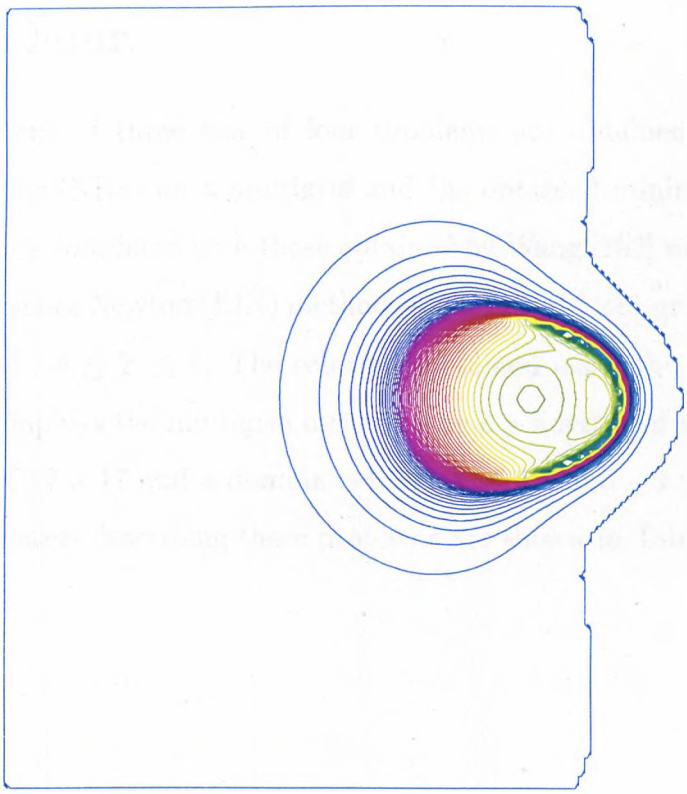

Figure 5.17: Pressure contour: $p_h = 1.05\,GPa$ and $U = 1.87 \times 10^{-10}$.

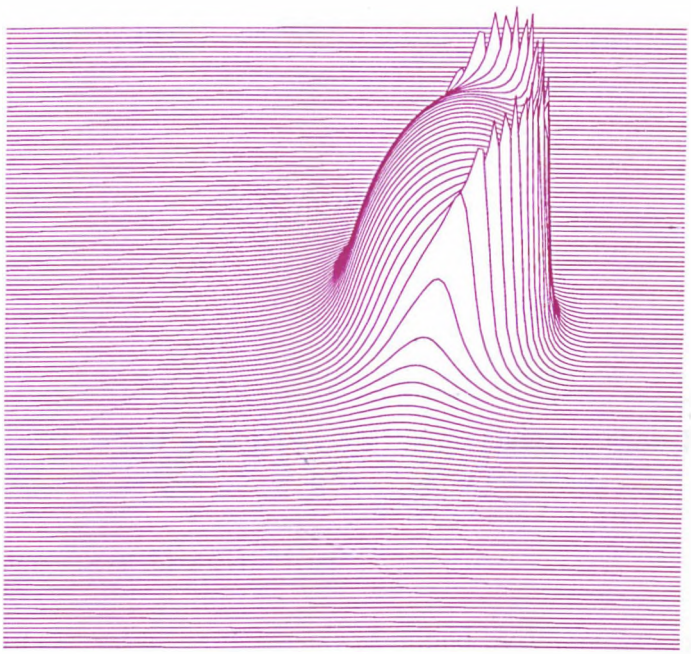

Figure 5.18: Pressure surface plot: $p_h = 1.05\,GPa$ and $U = 1.87 \times 10^{-10}$.

5.5 Case Four

Numerical solutions of three sets of four problems are obtained using the New Relaxation Scheme (NRS) on a multigrid and the obtained minimum and central film thicknesses are compared with those obtained by Wang [102] who has employed the Effective Influence Newton (EIN) method on a single 151×81 grid with a domain $-8 \leq X \leq 1$ and $-4 \leq Y \leq 4$. The solutions obtained using the New Relaxation Scheme (NRS) employs the multigrid method where a finest grid of 129×129 and a coarsest grid of 17×17 and a domain $-4.5 \leq X \leq 1.5$ and $-3 \leq Y \leq 3$ is used. The input parameters describing these problems are shown in Table (5.23).

Parameters	Set 1	Set 2	Set 3
Viscosity index α $[Pa^{-1}]$	$[0.50155 \times 10^{-8}$	to	$3.51433 \times 10^{-8}]$
Hertzian pressure p_h $[GPa]$	0.72	1.23	1.95
$\overline{\alpha} = \alpha\, p_h$	[4	to	69]
Material parameter G	[1136	to	7954]
Load parameter W	0.664×10^{-6}	3.311×10^{-6}	13.22×10^{-6}
Speed parameter U	[	1.344×10^{-10}	]
Moes parameter M	10	50	199
Moes parameter L	[5	to	32]

Table 5.23: Input parameters for the problems in Case Four.

5.5.1 Results and Discussion

The minimum and central film thicknesses obtained by Wang [102] using the Effective Influence Newton method (EIN) and the New Relaxation Scheme (NRS) which is developed and employed in this work are presented in Tables (5.25), (5.26), (5.27), (5.28), (5.29) and (5.30). A graphical representation is also shown in Figures (5.19), (5.20) and (5.21) where the material parameter G is plotted against the minimum and central film thicknesses using a logarithmic scale on both axes. Also shown in these Tables and Figures are the minimum and central film thicknesses predicted using the Hamrock and Dowson relationship (H-D) [47] which is given by equations (5.4) and (5.5) respectively. The discrepancy in the minimum and central film thicknesses obtained using Effective Influence Newton method (EIN) of Wang [102] and the New Relaxation Scheme (NRS) which is developed and employed in this work is minimal. The profiles of the pressure and the film thickness along the X-axis for the three problems are shown in Figures (5.22), (5.23) and (5.24). Generally, the type of material used determines the regime of lubrication which can either be elasto-hydrodynamic lubrication or purely hydrodynamic.

Table (5.16) shows a summary of the notation used in the Tables (5.25, 5.26, 5.27, 5.28, 5.29 and 5.30) and Figures (5.19, 5.20, 5.21, 5.22, 5.23 and 5.24).

Notation	Meaning
H-D	Hamrock and Dowson
EIN	Effective Influence Newton Method of Wang [102]
NRS	New Relaxation Scheme [74, 75]
Hm	Minimum film thickness
Hc	Central film thickness
P:G=7954	Pressure profile when G=7954
H:G=7954	Film thickness profile when G=7954

Table 5.24: Summary of notation used in the Tables and Figures to follow.

L	M	G	H-D	EIN	NRS
			(	$\times 10^{-6}$	)
5	10	1136	30.80	36.37	35.59
11	10	2727	47.30	55.41	55.45
20	10	4931	63.23	78.64	79.91
32	10	7954	79.92	105.15	108.89

Table 5.25: Minimum film thicknesses for $W = 0.664 \times 10^{-6}$ and $p_h = 0.72GPa$.

L	M	G	H-D	EIN	NRS
			(	$\times 10^{-6}$	)
5	10	1136	49.87	46.96	45.42
11	10	2727	79.33	73.57	73.73
20	10	4931	108.59	102.52	104.77
32	10	7954	139.90	135.25	138.87

Table 5.26: Central film thicknesses for $W = 0.664 \times 10^{-6}$ and $p_h = 0.72GPa$.

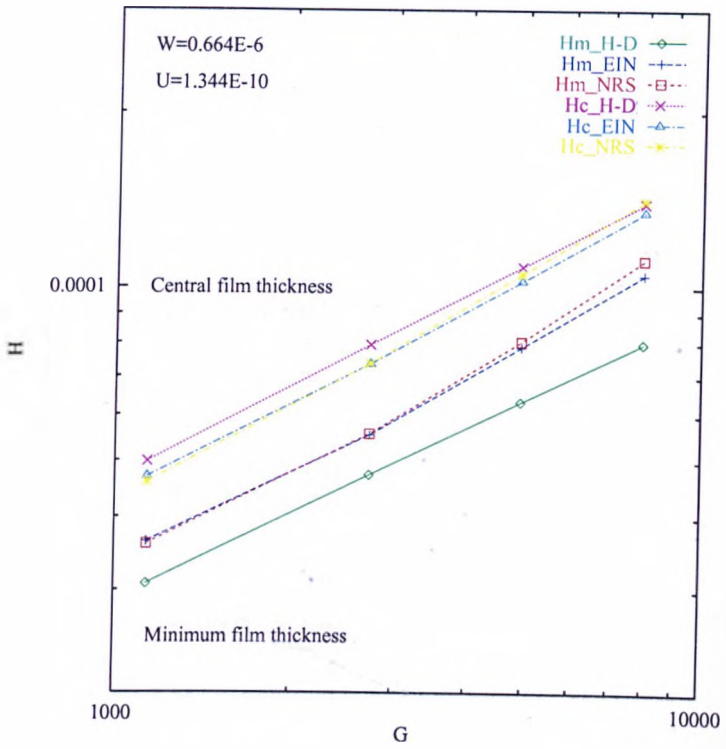

Figure 5.19: Minimum and central film thicknesses for $p_h = 0.72GPa$.

L	M	G	H-D	EIN	NRS
			(	$\times 10^{-6}$	)
5	50	1136	27.39	26.46	26.76
11	50	2727	42.07	42.61	42.97
20	50	4931	56.23	63.45	66.82
32	50	7954	71.08	89.22	98.71

Table 5.27: Minimum film thicknesses for $W = 3.311 \times 10^{-6}$ and $p_h = 1.23GPa$.

L	M	G	H-D	EIN	NRS
			(	$\times 10^{-6}$	)
5	50	1136	44.78	43.97	42.96
11	50	2727	71.23	69.63	70.69
20	50	4931	97.50	98.44	104.67
32	50	7954	125.63	131.67	146.67

Table 5.28: Central film thicknesses for $W = 3.311 \times 10^{-6}$ and $p_h = 1.23GPa$.

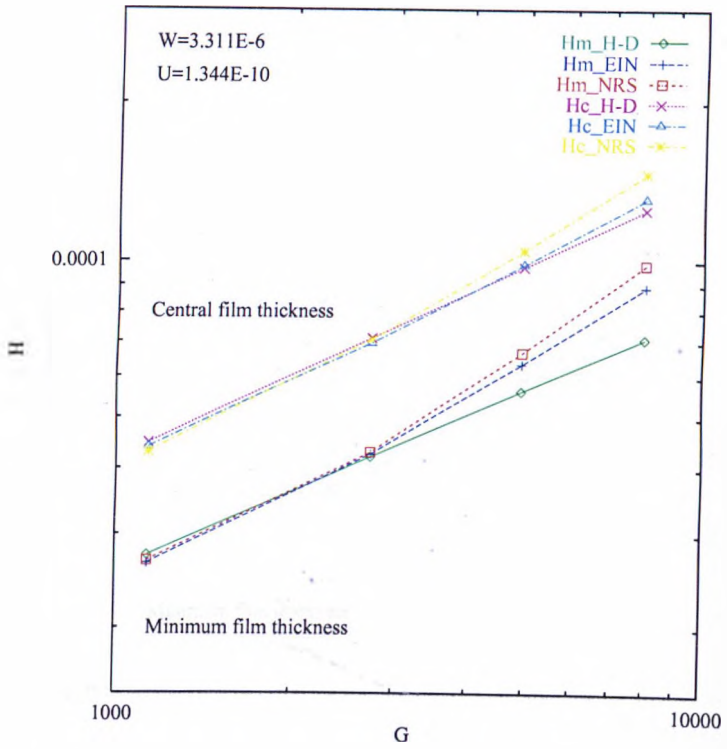

Figure 5.20: Minimum and central film thicknesses for $p_h = 1.23GPa$.

L	M	G	H-D (	EIN $\times 10^{-6}$	NRS)
5	199	1136	24.76	18.27	17.94
11	199	2727	38.02	30.29	29.49
20	199	4931	50.83	47.59	46.81
32	199	7954	64.25	68.38	69.83

Table 5.29: Minimum film thicknesses for $W = 13.22 \times 10^{-6}$ and $p_h = 1.95GPa$.

L	M	G	H-D (	EIN $\times 10^{-6}$	NRS)
5	199	1136	40.82	39.53	39.97
11	199	2727	64.92	63.61	64.76
20	199	4931	88.87	90.13	93.14
32	199	7954	114.50	122.91	127.35

Table 5.30: Central film thicknesses for $W = 13.22 \times 10^{-6}$ and $p_h = 1.95GPa$.

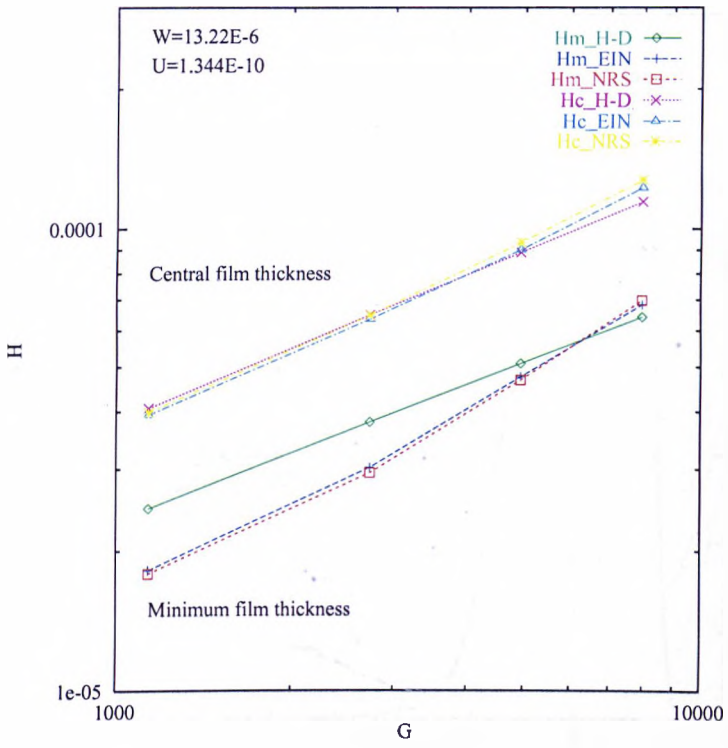

Figure 5.21: Minimum and central film thicknesses for $p_h = 1.95GPa$.

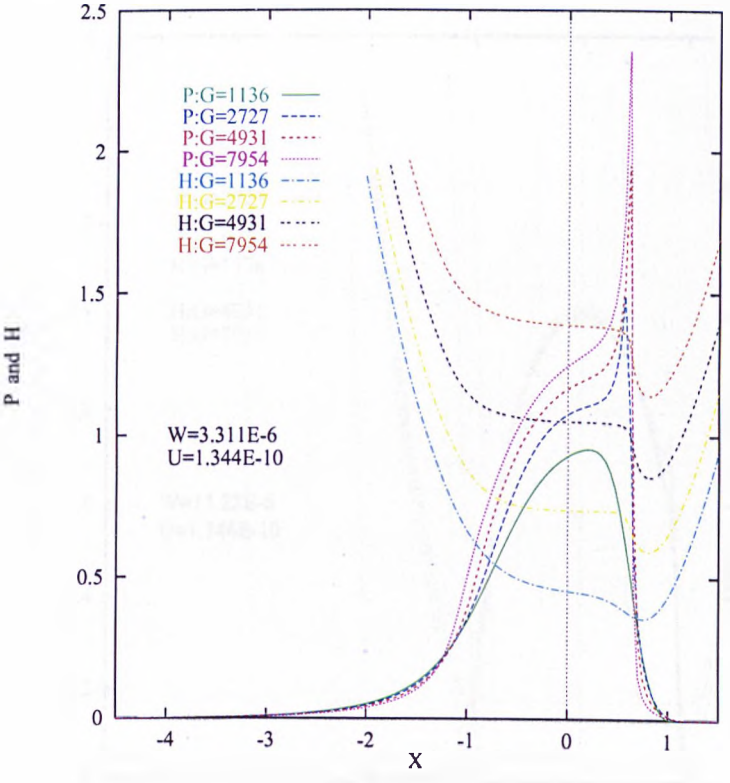

Figure 5.22: Pressure and film profiles for $p_h = 0.72GPa$ along the X axis.

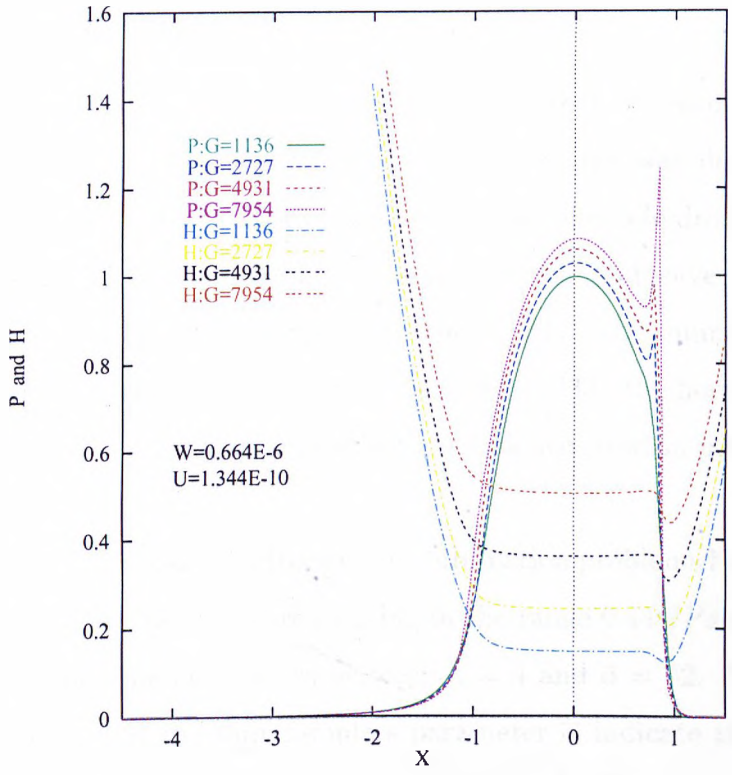

Figure 5.23: Pressure and film profiles for $p_h = 1.23GPa$ along the X axis.

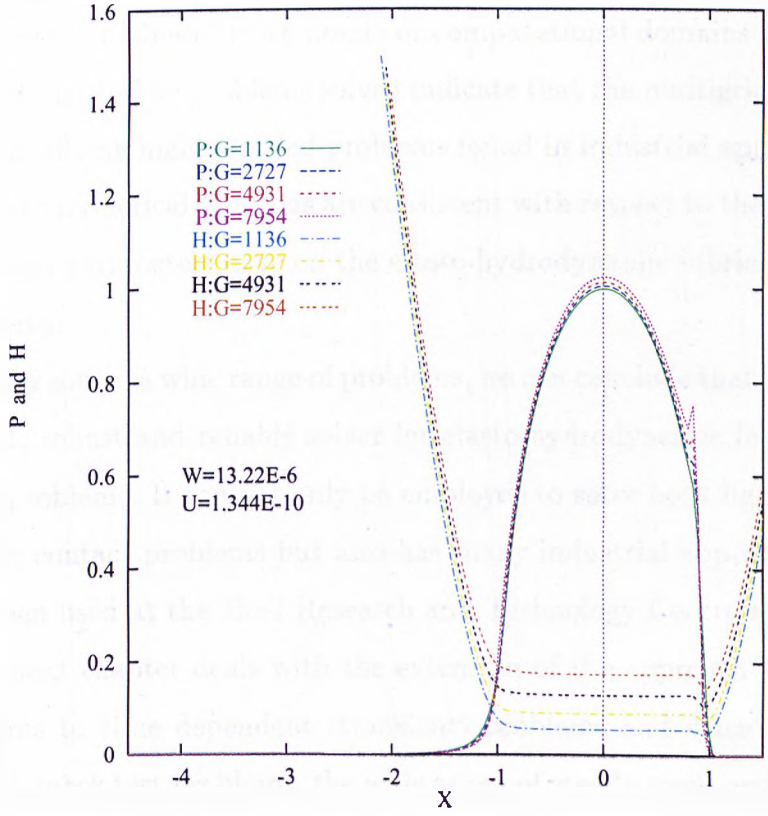

Figure 5.24: Pressure and film profiles for $p_h = 1.95GPa$ along the X axis.

5.6 Conclusion

The main intention in this chapter was to show the effectiveness of the multigrid solver for elasto-hydrodynamic lubrication problems which was described in the previous chapter. Numerical solutions of steady state elasto-hydrodynamic lubrication circular contact problems obtained using the multigrid solver are compared with those obtained using other numerical methods. The other numerical methods include the relaxation schemes of Venner [97] and Ehret [33], the homotopy method [4] which is used by Scales [75] and the effective influence Newton method of Wang [102].

A wide range of elasto-hydrodynamic lubrication problems have been solved with the maximum Hertzian pressure p_h lying in the range $0.44GPa$ and $3.68GPa$. The dimensionless parameter $\overline{\alpha}$ varies between $\overline{\alpha} = 4$ and $\overline{\alpha} = 82$. The maximum Hertzian pressure p_h and the dimensionless parameter $\overline{\alpha}$ indicate the load of the problem and the higher their values, the higher the load. The numerical solutions obtained using the multigrid solver are comparable with those obtained using other numerical schemes. Though some discrepancies do exist, these are mainly due to the use of different number of mesh points or computational domains and to the iterative methods used. The problems solved indicate that the multigrid solver is not only capable of solving highly loaded problems found in industrial applications but also the obtained numerical solutions are consistent with respect to the effects Hamrock and Dowson parameters have on the elasto-hydrodynamic lubrication circular contact problems.

Having solved a wide range of problems, we can conclude that the multigrid solver is a fast, robust and reliable solver for elasto-hydrodynamic lubrication circular contact problems. It can not only be employed to solve both lightly to highly loaded circular contact problems but also has many industrial applications and it has already been used at the Shell Research and Technology Centre at Thornton.

The next chapter deals with the extension of the approach used here for steady problems to time dependent (transient) problems and since there are no available bench mark test problems, the wide range of steady state problems solved in this chapter will be used as a guideline for the solutions of transient problems.

Chapter 6

TRANSIENT PROBLEMS

Over the past decade, the interest in elasto-hydrodynamic lubrication has moved on from steady state to time-dependent (or transient) problems. In practice, the need for a time-dependent approach is essential since, in general, the surfaces in contact are in relative motion and the load, the speed and the film thickness vary with time. The earlier numerical work on elasto-hydrodynamic lubrication was all based on steady state problems. The large computational costs and the complexities associated with these problems are the reasons why there has been a lack of development in the direction of transient problems.

Most of the recent work on transient problems [98] [32] is still concerned with studying surface features, especially surface roughness, but mainly looking at the line contact problems. Work on the point contact problems is still very limited. Up to this date, all the work done on the transient elasto-hydrodynamic lubrication problems makes use of fixed time steps. The time steps are usually chosen in an arbitrary way and no published work on variable time step methods or local error control is known to the author. Also of great importance is the issue of keeping computational costs to a minimum. This can be achieved by using an efficient convergence criterion which must give a true picture of the solution. Though the existing methods are commonly used, they can sometimes give misleading results

as described in Chapter 5.

This chapter will look at transient elasto-hydrodynamic lubrication problems by presenting the governing equations as differential algebraic equations. We will consider solutions to transient problems with fixed and variable time steps and also present a new convergence testing criterion when solving transient elasto-hydrodynamic lubrication problems. The new technique is used when solving differential algebraic equations and was originally developed by Shampine [90] for ordinary differential equations. This chapter will be concluded by presenting demanding test problems where the speeds of the two surfaces in contact are varied with time with the aim of zero and reversal entrainments. This is where the speeds of the two surfaces in contact are driven down to zero and then introducing a reversal entrainment, that is reversing the direction of flow using negative speeds. In general, when solving elasto-hydrodynamic lubrication problems, the oil entrainment is usually assumed to be in the positive X-direction.

6.1 Governing Equations

The governing equations (the Reynolds equation (2.19), the film thickness equation (2.22) and the force balance equation (2.24)) of elasto-hydrodynamic lubrication circular contact problems are introduced in Chapter 2. The only difference between the equations of steady state and transient elasto-hydrodynamic lubrication problems is in the Reynolds equation. In steady state elasto-hydrodynamic lubrication problems, the contribution from the squeeze term $\frac{\partial(\overline{\rho}H)}{\partial T}$, which describes the net flow rates due to the squeezing motion, in the Reynolds equation (2.41) is zero. However, when solving transient problems, the squeeze term must be introduced into the Reynolds equation.

Besides the squeeze term, the dimensionless Reynolds equation of transient problems is slightly different from that of steady state problems. However, this does not in any way affect the elasto-hydrodynamic lubrication model presented in Chapter 2 and has an added advantage of being flexible in the sense that it can also be used to solve steady state problems. A reference speed u_{ref} is introduced into

the model and is equal to the sum of the speeds at time $t = 0$ of the two surfaces in contact. As described in Chapter 2, the speeds of the two surfaces in contact are given by u_1 and u_2 and at time t, the sum u_s of the two speeds is given by

$$u_s(t) = u_1(t) + u_2(t)\,. \tag{6.1}$$

Hence, the reference speed u_{ref} is given by

$$u_{ref} = u_s(0)\,. \tag{6.2}$$

The non-dimensional Reynolds equation for a transient elasto-hydrodynamic lubrication circular contact problem is of the form

$$\frac{\partial}{\partial X}\left(\epsilon\frac{\partial P}{\partial X}\right) + \frac{\partial}{\partial Y}\left(\epsilon\frac{\partial P}{\partial Y}\right) - \left(\frac{u_s(t)}{u_{ref}}\right)\frac{\partial(\overline{\rho}H)}{\partial X} - \frac{\partial(\overline{\rho}H)}{\partial T} = 0 \tag{6.3}$$

where, as in a steady state problem,

$$\epsilon_{i,j} = \frac{\overline{\rho}(P_{i,j})\,H_{i,j}^3}{\overline{\eta}(P_{i,j})\,\lambda} \tag{6.4}$$

and $u_s(t)$ and u_{ref} are respectively defined above by equations (6.1) and (6.2). The reference speed u_{ref} prevents the solver from breaking down during zero entrainment, that is when the speeds of the two surfaces in contact are zero. The non-dimensional density $\overline{\rho}$ and viscosity $\overline{\eta}$ are obtained respectively, as in a steady state problem, using the Dowson and Higginson relation [30] and the Roelands equation and are given by equations (2.44) and (2.45). The constant λ, as in a steady state problem, is given by $\lambda = \frac{8\pi U}{W}\left(\frac{2}{3W}\right)^{1/3}$ where, as described in Chapter 2, the Hamrock and Dowson's load W and speed U parameters are respectively given by $W = \frac{F}{E'R_xR_x}$ and $U = \frac{\eta_0 u_e}{E'R_x}$ where, u_e is the entrainment speed. In general, the entrainment speed is the average of u_1 and u_2, but when solving transient problems, at every time step, it is the average of the two speeds at time $t = 0$, that is

$$u_e = \frac{u_s(0)}{2}\,, \tag{6.5}$$

where $u_s(t)$ is defined by equation (6.1).

The non-dimensional film thickness and force balance equations of transient problems are the same as in steady state problems. For completeness, as described in Chapter 2, they are respectively of the form

$$H(X,Y) = H_{00} + \frac{X^2}{2} + \frac{Y^2}{2} + \frac{2}{\pi^2}\int_{-\infty}^{\infty}\int_{-\infty}^{\infty}\frac{P(X',Y')\,dX'\,dY'}{\sqrt{(X-X')^2+(Y-Y')^2}} \tag{6.6}$$

and

$$\int_{-\infty}^{\infty}\int_{-\infty}^{\infty} P(X,Y)\,dX\,dY = \frac{2\pi}{3}. \tag{6.7}$$

The method employed to discretise the governing equations of transient elasto-hydrodynamic lubrication problems is the same as that used in steady state elasto-hydrodynamic lubrication circular contact problems as described in Chapter 2. However, when solving transient problems, the squeeze term $\frac{\partial(\overline{\rho}H)}{\partial T}$ in the Reynolds equation (6.3) must be taken into consideration.

As in steady state problems, the governing equations are discretised on a regular mesh over the computational domain

$$\{(X,Y) \in \Re^2 : X_a \leq X \leq X_b \ \ and \ \ -Y_a \leq Y \leq Y_a\},$$

with the oil entrainment in the positive X-direction and mesh spacings h_x and h_y in the X and Y directions respectively. At each non-boundary mesh point (i,j), $[(i-1)h_x + X_a, (j-1)h_y + Y_a]$, the discretised Reynolds equation (6.3) is given by

$$\begin{aligned} &h_x^{-2}(\epsilon_{i-\frac{1}{2},j}(P_{i-1,j} - P_{i,j}) + \epsilon_{i+\frac{1}{2},j}(P_{i+1,j} - P_{i,j})) + \\ &h_y^{-2}(\epsilon_{i,j-\frac{1}{2}}(P_{i,j-1} - P_{i,j}) + \epsilon_{i,j+\frac{1}{2}}(P_{i,j+1} - P_{i,j})) - \\ &\frac{u_s(t)\,h_x^{-1}}{u_{ref}}\left(\overline{\rho}_{i,j}H_{i,j} - \overline{\rho}_{i-1,j}H_{i-1,j}\right) - \frac{\partial\left(\overline{\rho}_{i,j}\,H_{i,j}\right)}{\partial T} = 0 \end{aligned} \tag{6.8}$$

where, the discretised form of the squeeze term $\frac{\partial(\overline{\rho}_{i,j}H_{i,j})}{\partial T}$ will be described below in Section 6.2.1. For convenience, as described in Chapter (2), the discretised forms of the film thickness equation (6.6) and force balance equation (6.7) are respectively of the form

$$H_{i,j} = H_{00} + \frac{X_{i,j}^2}{2} + \frac{Y_{i,j}^2}{2} + d_{i,j} \tag{6.9}$$

and

$$h_x\,h_y \sum_{i=1}^{m_x}\sum_{j=1}^{n_y} P_{i,j} - \frac{2\pi}{3} = 0. \tag{6.10}$$

6.2 Differential Algebraic Equations and the Backward Euler Method

When dealing with transient elasto-hydrodynamic lubrication problems, the discretised equations (6.8) and (6.9) can be represented as a system of Differential Algebraic Equations (DAE) [17]. Equation (6.8) can be written as

$$\underline{G}(\underline{P}, \underline{\hat{H}}, \underline{\hat{H}}') = 0 \tag{6.11}$$

where, $[\underline{\hat{H}}]_k = [\overline{\rho}_k \, H_k]$, $k = (i-1) \times m_x + j$ and $H_k = H_{i,j}$ for $(i = 1, \ldots, m_x \, ; \, j = 1, \ldots, n_y)$ where m_x and n_y are respectively the maximum number of mesh points in X and Y directions and equation (6.9) can be written as

$$\underline{F}(\underline{P}, \underline{H}) = 0 \, . \tag{6.12}$$

In order to understand differential algebraic equations, a property known as the *index* (or *nilpotency*) [17] is normally employed to classify the structure and analyse the behaviour of differential algebraic equations. This property is important because it gives an indication of numerical difficulties that might be encountered when solving a system of differential algebraic equations. In order to obtain the index of a system of differential algebraic equations, all or part of differential algebraic equations must be differentiated until they are converted into a system of ordinary differential equations. The number of differentiation steps required in this procedure is known as the index which can be defined as follows [17]: *The index of a differential algebraic equation* $S(t, y, y') = 0$ *is defined as the minimum number of times that all or part of* $S(t, y, y') = 0$ *must be differentiated with respect to* t *in order to determine* y' *as a continuous function of* y, t. In general, standard Ordinary Differential Equations (ODE), $\frac{\partial y}{\partial t} = f(t, y)$, has index zero and Differential Algebraic Equations (DAE) with index zero and one are easier to solve numerically than those with index greater than one.

In order to obtain the index of transient elasto-hydrodynamic lubrication problems, consider the differential algebraic equations (6.11) and (6.12). Equation (6.11) can also be written as

$$\underline{\hat{H}}' = \underline{\hat{G}}(\underline{P}, \underline{\hat{H}}) \tag{6.13}$$

and, if we differentiate equation (6.12) with respect to time t, we get

$$\frac{\partial \underline{F}}{\partial \underline{P}} \underline{P}' + \frac{\partial \underline{F}}{\partial \underline{H}} \underline{H}' = 0 \tag{6.14}$$

which, when multiplied through by $(\frac{\partial \underline{F}}{\partial \underline{P}})^{-1}$ gives, together with equation (6.13), a system of implicit ordinary differential equations. Hence, the index of transient problems in elasto-hydrodynamic lubrication is one. $\frac{\partial \underline{F}}{\partial \underline{P}}$ appears to be non-singular - its inverse being computed when solving elasto-hydrodynamic lubrication problems using the Newton-Raphson method [54, 68, 79] - but there is no proof of this.

When it comes to solving differential algebraic equations, many authors have done extensive work in developing solvers to deal with differential algebraic equations of the form $S(t, y, y') = 0$, e.g. SPRINT [8, 9], DASSL [17, 83] and LSODI [52]. Most of these solvers are based on the Backward Differentiation Formulas (BDF) which were introduced by Gear [39]. The concept of the backward differentiation formulas is that the derivative $y'(t)$ is approximated by a linear combination of the solution $y(t)$ at the current and previous mesh points. The simplest method for solving differential algebraic equations is to use the first order backward differentiation formula (or the backward Euler method) which will now be covered in the next section.

6.2.1 Backward Euler method

The backward Euler method is the simplest form of backward differentiation formulas [38, 42, 62] and is widely used to obtain solutions to differential algebraic equations of the form

$$S(t, y, y') = 0\,, \tag{6.15}$$

which is an initial-value [19, 38, 70] ordinary differential equation with a solution $y(t)$ over the interval $t_0 \leq t \leq t_f$ and $y(t_0) = y_0$ is known.

If the backward Euler method is used to obtain a solution to the differential algebraic equation (6.15), then the derivative $y'(t_{n+1})$ at time t_{n+1} must be approximated by a first order backward difference of $y(t)$, and the resulting system of non-linear equations is then solved for $y(t_{n+1})$. That is,

$$y'(t_{n+1}) \approx \frac{y(t_{n+1}) - y(t_n)}{\Delta t} \tag{6.16}$$

which, when substituted into the differential algebraic equation (6.15) gives

$$S\left(t_{n+1}\,,\,y(t_{n+1})\,,\,\frac{y(t_{n+1})-y(t_n)}{\Delta t}\right)=0 \tag{6.17}$$

where $\Delta t = t_{n+1} - t_n$.

When solving transient elasto-hydrodynamic lubrication problems, the discretised form of the squeeze term $\frac{\partial(\overline{\rho}_{i,j}\,H_{i,j})}{\partial T}$ shown in the Reynolds equation (6.8), is given by

$$\frac{\partial(\overline{\rho}_{i,j}\,H_{i,j})}{\partial T}=\frac{1}{\Delta t}\left((\overline{\rho}_{i,j}\,H_{i,j})_{n+1}-(\overline{\rho}_{i,j}\,H_{i,j})_n\right) \tag{6.18}$$

where, the subscript i,j denotes the grid point and the subscript n denotes time t_n. This means that the solution at the previous time step is required when solving transient elasto-hydrodynamic lubrication problems.

6.3 Local Error Estimates, Convergence Test and Time Stepping

The numerical solutions of transient elasto-hydrodynamic lubrication problems are obtained using the multigrid solver for elasto-hydrodynamic lubrication problems which is described in Chapter 4. When solving transient problems, extra operations, which were ignored in steady state problems, must be taken into consideration. This includes the evaluation of the local error estimates, the issue of when to stop the multigrid iterations (V-cycles) during each time step cycle and the issue of time stepping. The evaluation of the local error estimates is based on obtaining an approximation to the solution using a predictor. We will now outline these operations in turn and describe how they fit into the multigrid solver for elasto-hydrodynamic lubrication problems.

6.3.1 Local error estimates

The concept of local error estimates of a system of differential algebraic equations of the form

$$A\underline{y}' = B\underline{y} + \underline{g}(t) \tag{6.19}$$

is explained in detail by Petzold [83] and Brenan et al. [17]. They have shown that the local errors associated with these equations are of the form

$$(A - \Delta t\, B)\, \underline{e}_{local} = A\, \underline{le} \tag{6.20}$$

where, $\Delta t = t_{n+1} - t_n$ and $\underline{le}$ is the local truncation error given for the backward Euler method by

$$\underline{le} = \frac{1}{2}\left(\underline{y}_{n+1} - \underline{y}^{p}_{n+1}\right) \tag{6.21}$$

where, $\underline{y}^{p}_{n+1}$ is the predicted, denoted by superscript p, solution of $\underline{y}_{n+1}$ at time t_{n+1} and it is given by

$$\underline{y}^{p}_{n+1} = \underline{y}_{n+1} + \Delta t_{n+1}\left(\frac{\underline{y}_{n+1} - \underline{y}_{n}}{\Delta t_n}\right). \tag{6.22}$$

The local errors, $\underline{e}_{local}$, are usually calculated by forward and backward substitution using LU factorisation of $[A - \Delta t\, B]$, [83].

If we employ this strategy in transient elasto-hydrodynamic lubrication problems, then the differential algebraic equations (6.11) and (6.12) can respectively be rewritten as

$$\underline{\hat{G}}(\underline{\hat{H}}, \underline{P}) - \underline{\hat{H}}^{'} = 0 \tag{6.23}$$

where, $[\underline{\hat{H}}]_k = [\overline{\rho}_k\, H_k]$, $k = (i-1) \times m_x + j$ and $H_k = H_{i,j}$ for $(i = 1, \ldots, m_x\,;\, j = 1, \ldots, n_y)$ where m_x and n_y are respectively the maximum number of mesh points in X and Y directions and

$$\underline{H} - K\underline{P} - \underline{c} = 0 \tag{6.24}$$

where, the coefficient matrix K is used to evaluate the elastic deformation as described in Chapter 2.

The local errors associated with transient elasto-hydrodynamic lubrication problems can be obtained by formulating an equivalent system of equations to (6.20). The LU decomposition of $[A - \Delta t\, B]$ or its equivalent is not available and so the multigrid solver for elasto-hydrodynamic lubrication problems described in Chapter 4 is used to calculate the local errors associated with transient problems by solving equations (6.23) and (6.24). This is done at the end of each multigrid

cycle using the following algorithm: The equations for obtaining the local errors at the i,j th mesh point are of the form, [17],

$$\begin{bmatrix} -1-\Delta t\frac{\partial \hat{\underline{G}}}{\partial \underline{\hat{H}}} & -\Delta t\frac{\partial \hat{\underline{G}}}{\partial \underline{P}} \\ -\Delta t & \Delta t\,K \end{bmatrix} \begin{bmatrix} \underline{leH} \\ \underline{leP} \end{bmatrix} = \begin{bmatrix} -1 & 0 \\ 0 & 0 \end{bmatrix} \frac{1}{2} \begin{bmatrix} \underline{H}_{n+1} - \underline{H}^{p}_{n+1} \\ \underline{P}_{n+1} - \underline{P}^{p}_{n+1} \end{bmatrix} \tag{6.25}$$

where, the subscript n indicates time t_n, $\underline{leH}$ and $\underline{leP}$ are respectively the local errors in film thickness $\underline{H}$ and pressure $\underline{P}$ and $\underline{H}^{p}_{n+1}$ and $\underline{P}^{p}_{n+1}$ are respectively the predicted, denoted by superscript p, solutions of $\underline{H}_{n+1}$ and $\underline{P}_{n+1}$. In general, the predicted solution of $\underline{P}(t_{n+1})$ at time t_{n+1} is given by

$$\underline{P}^{p}_{n+1} = \underline{P}_{n+1} + \Delta t_{n+1}\left(\frac{\underline{P}_{n+1} - \underline{P}_{n}}{\Delta t_n}\right). \tag{6.26}$$

Let us consider the two equations of (6.25) more closely. First consider the second equation, which is simpler of the two equations and represents a relationship between the local errors in $\underline{H}$ and $\underline{P}$, that is

$$\underline{leH} = K\,\underline{leP}, \tag{6.27}$$

which implies that we can solve for local errors in either $\underline{H}$ or $\underline{P}$. Since when solving elasto-hydrodynamic lubrication problems, the multigrid solver is employed to solve for $\underline{P}$, which is then used to evaluate $\underline{H}$, we calculate the local errors in $\underline{P}$. Now consider the first equation which, using equation (6.24), can be rewritten as

$$-\Delta t\left(\frac{\underline{leH}}{\Delta t} + \frac{\partial \hat{\underline{G}}}{\partial \underline{\hat{H}}}\underline{leH} + \frac{\partial \hat{\underline{G}}}{\partial \underline{P}}\underline{leP}\right) = -\frac{K\,\underline{P}_{n+1} - K\,\underline{P}^{p}_{n+1}}{2}, \tag{6.28}$$

which must be rewritten in a different format because a multigrid solver is employed throughout this work to solve elasto-hydrodynamic lubrication problems and the Jacobian matrix of derivatives is not evaluated at any stage of the solution process. Consider the Taylor's theorem for 2 variables, that is

$$\hat{\underline{G}}(\underline{\hat{H}} + \underline{leH}, \underline{P} + \underline{leP}) \approx \hat{\underline{G}}(\underline{\hat{H}}, \underline{P}) + \frac{\partial \hat{\underline{G}}}{\partial \underline{\hat{H}}}\underline{leH} + \frac{\partial \hat{\underline{G}}}{\partial \underline{P}}\underline{leP} + h.o.t. \tag{6.29}$$

where, $\hat{\underline{G}}(\underline{\hat{H}}, \underline{P})$ represents the residual. Assuming that the residual is zero and using equation (6.23), equation (6.28) can be written in a different form as

$$\hat{\underline{G}}(\underline{\hat{H}}_{n+1} + \underline{leH}, \underline{P}_{n+1} + \underline{leP}) - \frac{\underline{\hat{H}}_{n+1} + \underline{leH} - \underline{\hat{H}}_{n}}{\Delta t} = \frac{K}{2\,\Delta t}\left(\underline{P}_{n+1} - \underline{P}^{p}_{n+1}\right) \tag{6.30}$$

where, the subscript n indicates time t_n and $[\underline{\hat{H}}]_k = [\overline{\rho}(P_k)\, H_k]$, $k = (i-1) \times m_x + j$ and $H_k = H_{i,j}$ for $(i = 1, \ldots, m_x\,;\, j = 1, \ldots, n_y)$ where m_x and n_y are respectively the maximum number of mesh points in X and Y directions.

Using equation (6.27), equation (6.30) can be rewritten as

$$\underline{\hat{G}}(\underline{\tilde{H}}_{n+1}, \underline{\tilde{P}}_{n+1}) - \frac{\underline{\tilde{H}}_{n+1} - \underline{\hat{H}}_n}{\Delta t} = \frac{K}{2\,\Delta t}(\underline{P}_{n+1} - \underline{P}^p_{n+1}), \tag{6.31}$$

where, $\underline{\tilde{H}}_{n+1} = \underline{\hat{H}}_{n+1} + K\underline{leP}$ and $\underline{\tilde{P}}_{n+1} = \underline{P}_{n+1} + \underline{leP}$. Equation (6.31) must be solved together with

$$\underline{\tilde{H}}_{n+1} - K\underline{\tilde{P}}_{n+1} - c = 0 \tag{6.32}$$

in order to obtain the local error in $\underline{P}$, $\underline{leP}$, at any i, j th mesh point. The local error in $\underline{H}$ may then be calculated using equation (6.27).

For a constant j, that is on the line $Y = j$, equation (6.31) is used to formulate a system of equations that is then solved simultaneously for $\underline{\tilde{P}}$. This concept is described in detail in Chapter 4. Having obtained the solution $\underline{\tilde{P}}$ on the entire computational domain, it is then used to evaluate the new film thickness $\underline{\tilde{H}}$, viscosities and densities on the entire computational domain. It is also used to calculate the local error in pressure using

$$||\underline{leP}||_w = ||\underline{\tilde{P}}_{n+1} - \underline{P}_{n+1}||_w \tag{6.33}$$

where, a weighted root mean square L_2-norm is used, i.e.

$$||\underline{leP}||_w = \sqrt{\frac{1}{m_x n_y} \sum_{i=1}^{m_x} \sum_{j=1}^{n_y} \left(\frac{leP_{i,j}}{w_{i,j}}\right)^2} \tag{6.34}$$

where, m_x and n_y are respectively the maximum number of grid points in the X and Y directions and at the i, j th mesh point, the weight depends on the absolute $(atol)$ and relative $(rtol)$ errors and the initial value of P at each time step, that is

$$w_{i,j} = atol + P^0_{i,j}\, rtol \tag{6.35}$$

where, $atol$ and $rtol$ are respectively the absolute and relative error tolerances. These tolerances can be specified by the user but for the solver to use the correct temporal accuracy, the spatial error [63, 7] must dominate the temporal error. This

concept is described in detail by Lawson et al. [63] and Berzins [7]. Hence, *atol* and *rtol* must be chosen so that the spatial error dominates and this can be achieved by controlling the local error in time so that it is a fraction of the local growth in the spatial error. However, since the spatial error may vary with time, the tolerances may also need to vary with time so that the spatial error stays in dominance at each time step. As an alternative, the tolerances can be chosen so that the local errors in time are an order of magnitude smaller than the spatial error, that is

$$||le|| < \varepsilon \, ||spatial \ error|| \tag{6.36}$$

where, ε is a small fraction, say less than 0.01. Hence, at each time step, the spatial error is computed and used to obtain the tolerances. We make use of this latter approach when solving transient elasto-hydrodynamic lubrication problems. This is achieved by taking a fraction of root mean square L_2-norm of the spatial error so that the L_2-norm of the local error in pressure, given by equation (6.33), is less than one, that is

$$||\underline{leP}||_w < 1.0 \, . \tag{6.37}$$

The root mean square L_2-norm of the spatial error is given by

$$||spatial \ error|| = ||\underline{P}^s - I_s^S \, \underline{P}^s|| \tag{6.38}$$

where, I_s^S is a restriction operator, described in Section 4.1.1, that restricts $\underline{P}^s$ to a coarser grid with mesh size S and $S = 2s$.

6.3.2 Convergence test

When solving transient elasto-hydrodynamic lubrication problems using the multigrid solver, we need to employ a strategy to decide when to terminate the multigrid iterations (V-cycles) during each time step. This strategy needs to be employed after each multigrid iteration in order to avoid doing extra work and improve the efficiency of the multigrid solver. Though the existing methods are commonly used, they can sometimes give misleading results as described in Chapter 5. Hence, a new convergence criterion for transient elasto-hydrodynamic lubrication problems

will be presented and employed in this work. It, referred here as convergence test, is similar to the one described by Brenan et al. [17] who employed it in DASSL [17, 83] and is based on the well-known result [90], that

$$||\underline{y}^* - \underline{y}^{m+1}||_w \leq \frac{\varrho}{1-\varrho}||\underline{y}^{m+1} - \underline{y}^m||_w \tag{6.39}$$

where, $\underline{y}^*$ is the exact solution, ϱ is an estimate of the rate of convergence of the iteration, w is a weight factor used when evaluating the norm and the superscript m is the iteration number. The iterations are continued until

$$\frac{\varrho}{1-\varrho}||\underline{y}^{m+1} - \underline{y}^m||_w < \tau \tag{6.40}$$

which is a convergence test developed by Shampine [90] and in DASSL $\tau = 0.33$. The reason for choosing 0.33 is that the error due to terminating the iteration does not affect the local error which is less than 1.0. According to Shampine [90], the choice of τ varies a great deal but, a very small tolerance τ does not necessarily improve the solution. The rate of convergence ϱ is given by

$$\varrho = \left(\frac{||\underline{y}^{m+1} - \underline{y}^m||_w}{||\underline{y}^1 - \underline{y}^0||_w}\right)^{1/m} \tag{6.41}$$

and according to Brenan et al., if $\varrho > 0.9$, the iteration is considered to have failed. The norms used in equations (6.40) and (6.41) are weighted root mean square L_2-norms as defined by equation (6.34).

When solving transient elasto-hydrodynamic lubrication problems, the convergence test employed in the multigrid solver is based on the solution pressure $\underline{P}$. This is the case because the multigrid solver is first employed to solve for $\underline{P}$ which is then used to evaluate the film thickness $\underline{H}$. The convergence test is carried out at the end of each multigrid cycle using equation (6.40), but $\underline{y}$ is replaced by $\underline{P}$. The tolerance τ in equation (6.40) is chosen to be 0.1 and with this choice, at every time step besides zero, between 2 to 3 multigrid iterations (V-cycles) are carried out by the multigrid solver.

6.3.3 Time stepping

A key feature associated with time-dependent (or transient) elasto-hydrodynamic lubrication problems is the concept of time stepping. When solving transient prob-

lems using the multigrid solver for elasto-hydrodynamic lubrication problems, a time step size must be assigned in order to drive the problem. The step size can be either chosen arbitrarily or evaluated within the solver using the local error estimates. If the step size is chosen arbitrarily by the user, then it is done once prior to solving the problem. However, if it is evaluated using the local error estimates, then it is done at the end of each time step.

The concept used to implement the variable time step method is to use the local error to only double or halve the step size as was done by Berzins and Furzland [10]. It is also important for variable step methods not to change the step size too frequently unless a decrease is called for. For this reason a step size increase is only considered after three successful steps.

An alternative method is that described by Brenan et al. [17]. They have based their strategy on the concept used by Shampine and Gordon [91]. The new step size is given by $r\Delta t_{n+1}$ where

$$r = (2\,||\underline{leP}||_w)^{-1/(k+1)} \tag{6.42}$$

where, k represents the order of the method. For the backward Euler method $k = 1$. According to Shampine et al. [91], even if r is reliable, some limits must be imposed on the new step size. The step size can either increase by a factor of two or decrease. However, if these two operations are not possible, then the step size is kept constant. The step size is increased if r is greater than or equal to two. If a decrease in the step size is required, then it is decreased by at least $r = 0.9$ and at most $r = 0.5$. The step size is decreased if r is less than or equal to one. A point to note is that when the step size is to be decreased, the estimate for r is taken at the face value whereas when it is to be increased, the estimate for r is not used in the evaluation of the new step size.

Solutions using both fixed and variable time step methods will be presented in this chapter. The next section will show the effectiveness of the new convergence criterion for solutions obtained using a fixed time step method.

6.4 Testing Convergence Criterion using a Fixed Time Step Method

The multigrid solver described in Chapter 4 is employed to solve a transient elasto-hydrodynamic lubrication circular contact problem using a fixed time step method. In order to show the effectiveness of the new convergence test, a comparison will be presented for solutions obtained with and without the convergence test described above. The main feature of this test problem is to study the effect of varying the speeds of the two surfaces in contact with time on the pressure and film thickness. The speeds of the two surfaces in contact are varied with time with the aim of zero and reversal entrainments. This is where the speeds are driven from a positive value down to zero (zero entrainment) and then introducing negative speeds (reversal entrainment). During the entire cycle of driving the problem from positive speeds down to zero and reversal entrainments, all the other input parameters defining the problem are left unchanged. Hence, the load of the problem remains the same at every time step. The input parameters of this test problem are shown in Table (6.1).

Parameters	Symbols	Values	Units
Reduced radius of curvature	R	1.27×10^{-2}	m
Reduced modulus of elasticity	E'	1.41×10^{11}	Pa
Load	w	14.96	N
Pressure viscosity index	α	2.1×10^{-8}	Pa^{-1}
Maximum Hertzian pressure	p_h	0.4468	GPa
Viscosity at ambient pressure	η_0	0.525	$Pa\,s$
Speed of surface 1	$u1$	5.0×10^{-2}	$m\,s^{-1}$
Speed of surface 2	$u2$	5.0×10^{-2}	$m\,s^{-1}$

Table 6.1: Input parameters

The dimensionless Hamrock and Dowson parameters G, W and U and the corresponding dimensionless Moes parameters M and L to the nearest integer are presented in Table (6.2).

Parameters	Values
Material parameter G	2961
Load parameter W	6.5782×10^{-7}
Speed parameter U	1.4659×10^{-11}
Moes parameter M	52
Moes parameter L	7

Table 6.2: Dimensionless parameters

This transient problem is solved on a domain $-3.0 \leq X \leq 3.0$, $-3.0 \leq Y \leq 3.0$ with 65 by 65 and 17 by 17 finest and coarsest grids respectively. The solutions are obtained for time $t = 0$ to $t = 3.0$ with reversal entrainment at time $t = 1.5$. At each time step, the speeds of the two surfaces in contact are reduced by 5.0×10^{-4} and the step size is kept constant at 0.01538. This problem is solved with and without the new convergence test. When the problem is solved using the new convergence test, the tolerance τ is set to 0.1 whereas when the solution is obtained without the new convergence test, 15 multigrid iterations (V-cycles) are carried out at every time step. The latter uses 15 V-cycles because that is what we would normally use in steady state problems.

6.4.1 Results and discussion

The central and minimum and film thicknesses obtained with and without the convergence test are respectively shown in Tables (6.3) and (6.4). There is little discernible difference in the values of central and minimum film thicknesses obtained with and without the new convergence test but, the times taken to obtain these results on an SGI R8000 were respectively 1.7 and 12.3 hours. Hence, by using the convergence test, the amount of work done is greatly reduced without affecting the accuracy of the solution.

Step	Time t	Hcent	Hmin
0	0.0000	1.9466E-05	1.1099E-05
40	0.6154	1.9614E-05	1.0805E-05
80	1.2308	1.9749E-05	9.6057E-06
100	1.5385	1.9900E-05	8.9634E-06
120	1.8462	2.0210E-05	8.5518E-06
160	2.4615	2.0624E-05	7.9192E-06
200	3.0769	1.6071E-05	8.0084E-06

Table 6.3: Central and minimum film thicknesses (ConvergenceTest).

Step	Time t	Hcent	Hmin
0	0.0000	1.9466E-05	1.1099E-05
40	0.6154	1.9611E-05	1.0809E-05
80	1.2308	1.9764E-05	9.6168E-06
100	1.5385	1.9936E-05	8.9863E-06
120	1.8462	2.0273E-05	8.6166E-06
160	2.4615	2.0689E-05	7.9356E-06
200	3.0769	1.5988E-05	8.0861E-06

Table 6.4: Central and minimum film thicknesses (No ConvergenceTest).

Figures (6.1) and (6.3) show respectively the profiles of pressure and film thickness along the X-axis for solutions obtained with the convergence test whereas Figures (6.2) and (6.4) show the same profiles but for solutions obtained without the convergence test. Figures (6.1) and (6.2) shows the effect on the pressure profiles of switching from positive to negative entrainments. During positive entrainment, a pressure spike is seen on the outlet region (+ve X-axis) and it moves gradually with time towards the central contact region. At reversal, which represents negative entrainment, a pressure spike begins to appear on the new outlet region (-ve X-axis). The effect of negative entrainment can also be seen from the profiles of film thickness shown in Figures (6.3) and (6.4). During the time cycle from positive to negative entrainments, not only does the constriction in the outlet region (+ve X-axis) gradually move with time towards the central contact region but also a

second constriction develops in the inlet region (-ve X-axis).

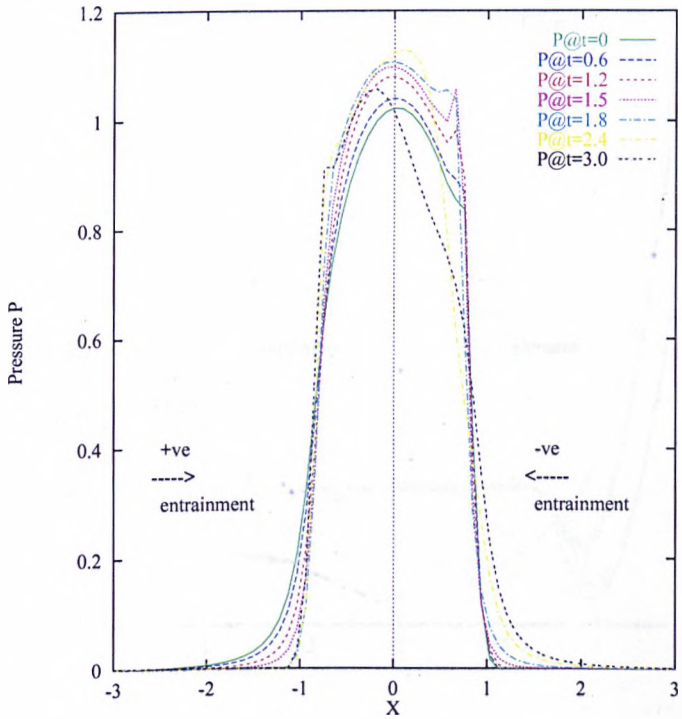

Figure 6.1: Pressure profiles along the X-axis (ConvergenceTest).

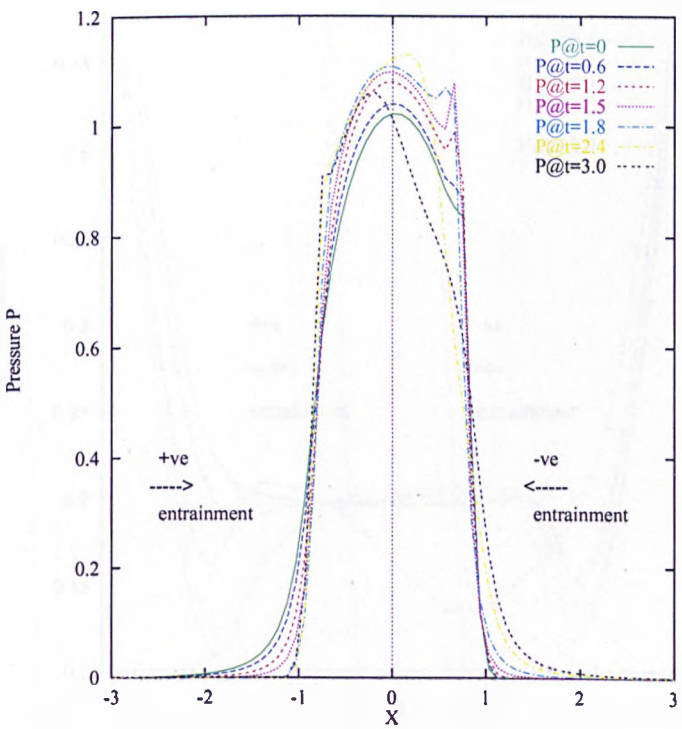

Figure 6.2: Pressure profiles along the X-axis (No ConvergenceTest).

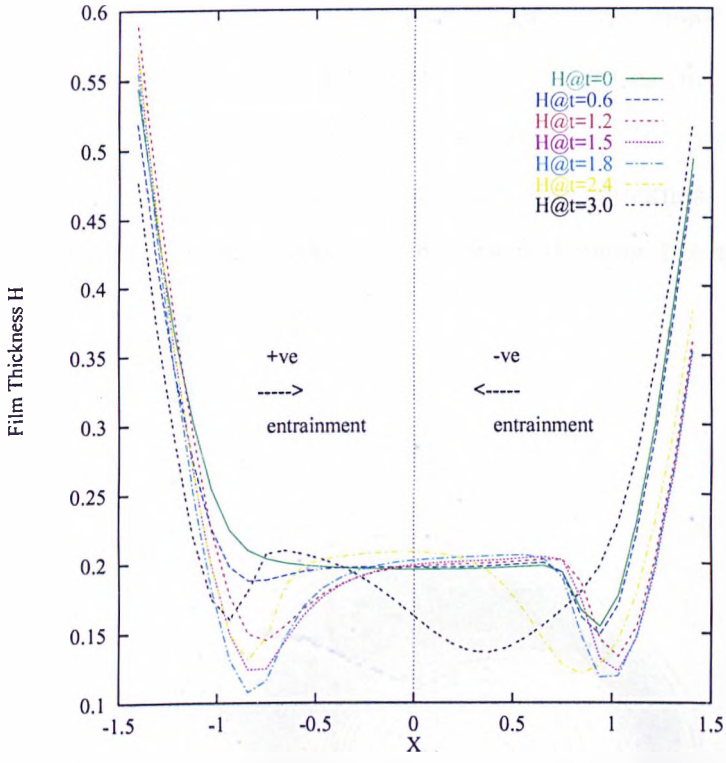

Figure 6.3: Film thickness profiles along the X-axis (ConvergenceTest).

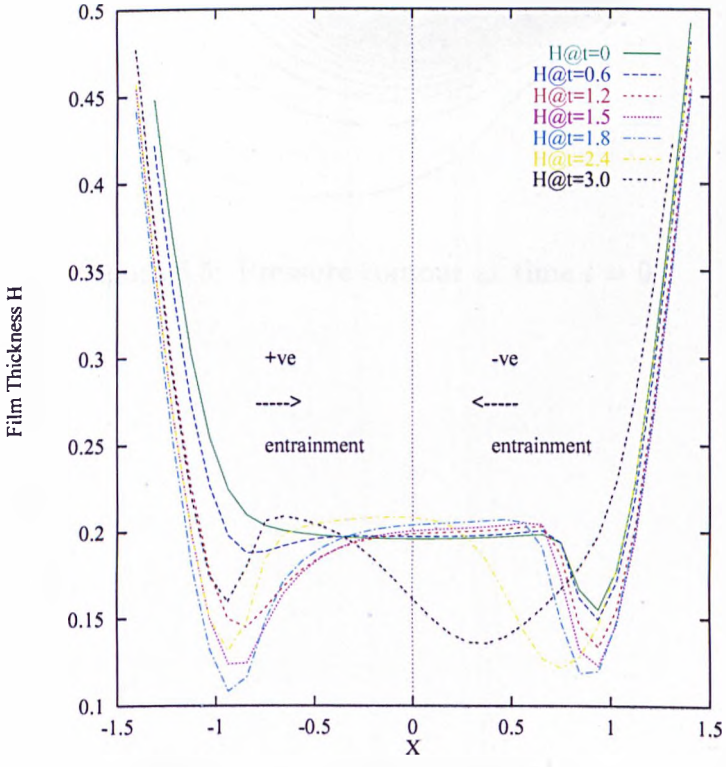

Figure 6.4: Film thickness profiles along the X-axis (No ConvergenceTest).

The effect of reversal entrainment can be seen more clearly from the contour and surface plots of pressure and film thickness. Figures (6.5), (6.6), (6.7), (6.8), (6.9) and (6.10) shows contour and surface plots of pressure and Figures (6.11), (6.12) and (6.13) shows contour plots film thickness at times $t = 0$, $t = 1.5$ and $t = 3.0$. All these profiles were obtained using the multigrid solver which employed the new convergence test.

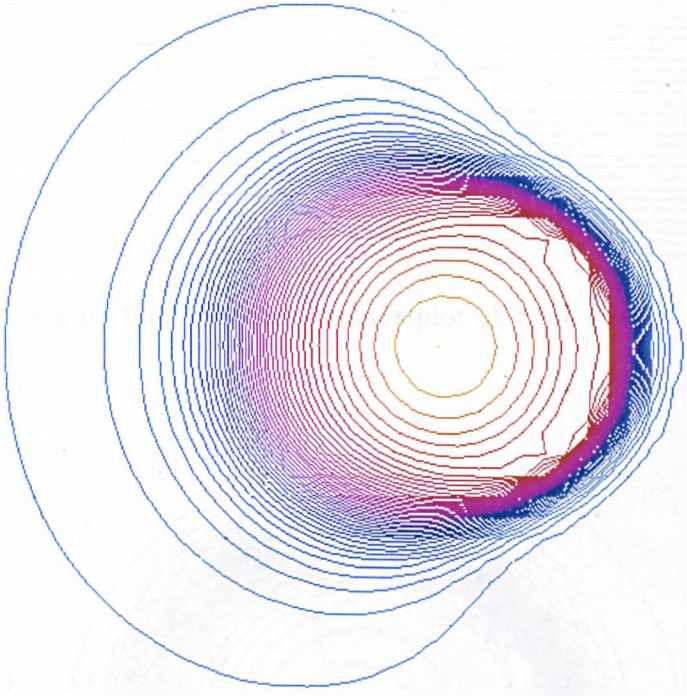

Figure 6.5: Pressure contour at time $t = 0$.

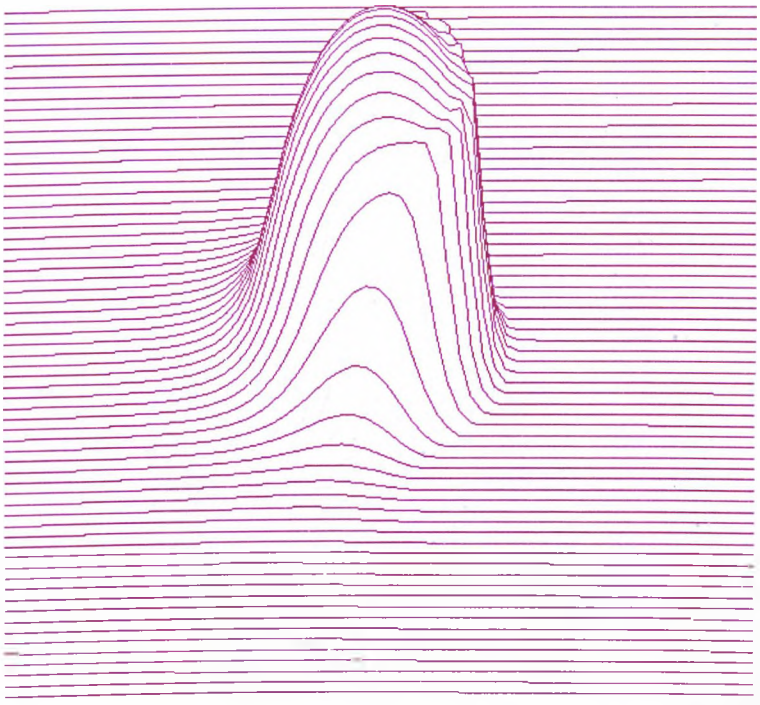

Figure 6.6: Pressure surface plot at time $t = 0$.

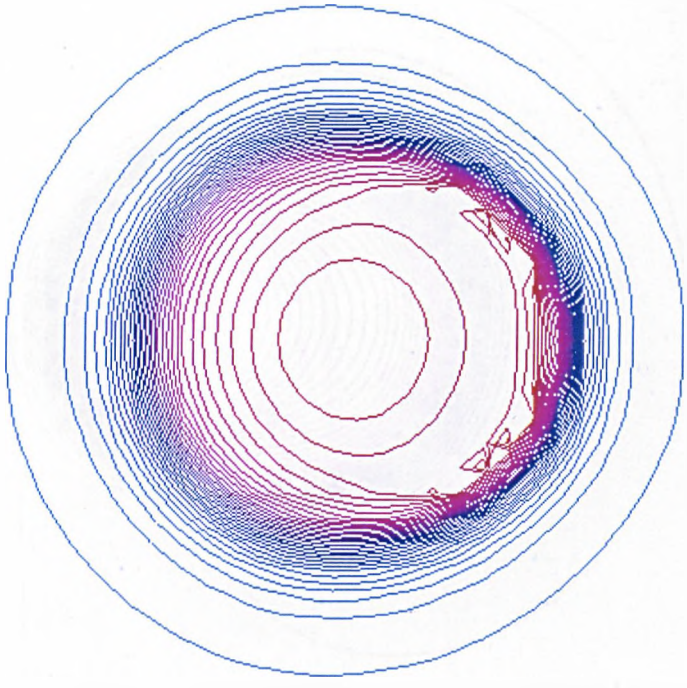

Figure 6.7: Pressure contour at time $t = 1.5$.

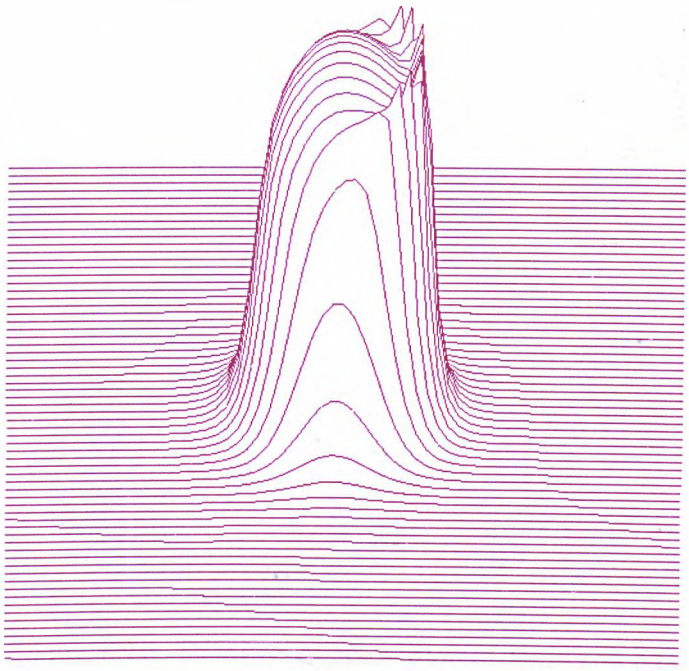

Figure 6.8: Pressure surface plot at time $t = 1.5$.

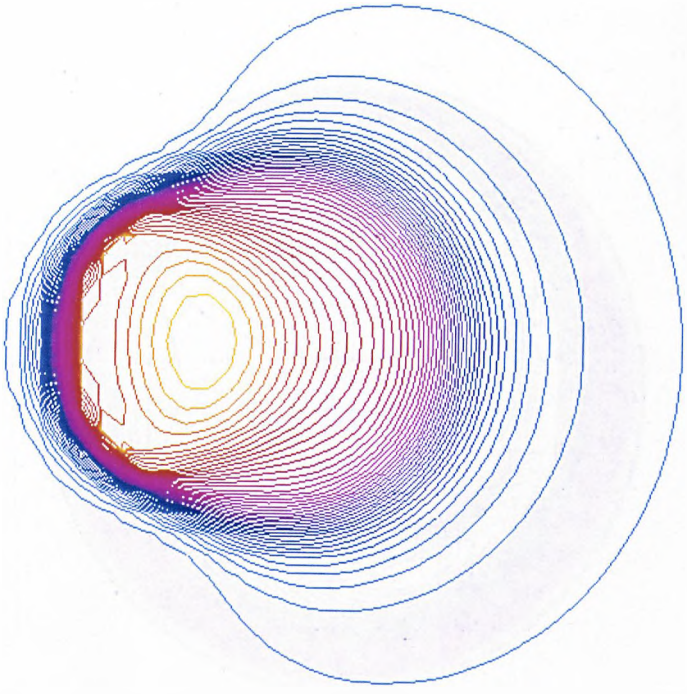

Figure 6.9: Pressure contour at time $t = 3.0$.

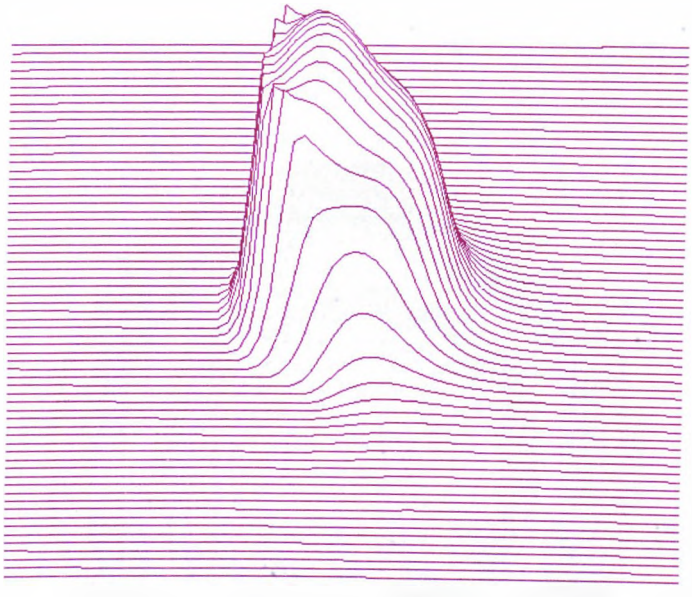

Figure 6.10: Pressure surface plot at time $t = 3.0$.

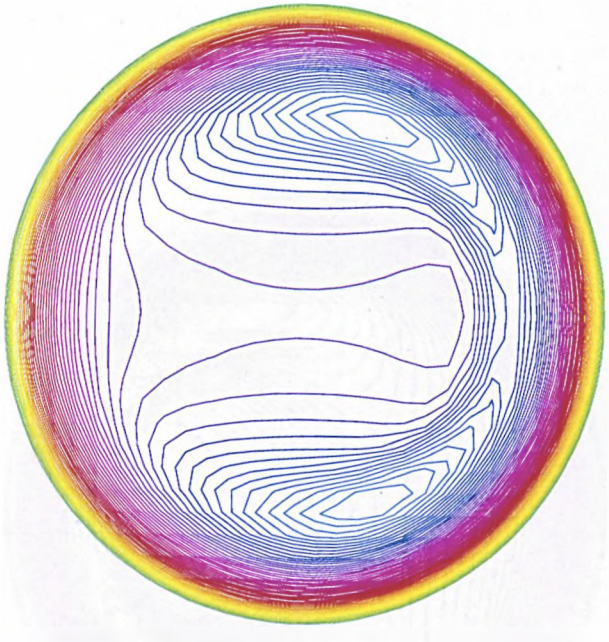

Figure 6.11: Film thickness contour at time $t = 0$.

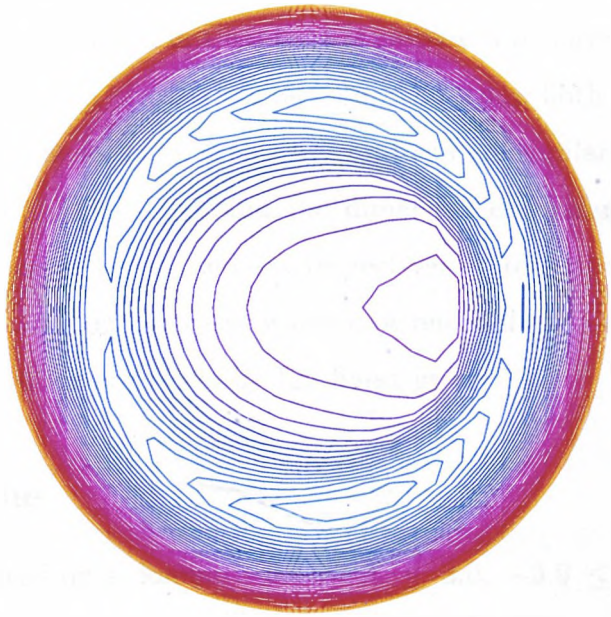

Figure 6.12: Film thickness contour at time $t = 1.5$.

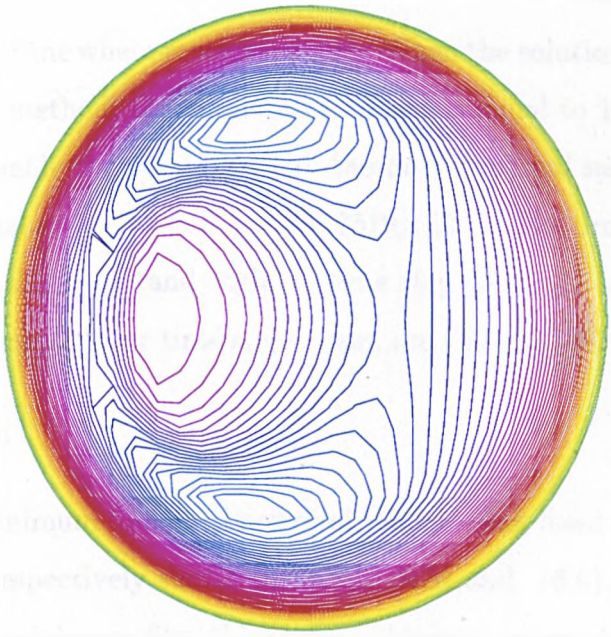

Figure 6.13: Film thickness contour at time $t = 3.0$.

6.5 Comparison of Fixed and Variable Time Step Methods

The multigrid solver described in Chapter 4 is employed to solve a transient elasto-hydrodynamic lubrication circular contact problem using both fixed and variable time step methods. The features of this test problem are similar to those described above in Section 6.4. The input and the dimensionless parameters of this test problem are the same as before and are respectively shown above in Tables (6.1) and (6.2). We will consider two cases where case one will use a 65 by 65 finest grid whereas case two will employ a 129 by 129 finest grid.

6.5.1 Case one

This problem is solved on a domain $-3.0 \leq X \leq 3.0$, $-3.0 \leq Y \leq 3.0$ with 65 by 65 and 17 by 17 finest and coarsest grids respectively. This problem is solved for time $t = 0$ to $t = 0.76$ with reversal entrainment at time $t = 0.38$. During the time cycle, the speeds of the two surfaces in contact are reduced by a fixed function of the simulation time t, that is

$$u_1(t) = u_1(0)\left(1 - \frac{t}{t_{reversal}}\right) \text{ and } u_2(t) = u_2(0)\left(1 - \frac{t}{t_{reversal}}\right), \qquad (6.43)$$

where $t_{reversal}$ is the time where reversal occurs. When the solution is obtained using the fixed time step method, the employed step size is equal to 1.0×10^{-3} whereas when using the variable time step method, the minimum and maximum step sizes are respectively equal to 1.0472×10^{-3} and 7.7519×10^{-3}. The times taken to obtain the two solutions using fixed and variable time step methods were respectively 7 and 5.4 hours and the number time steps taken are 750 and 670 respectively.

6.5.1.1 Results

The central and minimum film thicknesses obtained using fixed and variable time step methods are respectively shown in Tables (6.5) and (6.6). The discrepancy in the central and minimum film thicknesses obtained using the two methods is minimal and is approximately 5%. A point to note is that the step size in the fixed

time step method is approximately equal to the minimum step size in the variable step size method. Hence, the minimal discrepancies in the central and minimum film thicknesses obtained using the two methods.

Step	Time t	Hcent	Hmin
0	0.0000	1.9466E-05	1.1099E-05
200	0.2000	2.1236E-05	1.2423E-05
300	0.3000	2.2750E-05	1.3416E-05
400	0.4000	2.5687E-05	1.5510E-05
600	0.6000	3.6033E-05	2.2777E-05
700	0.7000	3.9775E-05	2.4361E-05
750	0.7500	4.1035E-05	2.4541E-05

Table 6.5: Central and minimum film thicknesses (65by65:Fixed TimeStep).

Step	Time t	Hcent	Hmin
0	0.0000	1.9466E-05	1.1099E-05
150	0.2162	2.0687E-05	1.1932E-05
250	0.3209	2.1968E-05	1.2723E-05
350	0.4256	2.4646E-05	1.4574E-05
550	0.6350	3.4214E-05	2.1303E-05
650	0.7398	3.7968E-05	2.3078E-05
670	0.7607	3.8573E-05	2.3292E-05

Table 6.6: Central and minimum film thicknesses (65by65:Variable TimeStep).

The profiles of pressure and film thickness along the X-axis obtained using the fixed time step method are respectively shown in Figures (6.14) and (6.16) whereas Figures (6.15) and (6.17) show the same profiles obtained using the variable time step method. The features described above in Section 6.4.1 are also observed in these figures.

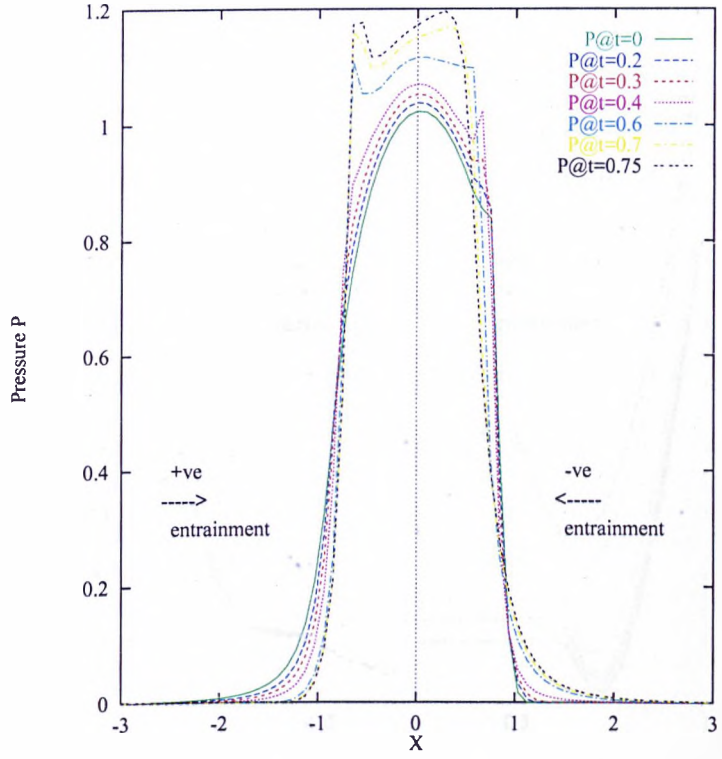

Figure 6.14: Pressure profiles along the X-axis (65by65:Fixed TimeStep).

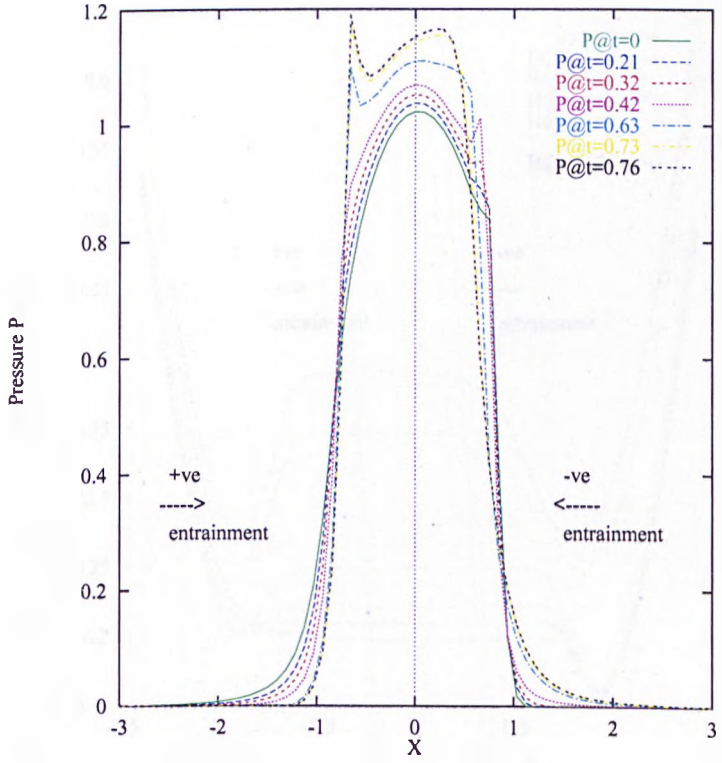

Figure 6.15: Pressure profiles along the X-axis (65by65:Variable TimeStep).

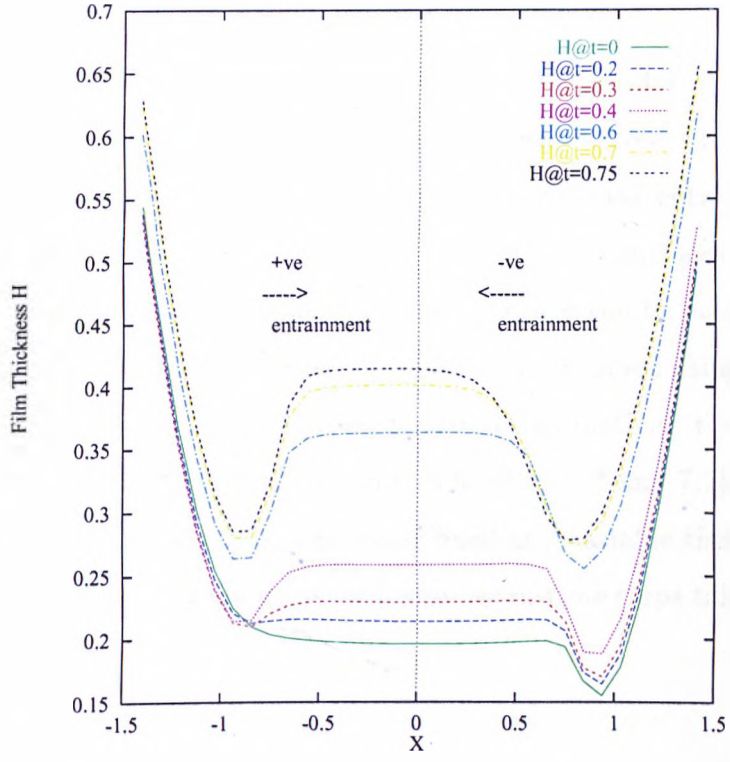

Figure 6.16: Film thickness profiles along the X-axis (65by65:Fixed TimeStep).

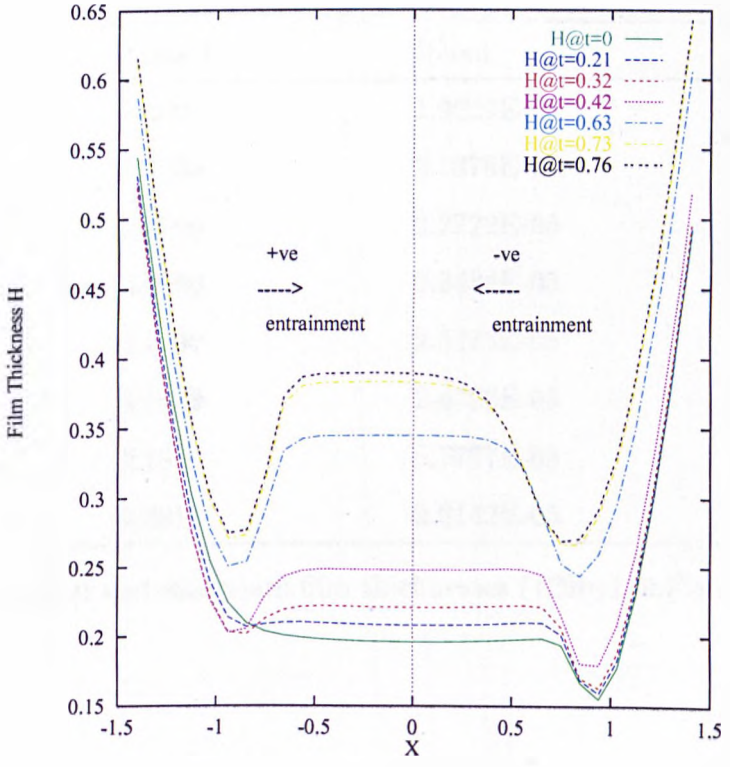

Figure 6.17: Film thickness profiles along the X-axis (65by65:Variable TimeStep).

6.5.2 Case two

This problem is solved on a domain $-3.5 \leq X \leq 3.5$, $-3.5 \leq Y \leq 3.5$ with 129 by 129 and 17 by 17 finest and coarsest grids respectively. For this case, the problem is solved for time $t = 0$ to $t = 0.2$ with reversal entrainment at time $t = 0.09$. During the time cycle, the speeds of the two surfaces in contact are reduced by a fixed function of the simulation time t as given by equation (6.43). A step size of 1.5×10^{-3} is employed when the solution is obtained using the fixed time step method whereas when using the variable time step method, the minimum and maximum step sizes are respectively equal to 9.6899×10^{-4} and 7.7519×10^{-3}. The times taken to obtain the two solutions using fixed and variable time step methods were respectively 16 and 7.6 hours and the number of time steps taken are 134 and 66 respectively.

6.5.2.1 Results

The central and minimum film thicknesses obtained using fixed and variable time step methods are respectively shown in Tables (6.7) and (6.8).

Step	Time t	Hcent	Hmin
0	0.0000	1.9229E-05	1.1038E-05
30	0.0450	2.1376E-05	1.2860E-05
50	0.0750	2.2722E-05	1.3937E-05
60	0.0900	2.3484E-05	1.4538E-05
80	0.1200	2.5275E-05	1.5947E-05
100	0.1500	2.6796E-05	1.7093E-05
120	0.1800	2.7777E-05	1.7690E-05
134	0.2010	2.8142E-05	1.7813E-05

Table 6.7: Central and minimum film thicknesses (129by129:Fixed TimeStep).

Step	Time t	Hcent	Hmin
0	0.0000	1.9229E-05	1.1038E-05
10	0.0446	1.9774E-05	1.1468E-05
20	0.0736	2.0375E-05	1.1922E-05
30	0.0959	2.1119E-05	1.2516E-05
40	0.1231	2.1864E-05	1.3073E-05
50	0.1521	2.2494E-05	1.3538E-05
60	0.1831	2.2929E-05	1.3785E-05
66	0.2006	2.3113E-05	1.3882E-05

Table 6.8: Central and minimum film thicknesses (129by129:Variable TimeStep).

The profiles of pressure along the X-axis obtained using the fixed time step and variable time step methods are shown in Figure (6.18). The two profiles at various times between $t = 0$ and $t = 0.2$ are displayed side by side in order to compare their differences. Similarly, the profiles of film thickness are shown in Figure (6.19).

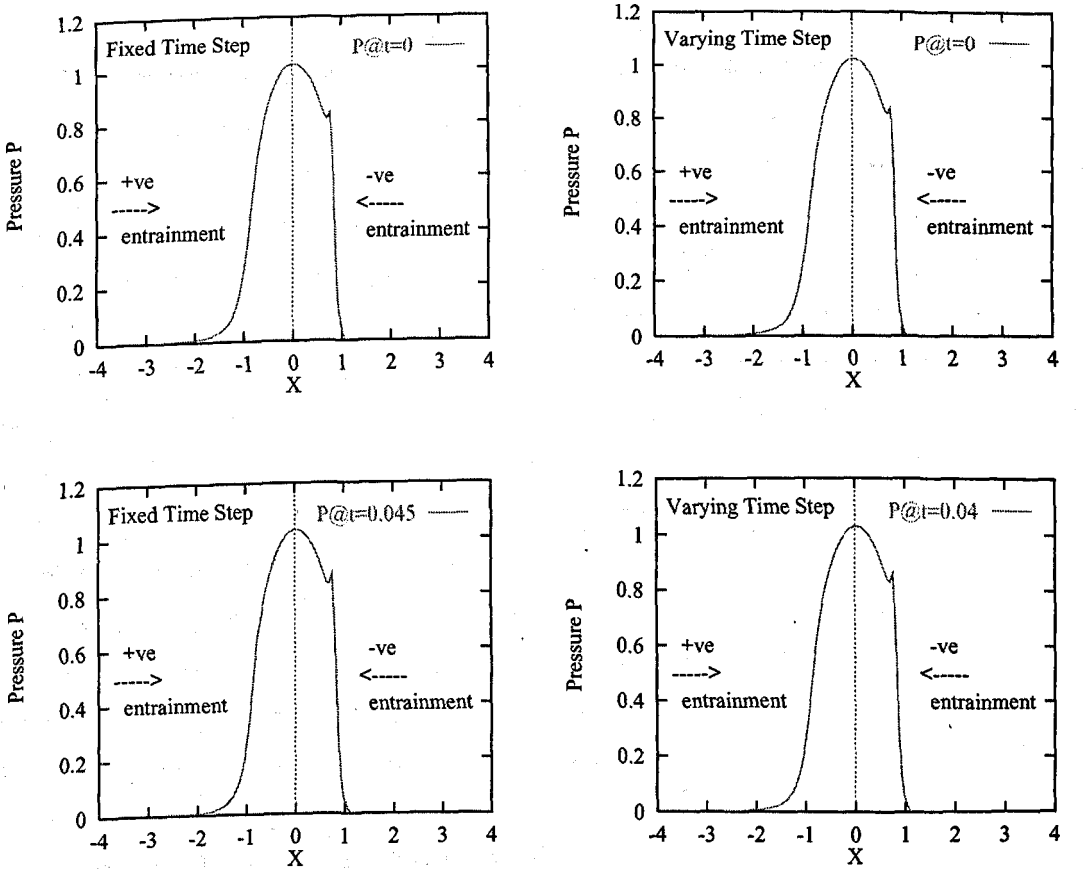

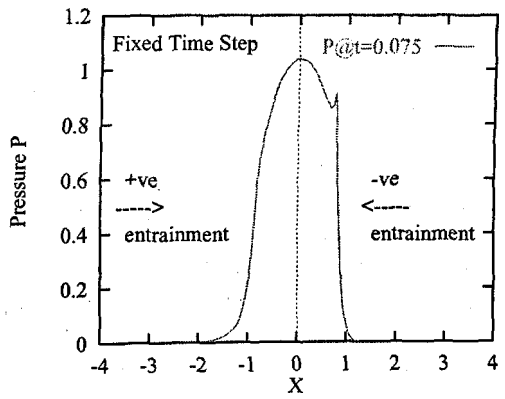
Fixed Time Step
P@t=0.075
Pressure P
+ve
----->
entrainment
-ve
<-----
entrainment
X

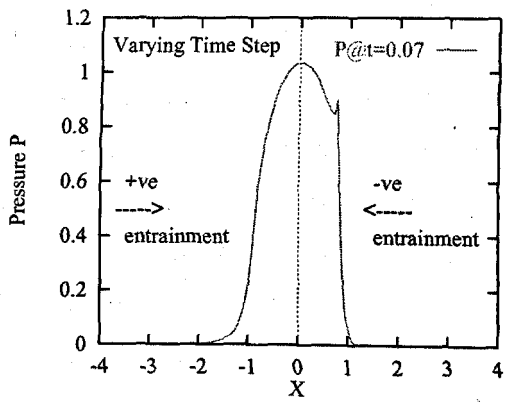
Varying Time Step
P@t=0.07
Pressure P
+ve
----->
entrainment
-ve
<-----
entrainment
X

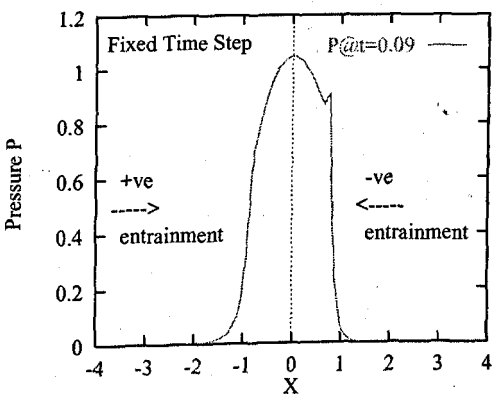
Fixed Time Step
P@t=0.09
Pressure P
+ve
----->
entrainment
-ve
<-----
entrainment
X

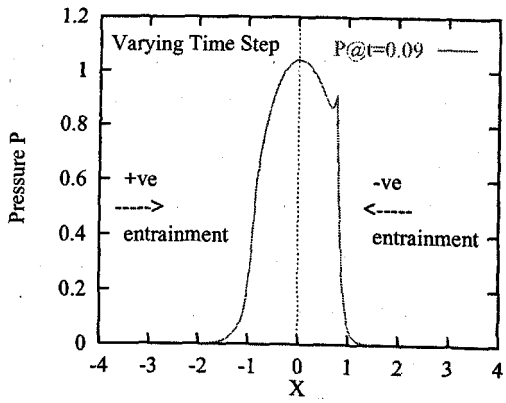
Varying Time Step
P@t=0.09
Pressure P
+ve
----->
entrainment
-ve
<-----
entrainment
X

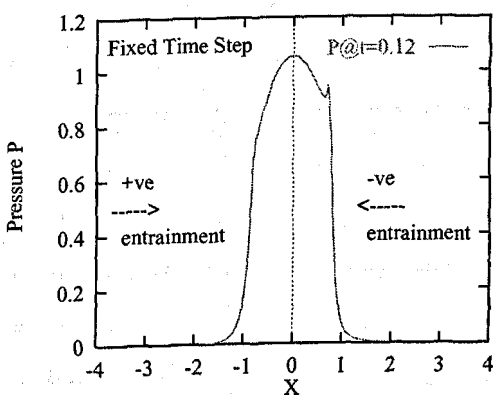
Fixed Time Step
P@t=0.12
Pressure P
+ve
----->
entrainment
-ve
<-----
entrainment
X

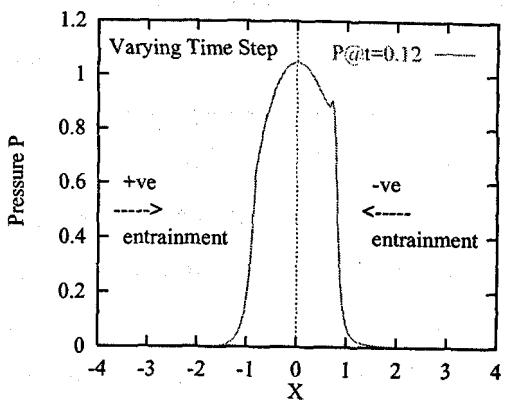
Varying Time Step
P@t=0.12
Pressure P
+ve
----->
entrainment
-ve
<-----
entrainment
X

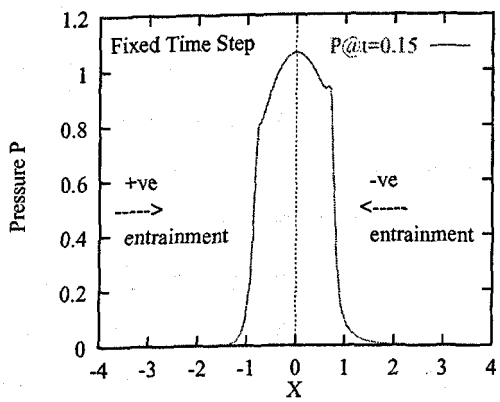
Fixed Time Step
P@t=0.15
Pressure P
+ve
----->
entrainment
-ve
<-----
entrainment
X

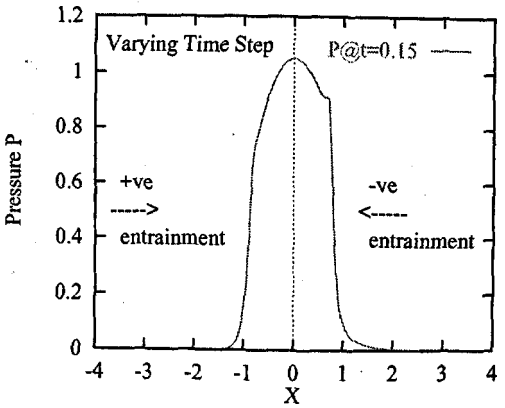
Varying Time Step
P@t=0.15
Pressure P
+ve
----->
entrainment
-ve
<-----
entrainment
X

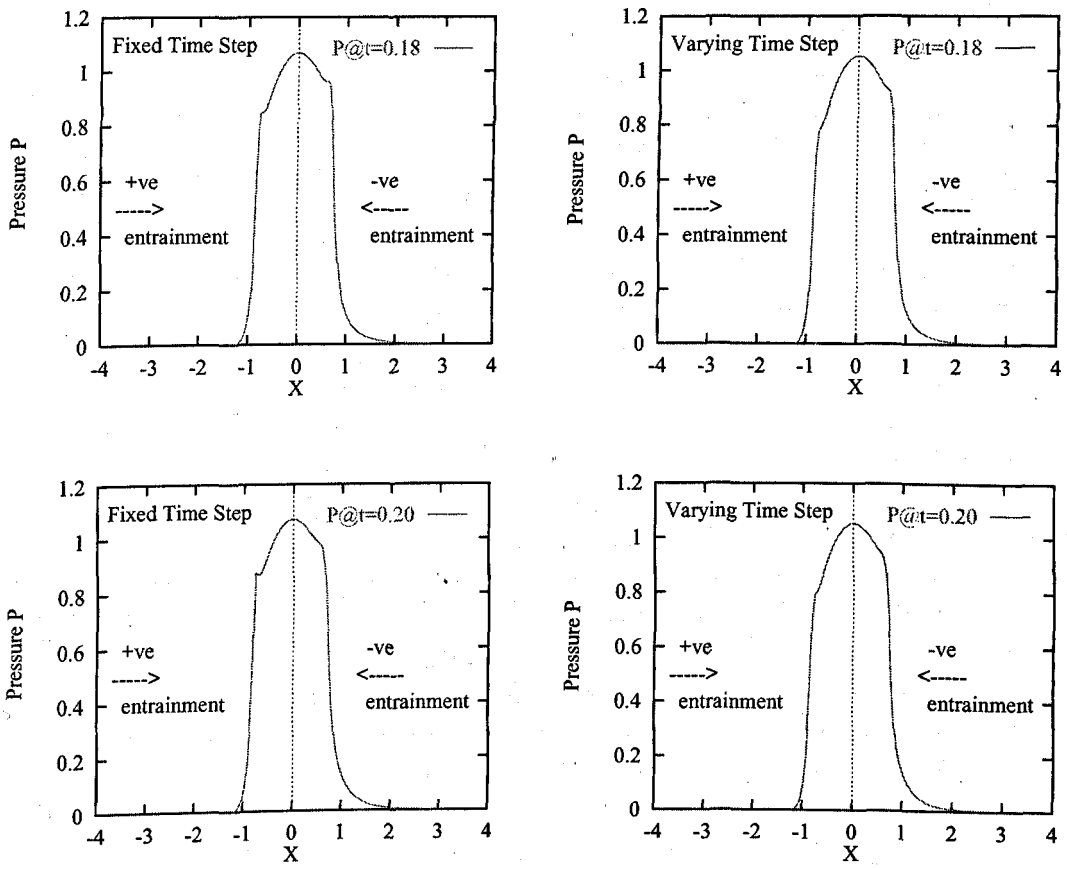

Figure 6.18: Pressure profiles along the X-axis (129by129).

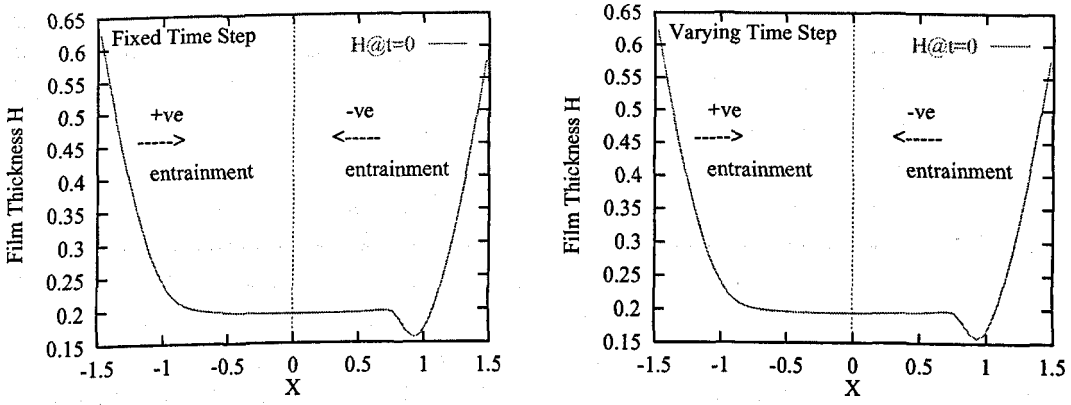

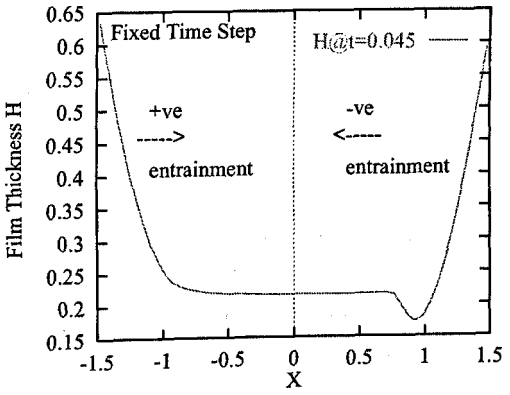
Fixed Time Step
H@t=0.045
+ve
----->
entrainment
-ve
<-----
entrainment
Film Thickness H
X

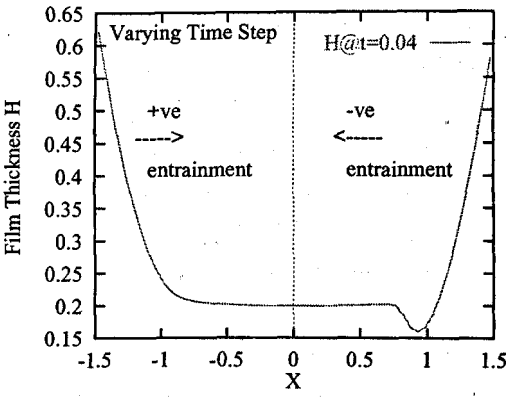
Varying Time Step
H@t=0.04
+ve
----->
entrainment
-ve
<-----
entrainment
Film Thickness H
X

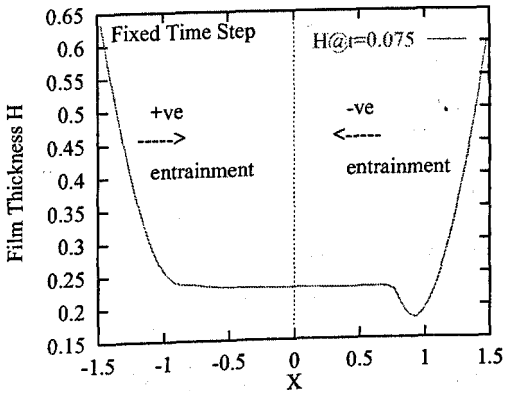
Fixed Time Step
H@t=0.075
+ve
----->
entrainment
-ve
<-----
entrainment
Film Thickness H
X

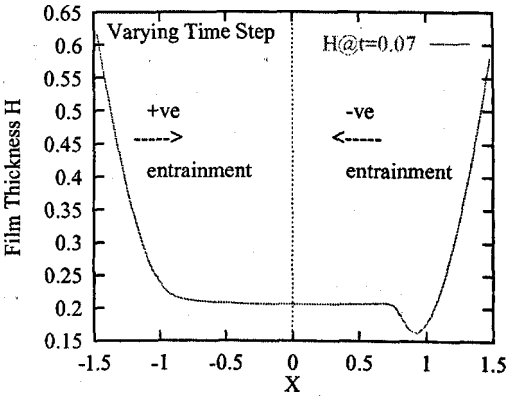
Varying Time Step
H@t=0.07
+ve
----->
entrainment
-ve
<-----
entrainment
Film Thickness H
X

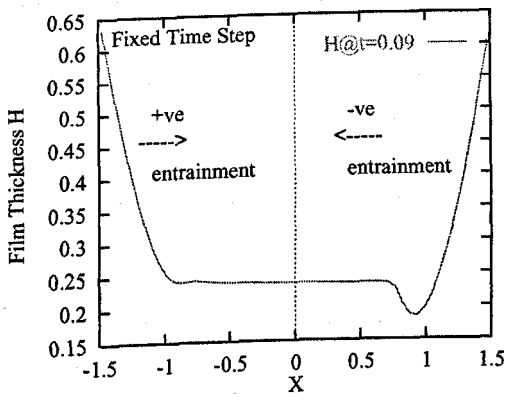
Fixed Time Step
H@t=0.09
+ve
----->
entrainment
-ve
<-----
entrainment
Film Thickness H
X

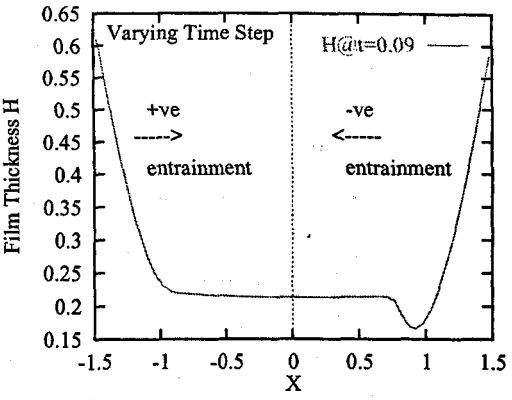
Varying Time Step
H@t=0.09
+ve
----->
entrainment
-ve
<-----
entrainment
Film Thickness H
X

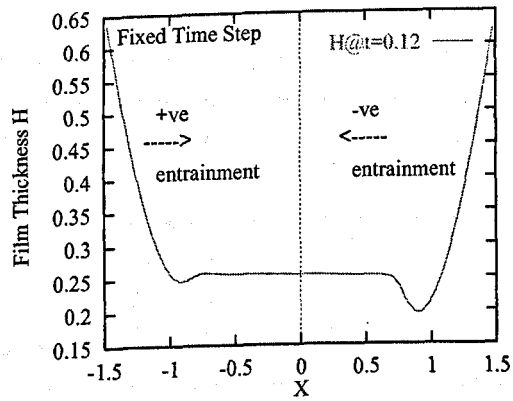
Fixed Time Step
H@t=0.12
+ve
----->
entrainment
-ve
<-----
entrainment
Film Thickness H
X

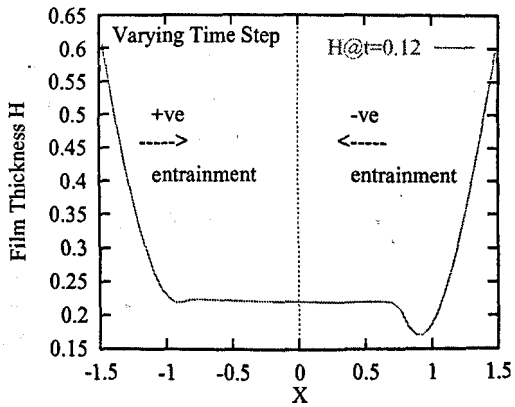
Varying Time Step
H@t=0.12
+ve
----->
entrainment
-ve
<-----
entrainment
Film Thickness H
X

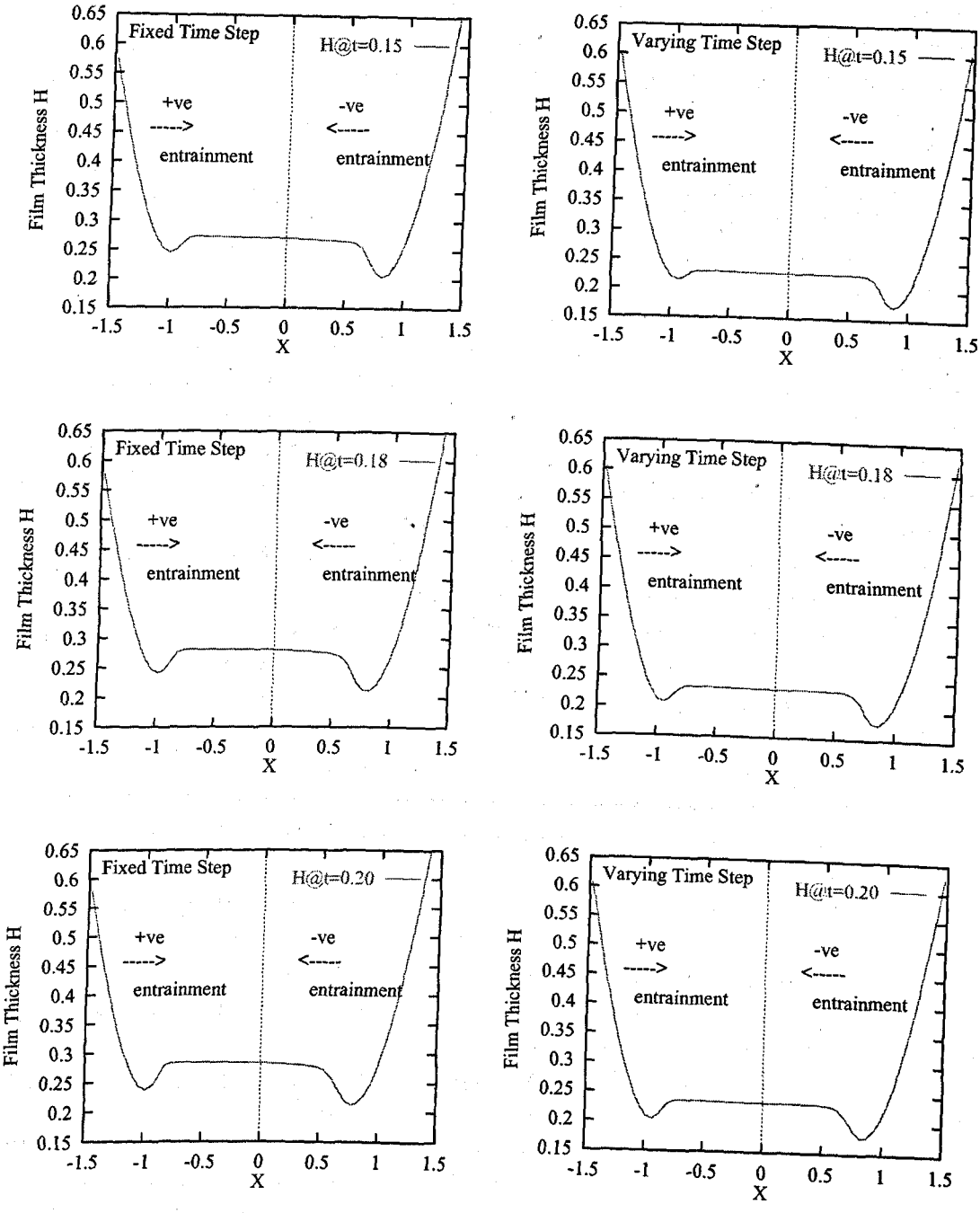

Figure 6.19: Film thickness profiles along the X-axis (129by129).

A graphical representation of the step sizes employed in the fixed and variable time step methods are shown in Figure (6.20). A logarithmic scale is used on both axes to plot time 't' against the step sizes 'Step Size' of the two methods. In the fixed time step method, the step size is constant and is shown as a straight line parallel to the X-axis which represents time t. The plot for the variable time step method starts off as a constant value and then begins to fluctuate between

3.8760×10^{-3} and 1.938×10^{-3} until it approaches reversal. At reversal the step size dips to a minimum value of 9.6899×10^{-4}. Just after reversal, the step size repeats the fluctuation pattern.

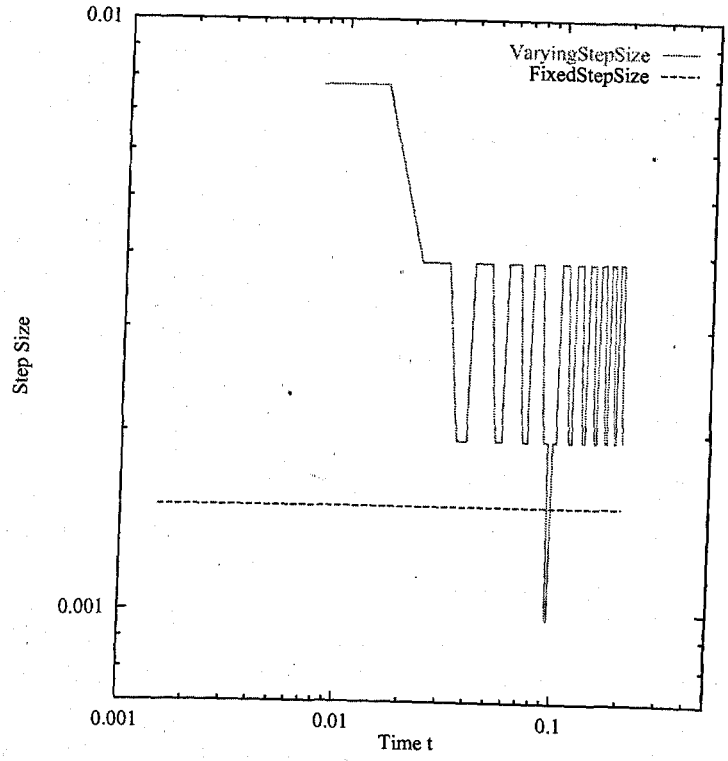

Figure 6.20: Graphical representation of fixed and variable step sizes.

6.5.3 Discussion

We will now analyse the solutions obtained using fixed and variable time step methods in the above two cases. For convenience, the solution in case one was obtained using a 65 by 65 finest grid whereas a 129 by 129 finest grid was employed in case two. In case one, there is not much to choose between the solutions obtained using the two methods and as expected, since the minimum step size in the fixed time step method is approximately equal to the minimum step size in the variable time step method, the discrepancy in the minimum and central film thicknesses obtained using the two methods is minimal. On a reasonably large mesh, as in case two, the variable time step method is much faster than the fixed time step method. However, though the discrepancy in the minimum and central film thicknesses obtained using the two methods is relatively large, their respective profiles of pressure and film

thickness are very similar. Since these problems are highly non-linear and due to the complexity of the problem being considered, that is zero and reversal entrainments, the variable time step method is quite sensitive to the step size when the time cycle approaches the zero and reversal entrainments. Hence, special measures need to be considered during zero and reversal entrainments. Besides this, the issue of discontinuity in the discretisation during reversal also needs to be addressed.

The combination of the multigrid method, differential algebraic equations and variable time steps is a novel approach for solving transient elasto-hydrodynamic lubrication problems. The results obtained using this approach are very encouraging and appear to be a step in the right direction although more work is needed.

6.6 Conclusion

The main concept of this chapter was to solve transient elasto-hydrodynamic lubrication problems using the multigrid solver of Chapter 4. This has been illustrated by solving very demanding test problems using fixed and variable time step methods. It is demanding in the sense that the problem undergoes a rapid change from positive to negative entrainments, that is the speeds of the two surfaces in contact are driven down to zero and then a reversal entrainment is introduced by reversing the direction of flow.

We have illustrated in this chapter the effectiveness of the new convergence criterion when solving transient elasto-hydrodynamic lubrication problems. By introducing the new concept for testing the convergence criterion, the amount of work done is reduced without affecting the accuracy of the solution. We have also illustrated that the variable time step method can be used to solve transient elasto-hydrodynamic lubrication problems and that this is a promising approach with regard to reducing the computational cost in solving such problems.

From the obtained fixed and variable time step solutions, we can conclude that the multigrid solver developed in Chapter 4 is very robust and capable of solving highly demanding elasto-hydrodynamic lubrication problems.

Chapter 7

CONCLUSION

The main object of the work presented in this thesis was to develop an efficient, robust and general purpose numerical solver for steady-state and time-dependent (or transient) elasto-hydrodynamic lubrication circular contact problems. The solver is based on the FDMG Multigrid Software [92] and a new relaxation scheme which is developed in this work. These problems are very important in engineering applications and by developing a general purpose numerical solver, mainly for industrial applications, engineers will be able to solve a wide range of these problems under different operating conditions.

The mathematical model describing isothermal (Newtonian) elasto-hydrodynamic lubrication circular contact problems is highly non-linear consisting of a complex system of coupled integro-differential equations. The model is made up of three equations with a pressure dependent viscosity and density. The three equations are the Reynolds equation, the film thickness equation and the force balance equation and the main feature of the model is the cavitation boundary condition $P \geq 0$. Due to the complexity of these problems, solutions can not be obtained analytically and numerical methods must be used. This is achieved by discretising the governing equations at every point on the computational domain using a finite difference scheme.

Over the years, dating back to the 1970's, many numerical schemes have been developed to solve elasto-hydrodynamic lubrication problems. Most of these schemes are based on the direct iterative methods which are not only expensive computationally but are also restrictive under severe operating conditions, such as high loads. Hence, most of the earlier work on elasto-hydrodynamic lubrication problems was based on line contact and lightly loaded point contact problems. However, new methods are emerging but they are still restrictive in one form or another. Examples of these new methods include the effective influence Newton method of Wang [102] and homotopy method [4] used by Scales [75].

A major breakthrough was achieved by Lubrecht [68] who introduced the multigrid method in solving elasto-hydrodynamic lubrication problems. The use of the multigrid method tackled the problem of large CPU times but the problem of instability associated with highly loaded point contact problems was still an issue. Following Lubrecht's work, Venner [97] developed a relaxation scheme which was used with the multigrid method to solve elasto-hydrodynamic lubrication problems. This enabled Venner to solve highly loaded point contact problems using a large number of mesh points. Hence, the issue of instability was resolved and problems that were previously unsolvable could now be solved routinely. However, the relaxation scheme of Venner is not only difficult to understand because it is not presented in its entirety but also difficult to implement due to its complexity.

A new relaxation scheme to solve elasto-hydrodynamic lubrication problems is presented in this work which uses the same principle as Venner in that different relaxation schemes are employed on the same computational domain. The manner in which the new relaxation has been developed is based on the behaviour of the Reynolds equation of the elasto-hydrodynamic lubrication model. The coefficient ϵ of the Reynolds equation varies several orders of magnitude over the computational domain and is the main cause for numerical instabilities when solving highly loaded problems. This means that whichever relaxation scheme is employed to solve these problems, it must be able to cope with extreme values of the coefficient ϵ of the Reynolds equation. This then leads to a stable error smoother over the entire domain. Based on this concept, the new relaxation scheme for solving elasto-

hydrodynamic lubrication problems makes use respectively of the Jacobi and the Gauss-Seidel line relaxation schemes in the contact and non-contact regions of the computational domain. The main concept of the new relaxation scheme developed in this work is that it is very simple and easy to implement and understand.

The new relaxation scheme is used with the FDMG Multigrid Software [92] to develop a multigrid solver for elasto-hydrodynamic lubrication problems (multigrid solver). However, due to the complexity of the elasto-hydrodynamic lubrication model, substantial modifications have been made to the original FDMG multigrid software. A wide range of steady-state problems have been solved using the multigrid solver and the obtained solutions are comparable with those obtained using other numerical methods. The maximum Hertzian pressure of steady-state problems solved in this work varied between $0.44GPa$ and $3.68GPa$ and the dimensionless parameter $\overline{\alpha}$ varied between $\overline{\alpha} = 4$ and $\overline{\alpha} = 82$. The maximum Hertzian pressure p_h and the dimensionless parameter $\overline{\alpha}$ indicate the load of the problem. The higher the value of p_h and $\overline{\alpha}$, the higher the load of the problem.

Besides solving steady-state problems, the multigrid solver is also employed to solve transient problems. Fixed and variable time step methods are used to solve demanding transient problems. A new convergence testing criterion, based on [90], for transient problems has also been presented which reduces the amount of work done to solve these problems without affecting the accuracy.

Having solved a range of demanding steady-state and transient problems, we can conclude that the multigrid solver for elasto-hydrodynamic lubrication problems developed in this work is a fast, robust and general purpose solver for elasto-hydrodynamic lubrication circular contact problems. It is capable of solving both lightly to highly loaded problems found in industrial applications. The multigrid solver has many industrial applications and it has already been used at the Shell Research and Technology Centre at Thornton.

Bibliography

[1] X Ai. *Numerical analysis of elasto hydrodynamic lubricated line and point contacts with rough surfaces by using semi-system and multigrid methods.* PhD thesis, North Western University, Evanston, IL, 1993.

[2] X Ai and H.S Cheng. The influence of moving dent on point EHL contacts. *STLE Tribology Transaction*, v 37:pages 323–335, 1994.

[3] X Ai, H.S Cheng, and L Zheng. A transient model for micro-elastohydrodynamic lubrication with three dimensional irregularities. *Journal of Tribology*, v 115:pages 102–110, 1992.

[4] E.L Allgower and K George. *Numerical continuation methods.* Springer Verlag, 1990.

[5] D.A Anderson, J.C Tannehill, and R.H Pletcher. *Computational Fluid Mechanics and Heat Transfer.* Hemisphere Publishing Corporation, 1984.

[6] C Barus. Isothermals, isopiestics and isometrics relative to viscosity. *American Journal of Science*, v 45:pages 87–96, 1893.

[7] M Berzins. Global error estimation in the method of lines for parabolic equations. *SIAM, Journal of Sci. Stat. Comput.*, v 9(No 4):pages 687–703, 1988.

[8] M Berzins and R.M Furzeland. A user's manual for sprint: Part 1. Technical Report No 199, Department of Computer Studies, University of Leeds, Leeds, 1985.

[9] M Berzins and R.M Furzeland. A user's manual for sprint: Part 2. Technical Report No 202, Department of Computer Studies, University of Leeds, Leeds, 1986.

[10] M Berzins and R.M Furzeland. An adaptive theta method for the solution of stiff and non-stiff differential equations. *App. Num. Math.*, v 8:pages 1–19, 1992.

[11] S Biswas and R.W Snidle. Calculation of surface deformation in point contact EHD. *Journal of Lub. Tech.*, v 99:pages 313–317, 1977.

[12] A Brandt. Multi-level adaptive solutions to boundary-value problems. *Mathematics of Computation*, v 31:pages 333–390, 1977.

[13] A Brandt. Multigrid techniques: 1984 guide with applications to fluid dynamics. *Available as G.M.D. Studien No. 85, from G.M.D FIT, Postfach 1240, D-52 05, St Augustin 1, Germany*, 1984.

[14] A Brandt and N Dinar. Multigird solutions to flow problems. In S.V Parter, editor, *Numerical methods for partial differential equations.* Academic, New York, 1979.

[15] A Brandt and A.A Lubrecht. Multilevel matrix multiplication and fast solution of integral equations. *Journal of Computational Physics*, 90:pages 348–370, 1990.

[16] A Brandt and C.H Venner. Multilevel evaluation of integral transforms with asymptotically smooth kernels. Technical report, The Weizmann Institute of Science, Israel, 1995.

[17] K.E Brenan, S.L Campbell, and L.R Petzold. *Numerical Solution of Initial-Value Problems in Differential-Algebraic Equations.* Elsevier Science Publishing Co., 1989.

[18] W.L Briggs. A multigrid tutorial. *SIAM, Philadelphia, Pennsylvania, ISBN 0-89871221-1*, 1987.

[19] R.L Burden and J.D Faires. *Numerical Analysis.* PWS Kent, 1993.

[20] L Chang. An efficient and accurate formulation of the surface deflection matrix in leastohydrodynamic point contacts. *Journal of Tribology*, v 111:pages 642–647, 1989.

[21] L Chang. Traction in thermal elastohydrodynamic lubrication of rough surfaces. *Journal of Tribology*, v 114:pages 186–191, 1992.

[22] L Chang, T.F Conry, and C Cusano. An efficient, robust, multi-level computational algorithm for elasto hydrodynamic lubrication. *Journal of Tribology*, v 111:pages 193–199, 1989.

[23] L Chang, C Cusano, and T.F Conry. Effects of lubrication rheology and kinematic conditions on micro-elastohydrodynamic lubrication. *Journal of Tribology*, v 111:pages 344–351, 1989.

[24] H Cheng. A numerical solution of the elasto-hydrodynamic film thickness in an elliptical contact. *Trans. ASME, Journal of Lubrication Technology*, v 92(No. 1):pages 155–162, 1970.

[25] R.J Chittenden, D Dowson, J.F Dunn, and C.M Taylor. A theoretical analysis of the isothermal elastohydrodynamic lubrication of concentrated contacts. *Proc. R. Soc. London*, v 397:pages 245–269 and 271–294, 1985.

[26] T.F Conry, S Wang, and C Cusano. A Reynolds-Eyring equation for elastohydrodynamic lubrication in line contacts. *Journal of Tribology*, v 109(No. 4):pages 648–658, 1987.

[27] A.W Crook. The lubrication of rollers. *Phil. Trans.*, A 250:page 387, 1958.

[28] D Dowson and B.J Hamrock. Numerical evaluation of the surface deformation of elastic solids subjected to a Hertzian contact stress. *ASLE Trans.*, v 19(No. 4):pages 279–286, 1976.

[29] D Dowson and G.R Higginson. A numerical solution to the elastohydrodynamic problem. *Journal of Mech. Eng. Science*, v 1(No.1):pages 7–15, 1959.

[30] D Dowson and G.R Higginson. Elasto-hydrodynamic lubrication, the fundamentals of roller and gear lubrication. *Pergamon Press, Oxford, Great Britain*, 1966.

[31] D Dowson and D Wang. An analysis of the normal bouncing of a solid elastic ball on an oily plane. *WEAR*, v 179:pages 29–37, 1994.

[32] P Ehret, D Dowson, and C.M Taylor. Time dependent solutions with waviness and asperities in EHL point contacts. *23rd Leeds-Lyon Symposium on Tribology*, 1996.

[33] P Ehret, D Dowson, C.M Taylor, and D Wang. Analysis of EHL point contact with multigrid methods. *IMechE Part C*, 1996.

[34] A.M Ertel. Hydrodynamic lubrication based on new principles. *Akad.Nauk, SSSR Prikadnaya Mathematica i Mekhanika*, 3, 2:pages 41–52, 1939.

[35] H.P Evans and R.W Snidle. Inverse solution of Reynolds equation of lubrication under point contact elastohydrodynamic conditions. *Trans.ASME, Journal of Lubrication Technology*, v 103:pages 539–546, 1981.

[36] H.P Evans and R.W Snidle. The isothermal elastohydrodynamic lubrication of spheres. *Trans.ASME, Journal of Lubrication and Technology*, v 103:pages 547–557, 1981.

[37] H.P Evans and R.W Snidle. The elastohydrodynamic lubrication of point contacts at heavy loads. *Proc. Royal Society of London*, A382:pages 183–199, 1982.

[38] C.W Gear. *Numerical initial value problems in ordinary differential equations.* Prentice Hall, 1971.

[39] C.W Gear. The simultaneous numerical solution of differential-algebraic equations. *IEEE Trans. Circuit Theory CT-18*, pages 89–95, 1971.

[40] R Gohar. *Elastohydrodynamics.* Ellis Horwood, Chichester, England, 1988.

[41] A.N Grubin and I.E Vinogradova. Investigation of the contact of machine components. *Central Scientific Research Institute for Technology and Mechanical Engineering (Moscow)*, v 30 (DSIR translation 337), 1949.

[42] G Hall and J.M Watt. *Modern numerical methods for ordinary differential equations.* Clarendon Press, Oxford, 1976.

[43] B.J Hamrock. *Fundamentals of Fluid Film Lubrication.* NASA Reference Publication 1255, 1991.

[44] B.J Hamrock and D Dowson. Numerical evaluation of the surface deformation of elastic solids subjected to a Hertzian contact stress. Technical report, NASA, Washington D. C, 1974.

[45] B.J Hamrock and D Dowson. Isothermal elastohydrodynamic lubrication of point contacts, part i - theoretical formulation. *Journal of Lubrication Technology*, v 98:pages 223–229, 1976.

[46] B.J Hamrock and D Dowson. Isothermal elastohydrodynamic lubrication of point contacts, part ii - ellipticity parameter results. *Journal of Lubrication Technology*, v 98:pages 375–383, 1976.

[47] B.J Hamrock and D Dowson. Isothermal elastohydrodynamic lubrication of point contacts, part iii - fully flooded results. *Journal of Lubrication Technology*, v 99:pages 264–276, 1977.

[48] B.J Hamrock and D Dowson. Isothermal elastohydrodynamic lubrication of point contacts, part iv - starvation results. *Journal of Lubrication Technology*, v 99:pages 15–23, 1977.

[49] B.J Hamrock and D Dowson. *Ball Bearing Lubrication, The Elastohydrodynamics of Elliptical Contacts.* John Willey and Sons, 1981.

[50] B.J Hamrock and B.O Jacobson. Elastohydrodynamic lubrication of line contacts. *ASLE transactions*, v 27(No. 4):pages 275–287, 1984.

[51] H Hertz. The contact of elastic solids. *Journal Reine Angew Math*, v 92:pages 156–171, 1881.

[52] A.C Hindmarsh. Lsode and lsodi, two new initial value ordinary differential equation solvers. *ACM-SIGNUM Newsletters*, v 15:pages 10–11, 1980.

[53] K.P Hou, D Zhu, and S.Z Wen. A new numerical technique for computing surface elastic deformation caused by a given normal pressure distribution. *Journal of Tribology*, v 107:pages 128–131, 1985.

[54] L.G Houpert and B.J Hamrock. A fast approach for calculating film thicknesses and pressures in elastohydrodynamically lubricated contacts at high loads. *Journal of Tribology*, v 108:pages 411–420, 1986.

[55] A Iserles. *A first course in the numerical analysis of differential equations.* Cambridge University Press, 1996.

[56] F.L Jen and Y.C Hsiaw. A numerical solution for calculating elastic deformation in elliptical contact EHL of rough surface. *Journal of Tribology*, v 113:pages 12–21, 1991.

[57] C Johnson. *Numerical solution of partial differential equations by the finite element method.* Cambridge University Press, 1990.

[58] M Kaneta. Effects of surface roughness in elastohydrodynamic lubrication. *JSME III*, v 35(No. 4):pages 535–546, 1992.

[59] M Kaneta, T Sakai, and H Nishikawa. Optical interferometric observations of the effects of a bump on point contact EHL. *Journal of Tribology*, v 114:pages 779–784, 1992.

[60] M Kaneta, T Sakai, and H Nishikawa. Effects of surface roughness on point contact EHL. *STLE Tribology Transactions*, v 36(No. 4):pages 605–612, 1993.

[61] H.P Kweh, C.C Evans, and R.W Snidle. Elastohydrodynamic lubrication of heavily loaded circular contacts. *Proc. Instn. Mech. Engrs*, v 203:pages 133–148, 1989.

[62] J.D Lambert. *Computational methods in ordinary differential equations.* Wiley, 1973.

[63] J Lawson, M Berzins, and P.M Dew. Balancing space and time errors in the method of lines for parabolic equations. *SIAM Journal of Sci. Stat. Comput.*, v 12(No 3):pages 573–594, 1991.

[64] R Lee and B.J Hamrock. Squeeze and entraining motion in noncomformal line contacts, part ii - elastohydrodynamic lubrication. *Journal of Tribology*, v 111, 1989.

[65] A.A Lubrecht. *The numerical solution of the elastohydrodynamically lubricated line and point contact problem using multigrid techniques.* PhD thesis, University of Twente, Enschede, ISBN 90-9001583-3, 1987.

[66] A.A Lubrecht and E Ioannides. A fast solution of the dry contact problem and the associated sub surface stress field using multilevel techniques. *Journal of Tribology*, v 113:pages 128–133, 1991.

[67] A.A Lubrecht, W.E ten Napel, and R Bosma. Multigrid, an alternative method of calculating film thickness and pressure profiles in elastohydrodynamically lubricated line contacts. *ASME Journal of Tribology*, v 108(No. 4):pages 551–556, 1986.

[68] A.A Lubrecht, W.E ten Napel, and R Bosma. Multigrid, an alternative method of solution for two dimensional elastohydrodynamically lubricated point contact calculations. *ASME Journal of Tribology*, v 109:pages 437–443, 1987.

[69] S.B Lui, J.J Ma, and X.Y Chen. Elliptic paraboloid method for calculating surface elastic deformation in EHL. *Tribology International*, v 26(No. 6):pages 443–448, 1993.

[70] M.J Maron and R.J Lopez. *Numerical Analysis: a practical approach.* 1991.

[71] H.M Martin. Lubrication of gear teeth. *Engineering (London)*, pages 102 and 199, 1916.

[72] A Meldahl. Contribution to the theory of the lubrication of gears and of the stressing of the lubricated flanks of gear teeth. *Brown Boveri Review*, v 28(No. 11):page 374, 1941.

[73] H Moes. Discussion on a paper by D. Dowson. *Proc. Inst. Mech. Engrs.*, v 180:pages 244–245, 1965.

[74] E Nurgat and M Berzins. A new relaxation scheme for solving EHL problems. *23rd Leeds-Lyon Symposium on Tribology*, 1996.

[75] E Nurgat, M Berzins, and L Scales. Solving EHL problems using iterative, multigrid and homotopy methods. Review stage of publication in the Journal of Tribology, 1997.

[76] Department of Education and Science. Lubrication (tribology), education and research. Technical report, Department of Education and Science, HMSO, London, 1966.

[77] K.P Oh. The numerical solution of dynamically loaded elastohydrodynamic contact as a nonlinear complementarity problem. *Journal of Tribology*, v 106:pages 88–95, 1985.

[78] K.P Oh and S.M Rohde. Numerical solution of the point contact problem using the finite element method. *International Journal for Numerical Methods in Engineering*, v 11:pages 1507–1518, 1977.

[79] H Okamura. A contribution to the numerical analysis of isothermal elasto hydrodynamic lubrication. *Leeds-Lyon Symposium on Tribology*, pages 313–320, 1982.

[80] K.F Osborn and F Sadeghi. Time dependent line EHD lurication using the multigrid/multilevel technique. *Journal of Tribology*, v 114:pages 68–74, 1992.

[81] N.P Petrov. Friction in machines and the effect of the lubricant. *Inzherernii Zhurnal St. Petersburg*, vs 1, 2, 3 and 4, 1883.

[82] A.I Petrusevich. Fundamental conclusions from the contact-hydrodynamic theory of lubrication. *Izv. Akad. Nauk. SSSR (OTN)*, v 2:page 209, 1951.

[83] L Petzold. Differential algebraic equations are not odes. *SIAM Journal Sci. Stat. Comput.*, v 3:pages 367–384, 1982.

[84] A.P Ranger, C.M.M Ettles, and A Cameron. The solution of the point contact elastohydrodynamic problem. *Proc. Roy. Soc. London, Ser. A*, v 346:pages 227–244, 1975.

[85] J.N Reddy. *An introduction to the finite element method.* McGraw-Hill International, 1984.

[86] O Reynolds. On the theory of lubrication and its application to Mr Beauchamp Tower's experiments, including an experimental determination of the viscosity of olive oil. *Philos. Trans. Roy. Soc. London*, v 177:pages 157–234, 1886.

[87] C.J.A Roelands. *Correlational aspects of the viscosity-temperature-pressure relationship of lubricating oils.* PhD thesis, Technische Hogeschool Delft, The Netherlands, 1966.

[88] F Sadeghi and P.C Sui. Subsurface stresses in rolling/sliding machine components. *Proceedings of 1988 International Compressor Engineeering Conference*, v 2:pages 629–638, 1988.

[89] A.G Schlijper, L.E Scales, and J.E Rycroft. Current tools and techniques for EHL modelling. *Tribology International*, v 29:pages 669–673, 1996.

[90] L.F Shampine. Implementation of implicit formulas for the solution of ODEs. *SIAM Journal of Sci. Stat. Comp.*, v 1(No 1):pages 103–118, 1980.

[91] L.F Shampine and M.K Gordon. *Computer solution of ordinary differential equations.* W.H Freeman and Co., 1975.

[92] G.J Shaw. FDMG multigrid software. Version 3.

[93] L.B Sibley and F.K Orcutt. Elastohydrodynamic lubrication of rolling contact surfaces. *Trans. Amer. Soc. Lub. Engrs.*, v 4(No. 2):page 234, 1961.

[94] C Taylor and J.F O'Callaghan. A numerical solution of the elastohydrodynamic lubrication problem using finite elements. *Journal Mechanical Engineering Science*, v 14(No. 4):pages 229–237, 1972.

[95] S.P Timoshenko and J.N Goodier. Theory of elasticity. *3rd ed. McGraw-Hill, New York*, 1982.

[96] B Tower. Second report on friction experiments (experiments on the oil pressure in a bearing). *Proc. Inst. Mech. Eng. (London)*, pages 58–70, 1885.

[97] C.H Venner. *Multilevel solution of the EHL line and point contact problems.* PhD thesis, University of Twente, The Netherlands, ISBN 90-9003974-0, 1991.

[98] C.H Venner, F Couhier, A.A Lubrecht, and J.A Greenwood. Amplitude reduction of waviness in transient EHL line contacts. *23rd Leeds-Lyond Symposium Tribology*, 1996.

[99] C.H Venner and A.A Lubrecht. Numerical simulation of a transverse ridge in a circular EHL contact under rolling/sliding. *Journal of Tribology*, v 116:pages 751–761, 1994.

[100] C.H Venner, A.A Lubrecht, and W.E ten Napel. Numerical simulation of the overrolling of a surface feature in an EHL line contact. *Journal of Tribology*, 1991:pages 777–783, 1991.

[101] C.H Venner, W.E ten Napel, and R Bosma. Advanced multilevel solution of the EHL line contact problem. *Journal of Tribology*, v 112:pages 426–431, 1990.

[102] D Wang. *Elastohydrodynamic lubrication of point contacts for layers of soft solids and for monolithic hard materials in the transient bouncing ball problem.* PhD thesis, Department of Mechanical Engineering, University of Leeds, 1994.

[103] C Weber and K Saalfeld. Schmierfilm bei walzen mit verformung. *Zeits. ang. Math. Mech*, v 34(Nos. 1-2):page 54, 1954.

[104] L.D Wedeven and C Cusano. Elastohydrodynamic film thickness measurements of artificially produced surface dents and grooves. *ASLE Trans.*, v 22:pages 369–381, 1979.

[105] P Wesseling. *An introduction to multigrid methods.* John Wiley , Chichester, England, 1992.

[106] S.R Wu. A penalty formulation and numerical approximation of the Reynolds-Hertz problem of elasto-hydrodynamic lubrication. *International Journal of Engineering Science*, v 24:pages 1001–1013, 1986.

[107] S.R Wu and J.T Oden. Convergence and error estimates for finite element solutions of elastohydrodynamic lubrication. *Comput. Math. Applic.*, v 13(No. 7):pages 583–593, 1987.

[108] S.R Wu and J.T Oden. A note on applications of adaptive finite elements to elastohydrodynamic lubrication problems. *Communications in Applied Numerical Methods*, v 3:pages 485–494, 1987.

[109] D Zhu and H.S Cheng. Effect of surface roughness on the point contact EHL. *ASME Journal of Tribology*, v 110:pages 32–37, 1988.